Aus dem Institut für Medizintechnologie

der Universität Heidelberg und der Hochschule Mannheim

(Geschäftsführender Direktor: Prof. Dr. med. Norbert Gretz)

# Investigation of Cancerous Tissues by MALDI Mass Spectrometry Imaging

## -

## Imaging of proteolytic activity in frozen tissue and standardised on-tissue digestion

Inauguraldissertation

zur Erlangung des akademischen Grades Doctor scientiarum humanarum

(Dr. sc. hum.)

der

Medizinischen Fakultät Mannheim

der Ruprecht-Karls-Universität

zu

Heidelberg

vorgelegt von

Katrin Miriam Erich

aus

Bad Dürkheim a.d.W.

2019

Dekan: Prof. Dr. med. Sergij Goerdt
Referent: Prof. Dr. rer. nat. Carsten Hopf

*Für meine Tochter und meinen Ehemann, die
viel Zeit opferten und mich stets unterstützen...*

# TABLE OF CONTENT

Page

# ABBREVIATIONS

| | |
|---|---|
| ABC | Ammonium bicarbonate |
| ABPP | Activity-based protein profiling |
| ACC | 7-amino-4-carbamoylmethylcoumarin |
| ACE | Acetylcholinesterase |
| ACN | Acetonitrile |
| AEBSF | 4-(2-aminoethyl)benzenesulfonyl fluoride hydrochloride |
| AMC | Asp-7-amino-4-methyl-coumin |
| BCA | Bicinchoninic acid |
| BSA | Bovine serum albumin |
| CHCA | A-cyano-4-hydroxycinnamic acid |
| CMC | Carboxymethyl Cellulose |
| CV | Coefficient of variation |
| ddH2O | Ultra-pure water |
| DHB | 2,5-dihydroxybenzoic acid |
| DMSO | Dimethyl sulfoxide |
| ECM | Extracellular matrix |
| EDTA | Ethylenediaminetetraacetic acid |
| ESI | Electrospray ionisation |
| EtOH | Ethanol |
| FA | Formic acid |
| FFPE | Formalin-fixed paraffin-embedded |
| FRET | Fluorescence resonance energy transfer |
| FT-ICR | Fourier Transform Ion Cyclotron Resonance |
| FWHM | Full-width half maximum |
| GIST | Gastrointestinal stromal tumour |
| H&E | Hematoxylin & Eosin |
| HC | Hierarchical clustering |
| HCl | Hydrochloric acid |
| IQR | Inter-quartile-range |
| ITO | Indium Tin Oxide |
| LC-MS/MS | Liquid Chromatography-Tandem Mass Spectrometry |
| LFQ | Label-free quantification |
| $m/z$ | Mass to Charge |
| MAD | Mean absolute deviation |
| MALDI | Matrix-assisted laser desorption/ionization |
| MeOH | Methanol |
| MMP | Matrix metalloprotease |
| MRI | Magnetic Resonance Imaging |
| MS | Mass Spectrometry |
| MSI | Mass Spectrometry Imaging |
| NIR | Near-infrared |
| ON | Overnight |
| PBS | Phosphate buffered saline |
| PCA | Principal Component Analysis |

| | |
|---|---|
| PET | Positron emission tomography |
| PIM | Protease-inhibitor mixture |
| qPCR | Quantitative polymerase-chain reaction |
| RG | RapiGest SF Surfactant |
| ROI | Region of interest |
| RT | Room temperature |
| S/N | Signal-to-Noise ratio |
| SDS | Sodium dodecyl sulfate |
| SOP | Standard operating procedure |
| TCA | Trichloroacetic acid |
| TCEA-positive | CEA424-SV40TAg transgenic mice (C57BL6 background) with developed tumour |
| TCEP | Tris(2-carboxyethyl)phosphine |
| TFA | Trifluoroacetic acid |
| TGGA | The cancer genome atlas |
| TIC | Total Ion Current |
| TIMP | Tissue matrix metalloprotease inhibitor |
| TOF | Time of Flight |
| TPAA | Tissue protease activity assay |
| WHO | World health organisation |
| WT | Wild-Type |

# 1 INTRODUCTION

## 1.1 Classification of Proteases

The enzyme class 'hydrolases' and their subclass 'peptidases' (EC 3.4.-.-), defined by the Enzyme Commission in 1961, comprise any enzyme that hydrolyzes peptide bonds (synonyms: peptide hydrolase, protease, proteinase)[1,2]. The class is further divided into 'exopeptidases', which act at the terminus of the substrate's polypeptide chain and 'endopeptidases' that act internally in the polypeptide chain. Several sub-subclasses are defined, for example for exopeptidases: aminopeptidases (EC 3.4.11.-) that liberate a single amino acid at the N-terminus or dipeptidyl-peptidases and tripeptidyl-peptidases liberating two and three amino acids, respectively (EC 3.4.14.-). Furthermore, endopeptidases are divided into sub-subclasses based on their ) catalytic mechanisms (e.g. metalloproteases, serine- or cysteine proteases Table 1). The human *degradome* (the complete set of proteases) comprises in total 569 proteases, whereas the rat and mouse degradome seem to consist of even more proteases (644 and 629, respectively)[3]. Serine-type, cysteine-type and metallo carboxypeptidases (EC 3.4.16, EC 3.4.18 and EC 3.4.17, respectively) cleave with a similar catalytic mechanism but act on the C-terminus of the polypeptide chain liberating a single residue.

Based on two fundamental differences mammalian proteases can be separated in the catalytic mechanisms. Serine-, cysteine- and threonine-proteases perform **covalent catalysis**, where the nucleophile of the catalytic site is part of an amino acid. The amino acid histidine thereby works commonly as the base in the active centre. In contrast, metallo- and aspartic proteases use **non-covalent catalysis,** and an activated water molecule is the nucleophile. Here aspartate or glutamate residues serve as bases (as deprotonated acid, it takes the proton of the water molecule) for the catalytic mechanism. For metalloproteases, a coordinated zinc molecule polarizes the carbonyl group of the substrate, while it facilitates the deprotonation of the water molecule. The specificity of each protease is used to identify the single enzyme of each sub-subclass not being defined solely by the nature of the catalytic centre. The binding sites, surrounding the catalytic centre, favour specific amino acids and therefore ensure proteolytic activity when required[4]. With that mechanism, proteases display a high degree of specificity.

**Table 1: Sub-subclasses of endopeptidases with their respective enzyme commission number**

| Sub-subclass | EC | Residue and molecule responsible for initiating cleavage of the peptide bond | Number of proteases in human degradome[3] | MEROPS database identifier |
|---|---|---|---|---|
| Serine endopeptidase | EC 3.4.21.- | Hydroxyl group of serine | 176 | S |
| Cysteine endopeptidase | EC 3.4.22.- | Thiol group of cysteine | 150 | C |
| Aspartic endopeptidase | EC 3.4.23.- | Carboxyl group of two aspartates | 21 | A |
| Metalloendopeptidase | EC 3.4.24.- | Zinc ion bound in the active centre | 194 | M |
| Threonine endopeptidase | EC 3.4.25.- | Hydroxyl group of threonine | 28 | T |

In the case of trypsin, a well-known serine-protease (EC 3.4.21.4) found in the mammalian digestive system, the bindingsites target positively charged amino acids. Therefore cleavage only occurs, when a lysine (Lys, K) or arginine (Arg, R) is attached to the binding site. A following proline (Pro, P) disturbs the interaction and impedes the cleavage process. The hydrolysis of the peptide bond is irreversible, because, on the one hand, the reaction equilibrium favours two amino acids, on the other hand, there is no enzyme counterpart to repair already cleaved proteins. As no turn-back process is implemented in biological processes, proteases should only be active when needed. In order to achieve this, they are expressed as *zymogens* (inactive precursors) and activated when needed by complex signalling cascades to ensure target amplification of the desired biological effect[5–7]. The group of matrix metalloproteases (MMPs) is further controlled by tissue matrix metalloprotease inhibitors (TIMPs), which together with hormones, cytokines and growth factors regulate their expression[8].

Initially, the role of protein degradation was attributed to food digestion and intracellular protein turnover[9]. Nowadays it is known, that proteolysis is related to key physiological processes like blood clotting, cell-cell progression, cell proliferation, cell death, DNA replication, tissue remodelling, and immune response[10].

### 1.1.1 The role of proteases in disease

A gain-of-function and loss-of-function of proteases result in several pathological conditions, such as cardiovascular-[11], inflammatory-[12], neurodegenerative-[13], infective diseases[14] as well as cancer[3].

With cancer intracellular and extracellular proteases are associated with tumour growth, survival, angiogenesis, invasion, inflammation, and metastasis[15,16]. It has been shown, that intracellular Caspases, which play a fundamental role in apoptosis, are related to tumour growth[17,18]. By degrading extracellular components Cathepsins allow tumour cells to invade surrounding tissue, blood and lymph vessels[19,20]. Trypsin, as another example, is involved in proliferation, invasion, and metastasis of colorectal cancer[21]. Furthermore, MMPs are released by tumour cells and tumour-surrounding stromal cells, and also degrade ECM to enable invasive tumour growth[22–24]. Deubiquitylases, Autophagins, ADAMTSs (short term for a disintegrin and metalloproteinase with thrombospondin motifs), Neprilysin, Kallikreins, and other proteases are also involved in tumour progression[3]. It is thus of great importance to know the molecular mechanism of proteases. For this reason, the *MEROPS – the peptidase database*[a] was developed, where known proteases, their related substrates, and inhibitors are listed[25]. An additional MEROPS identifier was developed, which indicates the catalytic type directly[26] (Table 1). Additional information is summed up in the *Degradome database*[b]*,* that comprises mammalian proteases and their associated diseases[27]. Whole genomic sequences from multiple organisms (human, chimpanzee, mouse, and rat), genetic diseases, protease structures, and protease inhibitors are implemented.

Excessive proteolysis can be reduced by therapeutic inhibitors, which are therefore widely investigated by pharmaceutical companies[14,28]. The development of angiotensin-converting enzyme (ACE) inhibitors used to treat hypertension, heart failure, and heart attack was a major success. About 20 different inhibitors (e.g. Captopril – Bristol-Myers Squibb, Lisinopril - AstraZeneca, Cilazapril – Roche) successfully target ACE, a metalloprotease of the renin-angiotensin system. In contrast, all MMP inhibitors combating cancer (e.g. marimastat – British Biotech,

---

[a] http://merops.sanger.ac.uk

[b] http://degradome.uniovi.es

prinomastat – Aguron or neovastat – Aeterba) failed in clinical trials due to severe side effects or lack of clinical benefit. Reasons for this are the fact that most inhibitors targeted broad-spectrum MMPs, and little was known about the diversity of MMPs. Secondly, the inhibitors seem ineffective against late-stage tumours (of the patients) but showed an effect in early stage tumour models[14].

### 1.1.2 Relevant proteases in gastric cancer

Gastric cancer used to be the leading cause of cancer deaths worldwide. It is separated anatomically into gastric adenocarcinomas (non-cardia) and gastro-esophageal-junction adenocarcinomas (cardia). Although most gastric cancers are gastric adenocarcinomas, the variety in architecture and growth, cell differentiation, histogenesis, and pathogenesis is high[29]. According to Lauren classification, four histological types are defined: diffuse (poorly differentiated, solitary tumour), intestinal (well differentiated, glandular structures), mixed and indeterminate[30]. A WHO classification comprises five histological classifications (tubular, papillary, mucinous, poorly cohesive, rare variants). The most commonly used system is the American Joint Committee on Cancer TNM (tumour, node, metastasis) staging[31].

In order to complement the preexisting classification based on histopathologic and anatomic criteria molecular and genetic findings were added. In a training set for supervised classification of 36 patients with localized gastric cancer three subtypes (proximal non-diffuse, diffuse, and distal non-diffuse) Shah *et al.* identified different gene expression patterns in >85 % of the samples[32]. Further, excessive studies have been performed to classify gastric cancer on a molecular level. Lei *et al.* compared the gene expression pattern of 248 gastric tumours and found three major subtypes: The **proliferative subtype** showed a high number of TP53 mutations (Tumour-suppressor gene 52; involved in regulation of apoptosis and DNA repair mechanism) and was grouped to the Lauren diffuse gastric cancer type. The **mesenchymal subtype** showed low TP53 mutations and a low level of CDH1 (gene for the protein E-Cadherin and also a tumour suppressor gene). This group had a histologic correlation to the Lauren diffuse type. The third group was named **metabolic subtype** having also low TD53 mutation and was more sensitive to 5-fluorouracil (5-FU, a cytotoxic agent used in chemotherapy)[33]. As part of The Cancer Genome Atlas (TCGA), 295 gastric

adenocarcinomas were analyzed and a new classification in four subgroups on a molecular basis was proposed[34]:

1. *Tumour positive for Epstein-Barr virus* (EBV)
2. *Microsatellite unstable tumours* (MSI)
3. *Genomically stable tumours* (GS)
4. *Chromosomally unstable tumours* (CIN)

The EBV is a pathogen that is associated with gastric cancer since 1990[35]. The virus disrupts the genes responsible for cell cycle regulation, inflammation, and angiogenesis. Microbial infections with the *Helicobacter pylori (H. pylori)* also contribute to gastric tumorgenesis[36]. Microsatellite instability is due to repetitive DNA sequences and is a result of impaired DNA mismatch repair, such as single base mismatches, short insertions, and deletions. The authors saw this new classification as an additive to histopathology, while there certainly exists some differences between those disciplines. Clinical trials with target therapies for distinct populations of gastric cancer patients are required.

In 1990 the comparison of homogenates from gastric cancer tissue and normal gastric tissue showed differences in cathepsin B, cathepsin L, tissue plasminogen activator (t-PA) and urinary plasminogen activator (u-PA). These differences seemed to favour cancer invasion and metastasis[37]. In a study of 301 gastric cancer patients the loss of expression of caspase-1 correlated with poor patient survival in gastric cancer[38]. Further reduced caspase-2 expression was found as an indicative marker for early-stage gastric carcinogenesis[39]. The expression of Hepsin, a transmembrane serine protease, was shown to be downregulated in gastric cancer tissue, whereas high expression of Hepsin correlated with a poorer survival[40]. Allgayer *et al.* showed that it is possible to identify high-risk protease pattern (proteases/inhibitor systems): Cathepsin D, α-1-antichymotrypsin, α-1-antitrypsin and α-2-macroglobulin had a prognostic impact on gastric cancer and indicated high individual risk. Furthermore, Cathepsin D seemed to be a parameter for disease-free survival[41]. Highly sensitive methods are required in order to detect early gastric cancer. Labisso *et al.* showed that Cathepsins and MMPs were potential biomarkers for early gastric cancer. During the conventional endoscopic examination of the upper gastrointestinal tract, early gastric cancer is often missed. The use of imaging modalities, like specific probes with fluorophores, could help to overcome this obstacle[42].

## 1.2 Visualization of protease activity

Apart from the analysis of gene expression levels, where the sample preparation requires homogenization of the tissue, "smart" imaging reagents and optical instrumentation are used. Monitoring of enzymatic activity in the context of intact cells (*in vitro*) or even in whole organisms (*in vivo*) is possible with those reagents. In 1997 a substrate library (PS-SCL = Positional scanning substrate combinatorial library) to study protease preferences with the fluorophore Asp-7-amino-4-methyl-coumarin (AMC) was developed[43]. The fluorophore 7-amino-4-carbamoyl-methylcoumarin (ACC) which was applied in the same library, improved the method for protease substrate specificity investigation[44]. Fluorescent probes are designed based on the substrate of the protease of interest and carry a fluorophore. So after enzymatic conversion and excitation in the lower UV/VIS range, the emission spectrum with its maximum shifted to higher UV/VIS wavelength is measured.
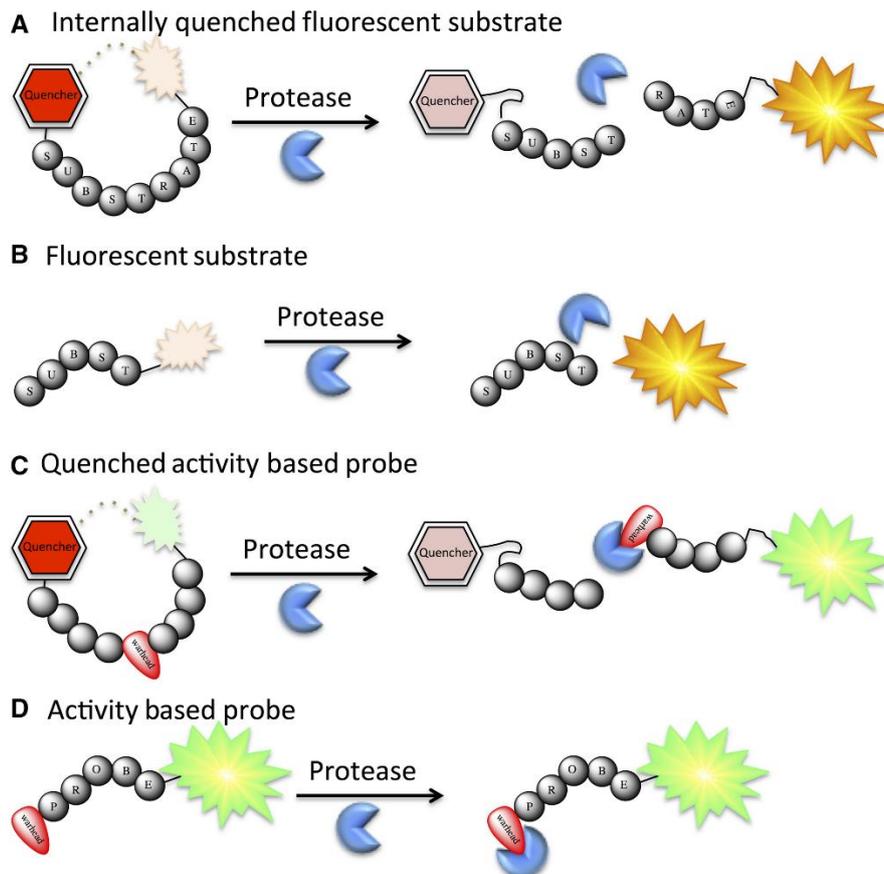


**Figure 1: Probe designs to monitor protease activity A** Initially quenched fluorophore is released after cleavage and emits photons **B** Fluorophore substrate emits photons when released **C** Quenched activity-based probe emits fluorescence after cleavage of the substrate **D** Activity-based probe tagged with a fluorophore attached to the target active centre of the enzyme. The figure is used with permission of John Wiley and Sons from Kasperkiewicz *et al.*[45] (License Number 4502511000947).

Figure 1 shows different designs of fluorescent substrates that emit characteristic photons after un-quenching or activation by proteases. Activity-based protein profiling (ABPP) was developed to target proteins in their native form and thus target the functional state of the enzyme[46,47]. Active enzymes can be distinguished from their inactive zymogen or inhibited form with that mechanism[48]. ABPP probes modify the enzyme by forming specific covalent bonds with the catalytic residue.

However, the reporter lacks in specificity, cell permeability, and rapid diffusion. The main drawback is the autofluorescence of the cellular environment. To produce higher signal-to-noise ratios, protease-responsive near infrared (NIR) probes have been developed. Substrate-enzyme specificity allows some targeted analysis of the protease, but also requires detailed knowledge for the appropriate probe design. Challenges like high chemical and photo-stability, non-toxicity, biocompatibility, and biodegradability impede the probe design and need to be overcome. Although these probes are used *in vitro* and *in vivo*, direct visualization and investigation of protease activity in tissue sections remain underexplored[49]. Only Withana *et al.* topically applied fluorescence-quenched activity-based probes to fresh-frozen tissue sections which enabled visualization of protease activity at cellular resolution[50].

## 1.3 Mass Spectrometry

About 100 years ago mass spectrometry (MS) began with J.J. Thomson and his discovery of the electron in 1897[51]. An early stage mass spectrometer, called parabola spectrograph, was build and refined in 1919 into the first mass spectrometer by Francis W. Aston[52]. A. J. Dempster was the one who developed the first electron impact source to enable analysis of elements and small molecules. With the development of Fourier transform ion cyclotron resonance[53](FT-ICR), magnetic sector double-focusing[54], time-of-flight (TOF)[55,56], and quadrupole[57] mass analysers the detectable mass range and resolution improved. To allow analysis of large and small-biomolecules the development of softer ionisation techniques like electrospray ionisation (ESI)[58] and matrix-assisted laser desorption/ionisation (MALDI)[59] was required. With less energy intake in the ion source fragmentation is reduced and the stability of the ionised molecules is improved.

In mass spectrometry chemical species (being elements or molecules) are ionised in the **ion source**, separated by their mass-to-charge ratio (*m/z*) in the **mass analyser**, and recorded in a **detector system** according to their relative abundance. The

developed systems are as different as chemical species can be. For biomolecules, soft ionization techniques and mass analyser with a high mass range are required to cover the biological diversity (i.e. lipids, peptides and proteins ranging up to several 100kDa). That is why MALDI and TOF-MS or FT-ICR-MS are often combined in order to analyse complex biological matrices.

### 1.3.1 The principle of MALDI mass spectrometry

MALDI MS requires the application of a matrix solution onto the sample or the matrix solution is mixed with a sample solution. During evaporation of the matrix solvent, the sample's analytes co-crystallise with the matrix forming a layer of analyte-matrix-crystals. Which molecules co-crystallise is dependent on their physicochemical properties and the properties of the used matrix. Some matrices prioritise smaller, other larger molecules[60]. The formation of crystal size is different for different matrices. The ions required for the separation in the mass analyser are generated by radiation with a pulsed focused laser beam (commonly neodymium-doped yttrium aluminium garnet (Nd:YAG) laser with a wavelength of 355 nm).

### 1.3.2 MALDI MS Imaging

In 1997 Caprioli *et al.* introduced MALDI MS as a method for mass spectrometry imaging (MSI) in order to combine classical tissue proteomics and histology[61]. It can help in therapeutic management and could confirm a diagnosis. In addition, MSI as a tool to discover new biomarkers can give semi-quantitative mapping information and can be used to evaluate tissue heterogeneity and complexity, where classical molecular pathological methods fail. For clinical research pathology tissues are the manifestation of many diseases, and morphological or molecular features are of great importance. The understanding of the molecular basis of diseases in particular, leads to insights into their mechanism and changes in tissue morphology[62]. Mass spectrometry combines the advantages of high sensitivity, molecular specificity, and detection of several classes of molecules (proteins, peptides, lipids, drugs and metabolites), thus providing unique insight into biological systems. As MALDI is a soft ionization technique, the analysis of a wide range of molecules is possible (100 Da – 30 kDa). In addition, MALDI predominantly produces singly charged molecules which makes interpretation of complex mixtures easier. The use of laser ionization allows the analysis of specific histologically relevant tissue regions and can be analysed in a pixel-to-pixel distance of 100 µm down to subcellular range[63].

To generate a MALDI MS image the matrix is applied onto the tissue in a homogeneous layer. Laser radiation is performed in a raster over the whole tissue, and mass spectra are generated for each x-y-position (Figure 5). As the laser permeates only the crystal layer on the tissue, the integrity of the tissue is preserved and histological staining after MALDI MS measurement is possible.
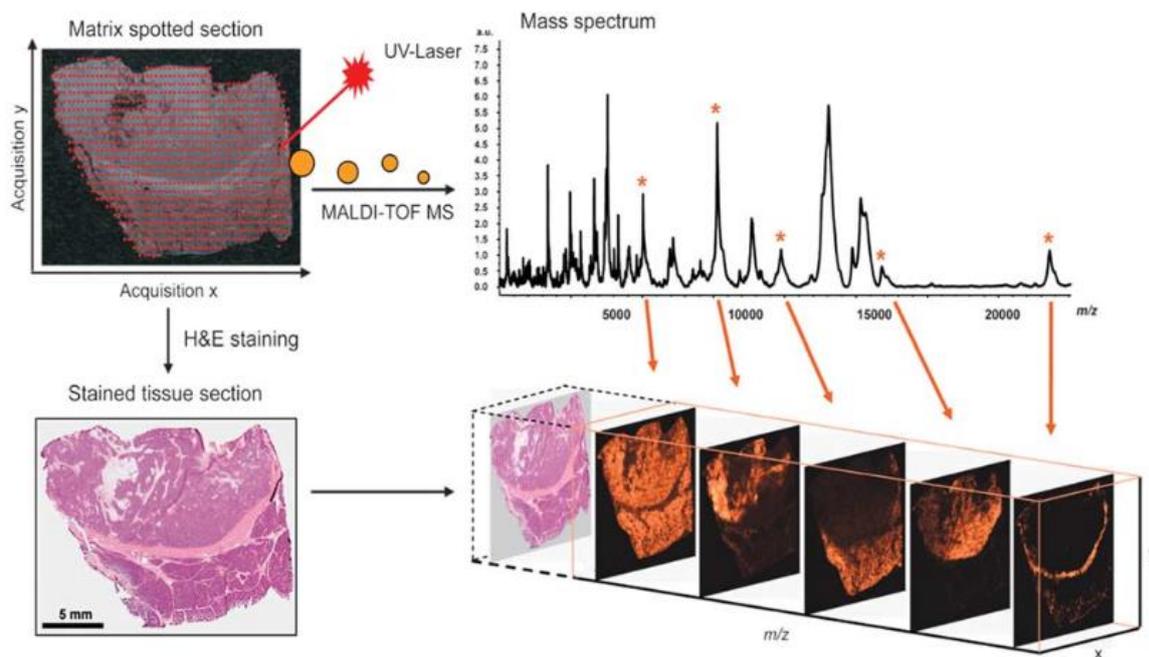


**Figure 2: Principle of MALDI mass spectrometry imaging** A clinically relevant tissue section is coated with a MALDI matrix. The solvent of the matrix extracts molecules from the tissue which then co-crystallize with the matrix molecules. In a raster process, the tissue is measured so, that at each position a laser shoots and ionizes the co-crystallized molecules, which are analysed in a time-of-flight (TOF) mass spectrometer. This results in mass spectra at each position of the measurement raster. The underlying tissue stays unaffected from the laser shots and can be histologically stained for histology-directed mass spectra. The figure is used with permission of Springer Nature from Aichler and Walch[64] (License Number 4498730581944).

### 1.3.3  The current method for tissue preservation

MSI is typically performed on fresh-frozen tissue[65], which is very rarely used as tissue preservation in a standardized manner for routine pathology. In contrast, formalin fixation and paraffin embedding (FFPE) preserves the morphology and cellular details and has thus become the standard preservation procedure[66]. The formaldehyde induces molecular changes in the form of cross-links between proteins, or between proteins and nucleic acids, with hydroxymethylene bridges. The coordinated bonds are responsible for the masking of epitopes and retaining the secondary structure of proteins. This process takes between 24 and 48 hours (until completeness[66]) and is not equalised for different hospitals, thus resulting into many observed variants in

immunohistochemistry (IHC) stainings[67]. After fixation in 10% neutral buffered formalin, the tissue is dehydrated in a series of grading alcohol concentration and then cleared in xylene. Finally, the tissue is embedded in paraffin.

Storing the FFPE tissue blocks at RT saves maintenance, space and labour costs that are required for frozen tissue storage. Clinical pathology departments routinely store large numbers of FFPE blocks, which are an extensive repository of tissue material[68]. With antigen retrieval methods IHC on FFPE samples was facilitated[69]. Further, antigen retrieval was used to extract DNA; RNA and proteins from FFPE tissue[70]. With improved deparaffinization and antigen retrieval methods, FFPE tissue allowed proteomic experiments in mass spectrometry[71,72]. In the top-down proteomics approach the purified protein is analysed in its intact form using tandem mass spectrometry (MS/MS)[73]. Here no enzymatic digestion is required, as the intact protein is trapped in an Ion Trap, FT-ICR or Orbitrap mass analyser and is further fragmented by e.g. electron-capture dissociation (ECD). 100% sequence coverage and full characterisation of proteoform can theoretically be achieved with that method. The proteoform is defined by the molecular form of the protein resulting from genetic variation, alternative splicing, and post-translational modifications. Further top-down methods lack dynamic ranges as abundant species are dominantly fragmented. Thus complex mixtures were more often analysed by shotgun or bottom-up proteomic experiments[74]. In bottom-up approaches the protein mixture is purified using gel electrophoreses. Then it is enzymatically digested and the resulting peptides are analysed by MS and MS/MS[75]. Few top-down studies using MALDI MSI had been performed but were limited to proteins <9kDa[76,77]. When the whole tissue slice is used for digestion (reflecting a bottom-up approach), the whole tissue proteome is theoretically accessible. Maier *et al.* showed that with MALDI MSI only a subset of proteins, compared to classical proteomics, is incorporated in the matrix crystals and can thus by identified[78]. Nevertheless, on-tissue digestion combined with MSI revealed the localization of proteolytic peptides and enables identification in MS/MS[79].

### 1.3.4 On-tissue digestion for MALDI MSI

In the last decade several researchers used on-tissue digestion for distribution analysis of proteolytic peptides. The preparative workflow is complex and requires multiple steps starting from dewaxing, heat-induced antigen retrieval, tissue digestion to MALDI

matrix embedding and MALDI MSI data acquisition (Figure 6). Additionally the published methods vary in analysed tissue specimen and used preservation technique.

Fresh-frozen tissue requires washing steps (in graded ethanol) to reduce lipids and salts which interfere with the enzymatic digestion[80]. The removal of paraffin and antigen retrieval is necessary for FFPE tissue. Those washing steps differ in the application of the solvent (pipetting or beaker), the solvent itself (buffers), duration (several minutes) and temperature. It had recently been investigated that the thickness of the FFPE slice also had an influence the result[81]. The enzyme and the enzyme application system allows the location of peptides after MALDI MSI. Exemplarily, Table 2 lists several publications with the used enzyme application systems, tissue specimen and preservation technique. The list does not cover all published methods, but emphasizes the diversity: The here listed methods use six different enzyme application systems ranging from microspotting to spray devices, with different application settings. On-tissue digestion has been performed on three preservation techniques: fresh-frozen (FF), FFPE and FFPE tissue microarrays (TMA). Tissue microarrays are paraffin blocks, where several hundred tissue cores (about 0.6 mm) are sorted in an array pattern[82].

**Table 2: Diversity of published instrumentation and material used for on-tissue digestion**

| FIRST AUTHOR | YEAR | TISSUE SPECIMEN | PRESERVATION TECHNIQUE | ENZYME APPLICATION DEVICES |
|---|---|---|---|---|
| GROSECLOSE et al.[83] | 2007 | brain and pituitary gland from rat | FF | microspotting chemical inkjet printer (chip-1000, Shimadzu biotech) |
| STAUBER et al.[84] | 2008 | rat brain slices | FFPE | microspotting chemical inkjet printer (chip-1000, Shimadzu biotech) |
| RONCI et al.[85] | 2008 | tissue surrogate, human breast cancer | FFPE | apply and drain solution |
| GROSECLOSE et al.[86] | 2008 | adenocarcinoma and squamous cell carcinoma | FFPE (TMA) | microspotting, portrait 630 |
| GRAVIUS et al.[87] | 2008 | human periprosthetic tissue | FFPE | spraying device ImagePrep (Bruker Daltonics) |
| STAUBER et al.[88] | 2010 | rat brain slices | FF & FFPE | microspotting chemical inkjet printer (chip-1000, Shimadzu biotech) |
| GUSTAFSSON et al.[89] | 2010 | human ovarian cancer | FFPE | microspotting chemical inkjet printer (chip-1000, Shimadzu biotech) |
| CASADONTE AND CAPRIOLI[90] | 2011 | biopsies | FFPE (TMA) | microspotting (portrait 630) |
| ENTHALER et al.[91] | 2012 | human skin from back and abdomen | FF | spraying device ImagePrep (Bruker Daltonics) |
| POWERS et al.[92] | 2014 | human tissues, mouse kidney, liver cancer, prostate tumour | FFPE (TMA) | spraying device ImagePrep (Bruker Daltonics) |
| DE SIO et al.[93] | 2014 | human brain, kidney, thyroid, small bowel | FFPE | spraying device ImagePrep (Bruker Daltonics) |
| CASADONTE et al.[94] | 2015 | renal biopsies | FFPE | spraying device ImagePrep (Bruker Daltonics) |
| HEIJS et al.[95] | 2015 | mouse brain | FF | spraying device SunCollect (SunChrom) |
| DIEHL et al.[96] | 2015 | rat brain slices | FF & FFPE | spraying device ImagePrep (Bruker Daltonics) |
| HOLST et al.[97] | 2016 | leiomyosarcoma, colorectal carcinoma | FFPE | spraying device SunCollect (SunChrom) |
| OETJEN et al.[98] | 2016 | rat brain | FFPE | spraying device ImagePrep (Bruker Daltonics) |
| MASCINI et al.[99] | 2018 | oral squamous cell carcinoma, oropharyngeal squamous cell carcinoma | FFPE (TMA) | spraying device SunCollect (SunChrom) |
| ANGEL et al.[100] | 2018 | liver with hepatocellular carcinoma, colorectal cancer, aortic valve tissue, porcine heart | FFPE | spraying device TM-sprayer (HTX Technologies) |

(FF = fresh-frozen; FFPE = formalin-fixed paraffin-embedded)

After digestion the choice of MALDI matrix influences the visualized peptides by the sample type or the molecular weight of the co-crystallizing molecules. The matrix application system also affects the resolution of the image. Large matrix droplets can lead to diffusion of analytes and thus limit lateral resolution. Furthermore, the size of the matrix crystal (and so resolution) is influenced by the application system, solvent, additives (salts), and temperature. The matrix droplets are ideally big enough to ensure efficient analyte extraction from the tissue and small enough to reach a high spatial resolution.

**Resolving power R** is defined as $m/\Delta m$ where $m$ is the mass and $\Delta m$ the peak width, precisely the full width at half maximum (FWHM). It is an instrument property that describes the ability of the MS to distinguish two adjacent ions. High resolution mass spectrometers like FT-ICR MS can yield resolving powers of 1,000,000. The **mass accuracy** (or mass measurement error) can be calculated by $\Delta m_i = (m_i - m_a)$ in Da or $\frac{(m_i - m_a)}{m_a} x\, 10^6$ in ppm (parts per million), where $m_i$ is the mass of the individual measurement and $m_a$ is the accurate mass[101]. In the case of MALDI-TOF MSI, the resolving power is 15,000 and mass accuracies of 0.1-0.01 Da are achieved[102]. FT-ICR instruments give better mass resolution and accuracy, at the expense of (much longer) measuring time. According to the law of error propagation errors in such a multi-step workflow multiply. The FFPE tissue preparation for MALDI MSI is therefore prone to high variability and requires an even more standardized protocol. For MALDI MS target measurements (in contrast to MALDI MSI experiments) reproducibility has already been a matter of interest. O'Rourke *et al.* stated that high throughput sample analysis with MALDI MS require robust and reproducible protocols[103]. This could be achieved by using nitrocellulose as it improves signal-to-noise, spot homogeneity, and reproducibility[104,105].

In a clinical context it has been suggested that on-tissue digestion of FFPE tissue can classify human pancreatic cancer[106], prostate tumours[107] and lymph node metastasis[99]. In another scenario the method is capable of successfully diagnosing amyloidosis, a disease with abnormal and accumulating protein folding resulting in harmful fibrils in tissue[94]. On-tissue digestion is also able to discover biomarkers by using hospital biopsy libraries as shown exemplarily for Parkinson disease[84].

### 1.3.5 Data processing and statistical analysis in MALDI MSI

For accurate and reliable results standardised data processing and interpretation is also necessary. The acquired spectra require preprocessing like baseline correction, noise removal, realignment and peak picking. Normalisation strategies are required to allow the comparison of different samples. Commercial software packages cover some of those steps and help investigate the distribution of specific ions of interest. As MSI produces very large datasets (several GB per tissue slice[108,109]), these software packages typically lack the ability of comparing several measurements in a multivariate statistical manner. In addition large datasets require long processing times. SCiLS Lab (SCiLS GmbH, Bremen) makes it possible to combine different measurements and perform basic statistics on them[96,100], but it is restricted to the predefined tools. Open source mathematics packages (e.g. R, R Studio) provide statistical tools, which can be applied to MSI datasets by trained statisticians.

In MALDI MSI the method development and validation has so far been rarely investigated. Diehl. *et al.* worked on the optimal preparation protocol for on-tissue digestion comparing different enzymes (Trypsin and LysC-Mix), digestion time and temperature, and MALDI matrices (DHB and HCCA)[96]. Using Principal Component Analysis (PCA) for mean and pixel-wise analysis they offered a recommendation of a standard operating protocol for FF and FFPE material. PCA is used to reduce the overall dimensionality of multidimensional data while the data variance is retained. Heijs *et al.* investigated the optimal digestion time (1.5h, 3h or 18h) by counting the picked peaks[95]. Later Oetjen *et al.* used fractional factorial design to find the optimal protocol for on-tissue digestion and proposed specific conditions regarding enzyme, incubation time and buffer system[98].

# 2  AIMS

**Part (I)** The current bioimaging methods for measuring active proteases focus on specifically designed tracer substrates that allow photometric monitoring of the activity of the targeted protease. Although these tracers can be used *in vivo* and *in vitro*, the synthesis of tracers that combine biocompatibility, specificity and photometric label is challenging. Mass spectrometry can be used label-free, as the measured *m/z* ratio is a physicochemical property of each molecule. MALDI MSI is an evolving technique combining the advantages of mass spectrometry and spatial resolution. It has already been shown that biomolecules like proteins, peptides, lipids, carbohydrates or glycans are detectable. So far it has not been explored whether MALDI MSI can be used for measuring protease activity in frozen tissue slices. Therefore part I of the present study had the following aims:

(1) To develop a method using MALDI MSI for monitoring tissue protease activity exemplarily on different porcine tissues.

(2) To validate the developed method by time- and concentration-dependency as well as by the production of specific degradation products. Further, to use a gastric tumour mouse model and evaluate differences in protease activity on tumorous tissue as compared to non-tumourous tissue.

(3) To demonstrate the transferability of the developed MALDI MSI method to relevant clinical samples by analysing the proteolytic activity of human tissue biopsies of gastroscopy.

**Part (II)** Methods that should be applied in clinical routine require a high degree of standardisation, in particular, if a workflow requires multiple steps. On-slide digestion of FFPE tissue for MALDI MSI is such a multi-step workflow that consists of dewaxing, antigen retrieval, digestion and imaging. Several protocols have been published, but little is known about suitable statistical scores for method comparison and standardisation. That is why the aims in part II of this study are the following:

(4) To develop scores suitable for standardisation (unbiased, low computational effort) of on-tissue digestion workflow for MALDI MSI by the use of clinical material processed with already published methods.

(5) To detect the best on-tissue digestion method for FFPE tissue and MALDI MSI in terms of repeatability and homogeneity of the application system.

## 3 MATERIALS AND METHODS

### 3.1 Materials

**Reagents**

| NAME | CATALOGUE NB. | COMPANY | LOCATION |
|---|---|---|---|
| 2,5 Dihydroxybenzoic Acid *(for endogenous digest experiments)* | A11459 | Alfa Aesar | Karlsruhe, GER |
| 2,5 Dihydroxybenzoic Acid *(for FFPE tissue digest)* | 8201346 | Bruker Daltonics | Bremen, GER |
| Acetone | 20067.320 | VWR | Darmstadt, GER |
| Acetonitrile *(for MALDI MS analysis)* | 83640.320 | VWR | Fontenay-sous-Bains, FRA |
| Ammonium bicarbonate | FL40867 | Fluka Analytical | Munich, GER |
| Ammonium formate | 84884.180E | VWR | Fontenay-sous-Bains, FRA |
| Bovine serum albumin | A2153 | Sigma Aldrich | Steinberg, GER |
| Bradford Reagent | B6916 | Sigma Aldrich | Steinberg, GER |
| Carboxymethyl Cellulose | 6190.1 | Carl Roth | Karlsruhe, GER |
| Casein (from bovine milk) | C7078 | Sigma Aldrich | Steinberg, GER |
| Citric acid monohydrate | 211018.1214 | AppliChem | Darmstadt, GER |
| Cytochrome C (equine heart) | C2506 | Sigma Aldrich | Steinberg, GER |

| | | | |
|---|---|---|---|
| Eosin G solution 0.5% | X883.1 | Carl Roth | Karlsruhe, GER |
| Ethanol absolute | 20821.330 | VWR | Fontenay-sous-Bains, FRA |
| Folin & Ciocalteau's phenol reagent | F9252 | Sigma Aldrich | Steinberg, GER |
| Formic acid | 069141 | Biosolve Chemicals | Dieuze, FRA |
| Hydrochloride acid | 9277.2 | Carl Roth | Karlsruhe, GER |
| L-tyrosine | T3754 | Carl Roth | Karlsruhe, GER |
| Magnesium sulfate | 0682.1 | Carl Roth | Karlsruhe, GER |
| Mayer's Hematoxylin | MHS16 | Sigma Aldrich | Steinberg, GER |
| Methanol | 8201346 | VWR | Fontenay-sous-Bains, FRA |
| Myoglobin (from equine skeletal muscle) | M0630 | Sigma Aldrich | Steinberg, GER |
| Pancreatin (from porcine pancreas) | P1625 | Sigma Aldrich | Steinberg, GER |
| Phosphate buffered saline | L0615 | biowest | Darmstadt, GER |
| Potassium hydrogenphosphate | 105104 | Merck | Darmstadt, GER |
| Protease Inhibitor Mix | P2714 | Sigma Aldrich | Steinberg, GER |
| RapiGest SF Surfactant 3-[(2-methyl-2-undecyl-1,3-dioxolan-4-yl)methoxy]-1-propansulfonat | 186001861 | Waters | Milford, USA |

| | | | |
|---|---|---|---|
| Rhodamine B | R6626 | Sigma Aldrich | Steinberg, GER |
| rLys-C (from E.coli) | V1671 | Promega | Madison, WI, USA |
| rLys-C-Trypsin-Mix | V5071 | Promega | Madison, WI, USA |
| Sodium bicarbonate | 8551.1 | Carl Roth | Karlsruhe, GER |
| Sodium carbonate | S2127 | Merck | Darmstadt, GER |
| Sodium dodecylsulfate | A0676 | AppliChem | Darmstadt, GER |
| Substance P acetate salt | 4010600 | BACHEM | Bubendorf, CHE |
| T-PER™ Tissue Protein Extraction Reagent | 78510 | Thermo Fisher Scientific | Rockford, USA |
| Trichloroacetic acid | T0699 | Sigma Aldrich | Steinberg, GER |
| Trifluoroacetic Acid | 8082600025 | Merck | Darmstadt, GER |
| TRIS buffer | A2264 | AppliChem | Darmstadt, GER |
| Tris(2-carboxyethyl)phosphine | 646547 | Sigma Aldrich | Steinberg, GER |
| Triton-X-100 | 108643 | Merck | Darmstadt, GER |
| Trypsin gold, mass spectrometry grade | V5280 | Promega | Madison, WI, USA |
| Xylene | 28973.328 | VWR | Fontenay-sous-Bains, FRA |
| α-cyano-4-hydroxycinnamic acid | 8201344 | Bruker Daltonics | Bremen, GER |

**<u>Equipment</u>**

| NAME | COMPANY | LOCATION |
|---|---|---|
| Aperio CS2 | Leica Biosystems | Nußloch, GER |
| Cryostat Leica CM 1950 | Leica Biosystems | Nussloch, GER |
| Decloaking Chamber | BioCare Medical | Concord CA,USA |
| Electro Multiscan Spectrum | Thermo Fisher Scientific | Rockford, USA |
| ImagePrep | Bruker Daltonics | Bremen, GER |
| Matrix application device Sun Collect with Dispenser Pump *(for MALDI matrix)* | SunChrom | Friedrichsdorf, GER |
| Matrix application device Sun Collect with Syringe Pump *(for enzymes and substrates)* | SunChrom | Friedrichsdorf, GER |
| RapiFlex MALDI TOF/TOF MS | Bruker Daltonics | Bremen, GER |
| solariX MALDI-FT-ICR MS | Bruker Daltonics | Bremen, GER |
| SunDigest device | SunChrom | Friedrichsdorf, GER |
| Ultraflex MALDI-TOF/TOF MS | Bruker Daltonics | Bremen, GER |

## Consumables

| NAME | COMPANY | LOCATION |
|---|---|---|
| MALDI ITO glass slides | Bruker Daltonics | Bremen, GER |
| Peptide calibration standard II | Bruker Daltonics | Bremen, GER |
| Protein calibration standard I | Bruker Daltonics | Bremen, GER |
| Starfrost adhesive slides | R. Langenbrinck | Emmendingen, GER |
| Water sensitive paper | Syngenta | Basel, CHE |

## Software

| NAME | COMPANY | LOCATION |
|---|---|---|
| BioTools | Bruker Daltonics | Bremen, GER |
| Excel | Microsoft | Redmond, USA |
| flexControl | Bruker Daltonics | Bremen, GER |
| flexImaging 4.1 | Bruker Daltonics | Bremen, GER |
| GraphPad Prism | GraphPad Software | La Jolla, USA |
| Image J | ImageJ (Wayne Rasband) | Maryland, USA |
| MATLAB R2017a | The Mathworks | Natick, USA |
| mMass - Open Source Mass Spectrometry Tool | By Martin Strohalm | |
| R (V 3.2.3.) | R Foundation of Statistical Computing | Vienna, AUT |
| Scils | SCiLS GmbH | Bremen, GER |
| Tableau | Tableau Software Inc. | Seattle, USA |

## 3.2 Tissue samples and ethics approval

**Porcine tissue**

Porcine tissue was collected from the local slaughterhouse, prepared in tissue blocks of 2 x 2 cm and immediately frozen to -80 °C.

**TCEA mouse model**

Transgenic CEA424-SV40 Tag C57BL/6 J mice developing spontaneous gastric carcinoma[110] were grown in our collaborating group of Dr. Elke Burgermeister (Prof. Dr. Matthias Ebert, Department of Medicine II, Medical Faculty Mannheim, Heidelberg University). Stomachs from TCEA-Tag positive mice and WT mice were collected and immediately frozen to -80 °C. All experiments have been ethically approved of Heidelberg University and government authorities (Az I-17/07).

**Human gastric biopsies**

Needle biopsies were taken from two patients undergoing gastroscopy (provided by Dr. Tobias Gropp (Department of Medicine II, Medical Faculty Mannheim, Heidelberg University) and immediately frozen to -80 °C. Studies were conducted in agreement with ethical guidelines by the Medical Ethics Committee II of the Medical Faculty Mannheim, Heidelberg (2014-633N-MA).

**Human FFPE tissue specimen**

Human liver and gastrointestinal-stromal tumour (GIST) tissue were preserved using standard fixation procedure of 10 % neutral buffered formalin for 24±4 h at RT followed by paraffin embedding (approval by the Medical Ethics Committee II of the Medical Faculty Mannheim, Heidelberg University #2015-868R-MA). Based on H&E stained consecutive tissue slices an expert pathologist (Prof. Dr. Alexander Marx, Director of the Institute of Pathology, University Medical Centre Mannheim, Heidelberg University ) has judged the tissue to be >98 % homogeneous (Figure 3).
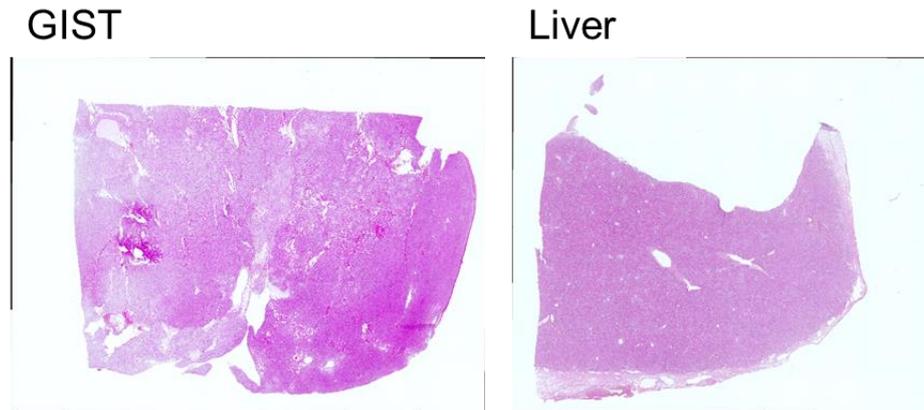
**Figure 3: H&E assessment of tissue homogeneity of FFPE preserved tissue** H&E staining of the two tissue samples GIST (left) and liver (right) was judged 98 % homogeneous by the expert pathologist Prof Dr Alexander Marx (Director of Institute of Pathology, University Medical Centre Mannheim).

## 3.3  Sample Preparation Methods

### 3.3.1  Preparation of tissue for monitoring endogenous protease activity

**Scores for evaluating spray quality**

To assess the spray quality substance P (20 pmol/µL in $H_2O$, 3 x 15 µL/min, Speed in X= Low 4, Speed in Y= Medium 1) was sprayed on Water Sensitive Paper WSP (Syngenta) in two different spray heights: Z-Position = 45.3 mm or 25.5 mm. The sprayed paper was scanned using Aperio CS2 (Leica Biosystems). The image was converted into grey scale 32-bit using the software ImageJ[111] (ImageJ) for quantitative analysis. Three equally sized and randomly chosen squares were analyzed for their mean grey scale value and the standard deviation in the squares. Values of three technical replicates were averaged.

For further investigation, the spray conditions porcine tissue was cut into 10 µm sections and melted on ITO-glass slides. On each tissue 3 x 1µL Rhodamine B (1 µg/ml in $H_2O$) were pipetted and dried under vacuum for 5 min. The slides were sprayed with substance P using the same two different spraying conditions. Rhodamine B spots were visually compared before and after spraying.

**H&E staining**

Sequential sections of frozen porcine tissue were sliced in 2 µm sections and melted on Starfrost adhesive glass slides (R. Langenbrinck). Nuclei were stained in Mayer's hematoxylin solution for 2 min. To remove the residual dye, slides were washed in tap water (3 min) and then dipped in distilled water. Staining is enhanced with a bath in

0.3 % acidic alcohol (0.3 % HCl in 70 % ethanol) for 30 sec, rinsed in distilled water and bathed in blueing solution (2 g/L sodium bicarbonate, 20 g/L magnesium sulfate in $H_2O$) for 2 min. Eosinophilic structures were stained in eosin solution 0.5 % (5 min) and washed in distilled water (1 min). Dehydration was performed in increasing ethanol-series (80 %, 96 %, 100 %) for 2 min each. After air-drying the slides, tissue was covered with Eukitt mounting medium and dried overnight (ON) before scanning. As TCEA mouse stomachs were H&E-stained after MALDI MSI (tissue remains intact, as laser shots only in matrix[112]), additional washing steps were required to remove the MALDI matrix. These steps comprise 50 %, 70 % and two times 100 % methanol baths (3 min each). Afterwards the tissue was washed in 100 % acetone (5 min) and rehydrated firstly in tap water and secondly in distilled water for 5 min each.

**Evaluation of endogenous protease activity on porcine tissue**

Porcine tissue blocks were sliced in 10 µm slices using cryostat CM 1950 (Leica Biosystems) with chamber- and head-temperature of -17 °C. Tissue slices were thaw-mounted on conductive ITO-slides. One slice of all the tissues was directly covered with MALDI matrix to assess the specificity of the methods. Further slides were desiccated for 5 min at RT and further dried in vacuum at 4°C for 15 min. To monitor the proteolytic activity a "digest" and a "no-digest" slide was prepared with sequential tissue sections (Figure 4).

To evaluate the incubation-time-dependency of proteolytic activity with and without inhibitor, four spots of 1 µL protease inhibitor mix 1x (PIM) were pipetted on the tissue slices. Further, 1 µL solvent of the PIM, namely $H_2O$ was pipetted on each tissue to assess solvent-related changes. The PIM is a mixture of protease inhibitors purchased by Sigma-Aldrich (), consisting of inhibitors listed in Table 3.

To evaluate inhibitor-concentration-dependency dilution series of the PIM were pipetted on the porcine tissue (1 µL of 0x, 0.1x, 0.5x, 0.5x, 1x, 2.5x and 10x PIM) at randomly chosen positions (N=2). Slides were kept on ice during the preparation procedure.
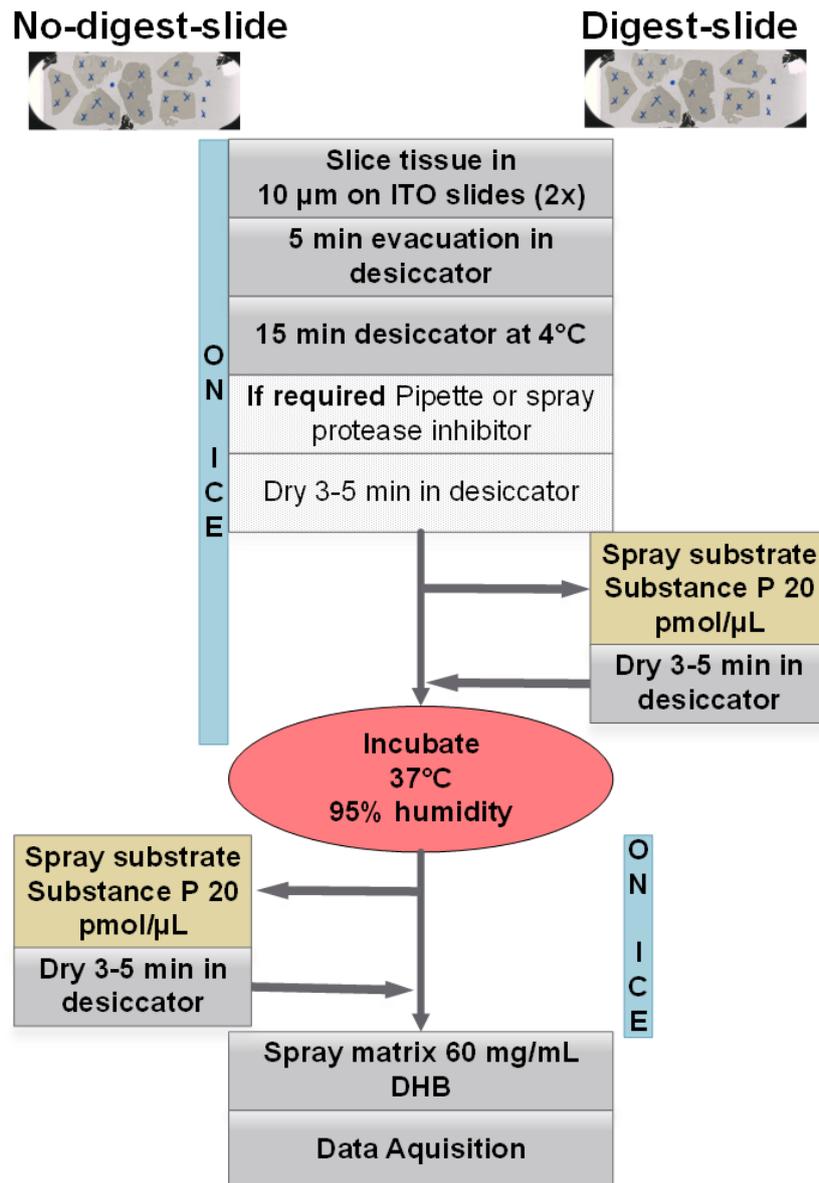
**Figure 4: Workflow of tissue preparation for monitoring proteolytic activity using substance P as a substrate**, One "digest" slide and one "no-digest" slide was prepared to bypass the variability of data introduced by measurements on different days and instrument conditions. For porcine experiments protease inhibitor-mix was pipetted onto the tissue to assess incubation-time-dependency and inhibitor-concentration-dependency. Substance P was sprayed onto the "digest" slide before and on the "no digest" slide after incubation at 37 °C and 95% humidity. During sample preparation the slides were kept on ice to prevent uncontrolled digestion.

**Table 3: Composition of protease inhibitor mix (PIM) in working solution concentration of 1x**

| Inhibitor | Final working concentration | Target proteases |
|---|---|---|
| *AEBSF* | 2 mM | Serine proteases |
| *Aprotinin* | 0.3 µM | Serine proteases |
| *Bestatine hydrochloride* | 116 µM | Aminopeptidases |
| *E-64* | 14 µM | Cysteine proteases |
| *EDTA* | 1 mM | Metalloproteases |
| *Leupeptin* | 1 µM | Serine- and cysteine proteases |

(AEBSF = 4-(2-aminoethyl)benzenesulfonyl fluoride hydrochloride; EDTA = ethylenediaminetetraacetic acid)

After drying the tissue under vacuum for 3-5 min, the digest slides were sprayed with tracer substrate substance P (20 pmol/µL in $H_2O$) with the following spray conditions: 3 x 15 µL/min, Y-distance 25.5 mm, Speed in X= Low 4, Speed in Y= Medium 1, on cool pad. This resulted in a final amount of 3.5 pmol/mm$^2$ substance P. After drying the slide briefly under vacuum, incubation was performed with both slides ("digest" and "no-digest"-slide) in different periods of time (15 min, 30 min, 45 min, 60 min, 120 min and 360 min) to assess time-dependent proteolytic activity. The incubation was one time performed in a standard cell culture oven at 37 °C and a second time in SunDigest incubation chamber (SunChrom) on a controlled condition of 37 °C and 95% humidity[c]. One incubation-time-dependency dataset consists of 60 single tissue datasets: 5 time-points x 6 organs x 2 conditions - digest and no-digest.

For the inhibitor-concentration-dependency and single-inhibitor experiment tissue was incubated for 60 min in the SunDigest incubation chamber at 37 °C and 95% humidity. Two full technical replicates were performed.

### 3.3.2  Adaptation of a tissue protease activity assay (TPAA)

**Optimisation of the extraction process**

The commercially available Tissue Protein Extraction Reagent T-PER (Thermo Fisher Scientific) is described to extract total protein amount under a mild condition in their active form. Conserved functionality is essential for a protease activity assay. A blank

---

[c] Experiments in SunDigest incubation chamber had been performed by Kevin Reinle in the context of his masterthesis: *Visualising endogeneous protease activity by MALDI Mass Spectrometry Imaging*, 2017

dilution series of T-PER were performed to evaluate the influencing absorption. Further, extraction of 500 mg/mL porcine spleen was performed with T-PER and extraction buffer (PBS / 1% (w/v) Triton-X-100 / 0.05% (w/v) SDS) at pH 7.5 and pH 3.2.

**Protease activity of porcine tissue**

Frozen porcine tissues were cut into 30 µm slices. Six slices were collected for one extraction. Extraction was performed in 500 mg/mL wet tissue. Samples underwent five cycles of sonication (5 min) and cooling on ice (2 min). The mixture was centrifuged (5 min, 10,000 x g), the supernatant was collected and placed on ice. Protein quantification was done by Bradford assay: Tissue extract was diluted 1:100 in $H_2O$. In a 96-well plate, 200 µL Bradford-reagent (1x) was mixed with 5 µL samples or calibration solution (500, 200, 100, 50, 0 µg/mL BSA in $H_2O$) and incubated for 25 min at RT in the dark. Absorption was measured at 595 nm.

Based on Cupp-Enyards protease activity assay for pure protein solution the tissue was tested for its proteolytic activity[113]. 500 µL casein (0.65% (w/v) in 50 mM $K_2HPO_4$) was placed at 37 °C (5 min). Then 100 µL protein extract was added and incubated for 10 min at 37 °C. The reaction was stopped by adding 500 µL 110 mM TCA and additional incubation for 30 min at 37 °C was performed. Protein precipitate was separated by centrifugation for 5 min at 10.000xg. Finally, 500 µL of 500 mM sodium carbonate and 100 µL Folin & Ciocalteau's phenol reagent was added to the supernatant and incubated at 37 °C for 30 min. Native pancreatin solution (1 mg/mL in $H_2O$), which is a protease extract from porcine pancreas (Sigma Aldrich), was used as positive control. Heat-denatured pancreatin solution (20 min, 95°C) was used as negative control. L-tyrosine dilution series (0.0055, 0.011, 0.022, 0.044, 0.055, 0.077 and 0.11 µmol) were prepared in tissue extraction buffer, which also serves for blank measurements. Absorbance was measured in 96-well plates at 660 nm and the activity calculation was performed by the following equation (1). Values were further multiplied by the quantified protein amount (mg/mL) to gain activity in U/mg.

$$Activity \left[\frac{unit}{mL}\right] = \frac{released\ tyrosine[\text{µmol}]\ x\ assay\ volume[mL]}{enzyme\ volume\ [mL]\ x\ incubation\ time\ [min]\ x\ measurement\ volume\ [mL]} \tag{1}$$

### 3.3.3 Monitoring protease activity in a gastric tumour mouse model and human biopsy

TCEA positive, wild-type mouse stomachs and human biopsies (normal gastric tissue and adenoma) were sliced in 10 µm tissue slices and melted on conductive ITO glass slides. ITO-slices with tissue were kept at RT for different time periods. To assess proteolytic activity each tissue was prepared two times, where one is used "without inhibitor (-)" and the other "with inhibitor (+)". Tissues were evacuated at RT for 5 min and then dried under vacuum at 4 °C for 15 min. The +inhibitor tissue was covered with PIM (1x) using 3 x 15 µL/min, Y-distance 25.5 mm, Speed in X= Low 4, Speed in Y= Medium 1, resulting in 0.2 µL/mm$^2$ PIM. After brief drying under vacuum, tracer substrate substance P (20 pmol/µL in H$_2$O) was sprayed on both tissues with the same spray settings (3.5 pmol/mm$^2$ substance P). All steps were performed on ice. An initial experiment for optimising the incubation time for mouse stomach tissue revealed that 30 min incubation time at 37 °C and 95% humidity in the SunDigest incubation chamber is superior to an incubation time of 60 min (Figure 26). After incubation the tissue was immediately covered with the MALDI matrix.

For selectivity evaluation one slice of all tissues was not covered with substance P. It was rather incubated and then covered with MALDI matrix. Further, ITO-slides with tissue of mouse stomach were kept at RT for different periods (0, 5, 10, 15, 60 min) to asses ageing-related changes of the spectra.

To evaluate the environmental influence of the tissue on the proteolytic activity, immediately after slicing TCEA positive stomachs tissues were rinsed with 2 x 1 mL 50 mM ammonium formate (pH 3 and pH 7). Results were compared with the standard proteolytic activity without the washing step (N=3).

### 3.3.4 Tissue preparation for quantitative proteomics analysis of mouse tissue extracts

For proteomics analysis three biological replicates of frozen TCEA-positive and WT mouse stomachs were cryosectioned into 6 x 60 µm slices and collected in vials (3 technical replicates for each WT sample, 2 technical replicates for all TCEA-positive samples). For direct MALDI MSI one slice (10 µm) of each tissue was thaw-mounted onto ITO-slides and vacuum-dried. The aim was to determine the tumour location in TCEA-positive mouse stomachs based on the local distribution of PC(34:1)+K$^+$. After that, further slices were produced.
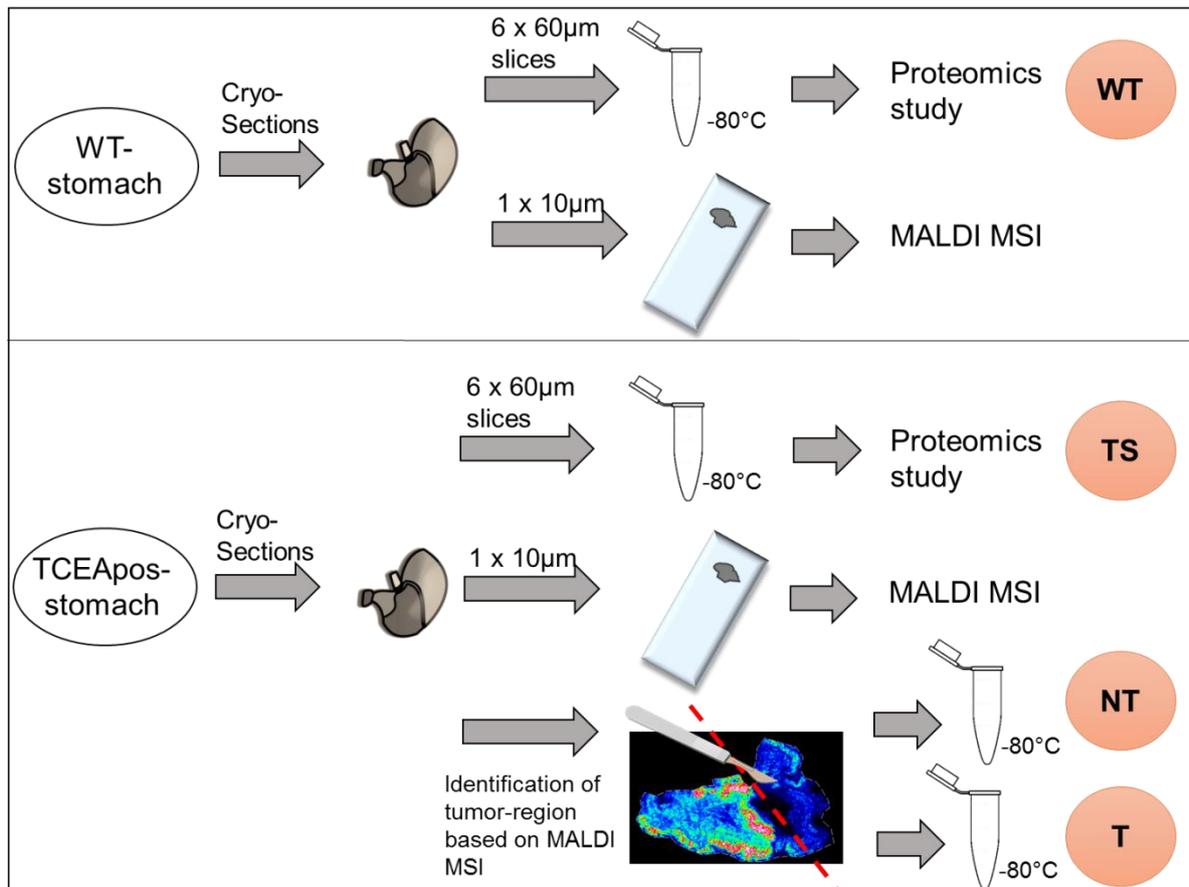
**Figure 5: Preparation of mouse stomachs for quantitative proteomics analysis** Frozen tissue (wild-type = WT and tumour containing stomach = TS) was cut into 6 x 60 µm slices on a cryostat. For WT 3 technical replicates were collected and for TS 2 technical replicates were collected in vials. One slice (10 µm) of each tissue was thaw-mounted onto ITO-slides for acquiring MALDI MSI. According to Hinsenkamp *et al.* PC(34:1)+K^{+} is enriched in the tumour[114], its location in TCEA positive stomachs was determined. The tumour-regions (T) were manually excised from non-tumour tissue (NT) and collected in vials. Vials containing tissue were stored at -80 °C until further processing.

Tumour-regions and non-tumour regions were excised manually, collected in separate vials and stored at -80 °C until further processing (Figure 5).

Further processing, data acquisition, and data analysis were kindly performed by our collaboration partners of the German Cancer Research Center (DKFZ), group of Prof. Dr. Jeroen Krijgsveld. The detailed description of procedures and results were described in Erich et al[115].

### 3.3.5 MALDI Matrix application

All tissues for assessing endogenous proteolytic activity were covered with MALDI matrix DHB (60 mg/mL in 50% ACN/ 49.5% $H_2O$/ 0.5% TFA) using the SunCollect dispenser system (10, 15, 20, 20, 20 µL/min flow, 300 mm/min speed).

### 3.3.6 Preparation of FFPE tissue for the development of statistical scores

The tissue blocks were cut in 2 µm slices using standard microtome instrument (at Institute of Pathology, University Medical Centre Mannheim). One slice of each tissue was placed on indium-tin-oxide (ITO)-slides (Bruker, Bremen) and dried at RT ON. In order to reveal the ideal method published in terms of reproducibility and homogeneous application, five different methods were tested based on four well-documented and published methods[90,94–96]. For easy assessment of similarities and differences in the multistep process Figure 6 describes the methods in all details. Each method was performed in three technical replicates. The detailed spray settings for all five methods were summarised in Table 4.

**Score evaluation for digest efficiency**

To find a suitable standard protein for monitoring the digest efficiency myoglobin (100 µM in ddH$_2$O) and cytochrome c (100 µM in ddH$_2$O) were prepared. These two proteins have a low molecular weight (16.7 kDa and 12.4 kDa, respectively) and are measurable in linear mode using MALDI MSI. An ITO slide with human liver was deparaffinised according to method I, II and III (steps are identical). Standard proteins were pipetted three times with 1 µL on one tissue and on the ITO slide before incubation ("digest"). The whole slide was sprayed with trypsin (0.1 µg/µL in 90% 100 mM ABC buffer/10% ACN) according to method I. After the incubation time of 2 h at 37 °C with 95 % humidity in SunDigest device (SunChrom, Friedrichsdorf), 1 µL standard protein solutions were pipetted three times on the second tissue and on the ITO slide. Prior to data acquisition the slide was covered with MALDI matrix DHB with method I.

1 µL of standard protein cytochrome C (1 mg/mL in ddH$_2$O) was pipetted on the slide next to the tissue before and after the incubation to monitor the protease activity in the method-comparison-experiments.

| | **All start with FFPE tissue 2 µm** | | | | |
|---|---|---|---|---|---|
| | **Method I** *Casadonte et. al. (2011) with SunCollect Sprayer* | **Method II** *Casadonte et. al. (2015)* | **Method III** *Casadonte et. al. (2011) with Heijs et. al. (2015)* | **Method IV** *Diehl et. al. (2015) using HCCA* | **Method V** *Diehl et. al. (2015) using DHB* |
| **Dewaxing** | 2x3min Xylol EtOH 100-100-96-70% (1min each) 2x3min H$_2$O | 2x3min Xylol EtOH 100-100-96-70% (1min each) 2x3min H$_2$O | 2x3min Xylol EtOH 100-100-96-70% (1min each) 2x3min H$_2$O | melt 1h. 60°C 2x5min Xylol 2x2min EtOH | melt 1h. 60°C 2x5min Xylol 2x2min EtOH |
| **Re-hydration** | In 10mM Tris buffer, pH 9.0 | In 10mM Tris buffer, pH 9.0 | In 10mM Tris buffer, pH 9.0 | 2x3min 10mM ABC-buffer | 2x3min 10mM ABC-buffer |
| **Antigen-Retrieval** | Decloaking chamber with 500mL water 95°C – 20min 90°C – 10min Cool down at RT | Decloaking chamber with 500mL water 95°C – 20min 90°C – 10min Cool down at RT | Decloaking chamber with 500mL water 95°C – 20min 90°C – 10min Cool down at RT | Microwave: 10mM citric acid pH6 (pulse boil for 10min, water bath- 30min, 98°C) Cool down 5 min | Microwave: 10mM citric acid pH6 (pulse boil for 10min, water bath- 30min, 98°C) Cool down 5 min |
| **Buffer exchange** | Exchange buffer to H$_2$0; Dry in exciccator | Exchange buffer to H$_2$0; Dry on filter paper | Exchange buffer to H$_2$0; Dry on filter paper | 2x1min 10mM ABC-buffer 5 min desiccator | 2x1min 10mM ABC-buffer 5 min desiccator |
| **Digest** | SunCollect: 100ng/µL Trypsin in 40mM ABC-buffer/10%ACN; 2h, 50°C 5x15µL/min (Low10, HIgh5) | Image Prep: 100ng/µL Trypsin in 40mM ABC-buffer/10%ACN; 1.5h, 37°C | SunCollect: 20ng/µL Trypsin in ddH$_2$O 37°C, 18h in 50% MeOH in saturated chamber | Image Prep: 100ng/µL Trypsin in 50mM ABC-buffer, 2h, 37°C | Image Prep: 100ng/µL Trypsin in 50mM ABC-buffer, 2h, 37°C |
| **Matrix** | SunCollect: 60mg/mL DHB in 50%ACN/0.2%TFA 10-15-20-20-20µL/min 300mm/min | Image Prep: HCCA 7mg/mL (in 50%ACN/0.5%TFA) | SunCollect: 25mg/mL DHB in 50% ACN/0.1%TFA | Image Prep: HCCA 5mg/mL (in 50%ACN/2%TFA) | Image Prep: DHB 30mg/mL in 50%MeOH/1%TFA |
| **Aquisition** | **50µm, UltrafleXtreme** | | | | |

**Figure 6: Overview of methods for FFPE tissue digestion** Method I and Method II are based on Casadonte and Caprioli[90], and R. Casadonte *et al.*[94], respectively. Method III is a combination of Dewaxing, Rehydration, Antigen-Retrieval and Buffer exchange of Method I / II with spraying conditions for digestion and matrix published by Heijs *et al.*[95]. Method IV and V are both published by Diehl *et al.*[96] and differ only in the chosen matrix and its application conditions.

**Table 4: Detailed setting for enzyme and matrix application of each method** The SunCollect system requires several settings to spray a defined amount of solvent. Those settings include X and Y vial distances and speed in X and Y direction. For matrix and enzyme application using the ImagePrep, the settings are saved in the named method files supplied by the supplier (Bruker Daltonics).

| Method | Enzyme application settings | Matrix application settings |
|---|---|---|
| I | SunCollect<br><br>*Vial X = 0.5 mm*<br><br>*Vial Y = 2 mm*<br><br>*Z-Offset = 1 mm*<br><br>*5 layers, each 15 µL/min*<br><br>*Z-Position = 45.28 mm*<br><br>*Speed in X = Low 10*<br><br>*Speed in Y = High 5* | SunCollect<br><br>*Vial Y = 2 mm*<br><br>*5 layers, 10, 15, 20, 20, 20 µL/min*<br><br>*Z-Position = 28 mm*<br><br>*300 mm/min* |
| II | ImagePrep<br><br>*TrypsinDeposition_nsh03.par* | ImagePrep<br><br>*HCCA_nsh04.par* |
| III | SunCollect<br><br>*Vial X = 0.3 mm*<br><br>*Vial Y = 0.3 mm*<br><br>*Z-Offset = 0 mm*<br><br>*5 layers, each 5 µL/min*<br><br>*Z-Position = 45.28 mm*<br><br>*Speed in X = Low 4*<br><br>*Speed in Y = Medium 1* | SunCollect<br><br>*Vial X = 0.5 mm*<br><br>*Vial Y = 2.0 mm*<br><br>*Z-Offset = 0 mm*<br><br>*3 layers, 10, 35, 35 µL/min*<br><br>*Z-Position = 25.00 mm*<br><br>*Speed in X = Low 3*<br><br>*Speed in Y = Medium 1* |
| IV | ImagePrep<br><br>*TrypsinDeposition_nsh03.par* | ImagePrep<br><br>*HCCA_nsh04.par + one additional cycle* |
| V | ImagePrep<br><br>*TrypsinDeposition_nsh03.par* | ImagePrep<br><br>*DHB_nsh04.par + one additional cycle* |

## 3.4 MALDI MS imaging data acquisition methods

### Assessment of endogenous protease activity in porcine tissues

Porcine tissues were analysed using an UltrafleXtreme MALDI-TOF/TOF MS instrument in reflector positive mode and a mass range of 500-2500 Da. The lateral resolution was 200 µm, summing up 300 shots per pixel. External quadratic mass calibration was performed by using peptide standard II.

**Assessment of endogenous protease activity in a gastric tumour mouse model and human biopsy**

Mouse-derived samples and human biopsies were measured using a RapifleX MALDI-TOF MS instrument (Bruker Daltonics) with a lateral resolution of 50 µm (and 20 µm for the high-spatial resolution replicate experiment on mouse stomach), summing up 400 shots per pixel. The same slides were further analysed using 7T solariX XR MALDI FT-ICR MS instrument (Bruker Daltonics) in a mass range of 100 – 3000 Da and a raster width of 20 µm with 15 laser shots/pixel. Additional parameters were summed in Table 5. Spectra were recorded using 512 k (FID 0.2447 s) data point transient, corresponding to an estimated resolving power of 33,000 at *m/z* 400. With these settings the data size has a manageable size of 22 GB. Internal calibration was performed using a lock mass of *m/z* 780.551 [PC(34:2)+Na$^+$]. For verification of the substance P fragments on mouse stomachs, CID fragmentation was used with individually optimised voltages. Data analysis was done using Biotools 3.2 and Sequence Editor 3.2 software.

**Table 5: Parameters for FT-ICR MSI of mouse stomach tissue and human biopsy**

| | | |
|---|---|---|
| **Ion transfer** | Funnel 1 | 150 V |
| | Skimmer 1 | 15 V |
| | Funnel RF Amplitude | 70 Vpp |
| **Octapole** | Frequency | 5 MHz |
| | RF Amplitude | 350 Vpp |
| **Collision cell** | RF Frequency | 2 MHz |
| | RF Amplitude | 1200 Vpp |
| **Transfer optics** | Time of Flight | 1.5 ms |
| | Frequency | 4 MHz |
| | FR Amplitude | 350 Vpp |
| **Quadrupole** | Q1 Mass | 350 *m/z* |
| **Excitation mode** | Sweep excitation | ON |
| | Sweep step time | 15 µs |

**Acquisition of FFPE on-tissue digestion experiments**

Data acquisition was performed on an UltrafleXtreme MALDI TOF/TOF instrument (Bruker Daltonics) in reflector positive (RP) mode and in a mass range of 500-5000 Da. On each tissue slice, three squares (~ 110 pixels each) were randomly selected in the trypsin-coated part and in the "no-trypsin control". Those six squares per tissue slice were measured with 50 µm pixel-to-pixel resolution, medium laser size, and 500 shots per pixel. Standard protein spots were measured in the linear positive (LP) mode in a mass range of 2000-20,000 Da using a raster width of 200 µm and a large laser focus. Peptide method calibration was performed using external peptide calibration standard II for reflector positive mode. Protein linear method calibration was performed using protein calibration standard I and external quadratic calibration. All acquired datasets were converted into SCiLS Lab – files performing a baseline subtraction during the import (TopHat, width 200). Additionally, all datasets were exported into imzML format[116] for in-house computational analysis.

## 3.5 Data processing and statistical methods

### 3.5.1 Statistical analysis for digests by endogenous proteases in mouse stomach

TOF datasets were converted into imzML format[116] using the flexImaging converter. FT-ICR data were converted to imzML by an in-house conversion tool. Statistical analysis has been done by Denis Abu-Sammour explained in details in Erich *et al.*[115] FT-ICR datasets were uploaded to METASPACE[d][117] and are publicly available.

**Proteomics data processing**

Proteomics data were processed by Torsten Müller of the German Cancer Research Center (DKFZ), group of Prof. Dr. Jeroen Kriijgsveld, as described in Erich *et al.*[115].

Data is publicly available in ProteomeXchange Consortium via PRIDE repository (identifier PXD010369).

---

[d] http://metaspace2020.eu

### 3.5.2 Data processing for FFPE-tissue trypsin digests score development

**<u>Evaluation of the sequence coverage</u>**

To evaluate the sequence coverage of the myoglobin and cytochrome C digest spectra from reflector-positive measurements were analysed and compared to *in situ* digest using BioTools software and sequence editor applying a mass tolerance of 100 ppm. Further, the values for a number of matched peptides are extracted.

**<u>Calculation of Digest Efficiency DE%</u>**

For FFPE-tissue experiments the total ion current- (TIC-) normalised intensities of each intact signal of cytochrome C $[M+H]^+$, $[M+H]^{2+}$ and $[M+H]^{3+}$ were exported for the undigested and digested spot by SCiLS Lab. Digest efficiency was calculated for each signal using the following formula and was further averaged resulting in the DE% for the respective slide.

$$DE\% = \left( 1 - \frac{intensity_{digested}}{intensity_{undigested}} \right) \times 100\% \qquad \textbf{(2)}$$

For quantifying protease activity regions-of-interest (ROIs) were manually drawn on the tissue spots with inhibitor (+inhibitor) and randomly on tissue without (-inhibitor) inhibitor in flexImaging. Mean spectra were exported into mMass, where baseline-subtraction and peak-picking (S/N>5) were performed. Intensities for substance P signal in each ROI were exported into Excel. DE% was calculated as described in equation (2). (Graphical visualisation and regression analysis have been done in Prism 5.0).

**<u>Data processing for FFPE on-tissue trypsin digests</u>**

The here briefly explained computational analysis of FFPE tissue digest was performed by my colleague Denis Abu-Sammour. Raw data were imported as imzML files into R.3.2.3[118], where preprocessing and peak picking were performed. Further details are explained in the respective publication by Erich *et al.*[119] The resulting peak lists were used for pixel-wise and mean-spectra analysis.

To visualise the number of picked peaks in defined mass ranges, peaks were grouped in Excel and tables were visualised using Tableau – software or GraphPad. The shown mean spectra were TIC normed and visualised using mMass software.

**Correlation and fold-change analysis**

For the analysis of repeatability the peak lists of all replicates were combined to one merged peak list. This list contained all occurring *m/z* values and was generated with an in-house script in MATLAB (tolerance 100 ppm). These defined peaks consisted most likely of a mixture of underlying molecules[102]. This is due to the theoretical mass accuracy of 0.1 – 0 01 Da for TOF-instruments in the used mass range. As method variability was evaluated, the same experimental setup was repeated, and the composition of each peak should be consistent throughout the analysis. The coefficient of determination $R^2$ was calculated for all peaks and their respective intensities. The natural fold-change (*natFC*) was defined as the absolute value of either 5th or 95th percentile of all fold-changes comparison, whatever was higher (equation (3)).

$$natFC = \max(\left| 5^{th}\ FC\ percentile \right|, \left| 95^{th}\ FC\ percentile \right|) \qquad \textbf{(3)}$$

This score-based analysis has not only been performed on mean spectra as described here but also on pixel-wise analysis using computational power (in R) by my colleague Denis Abu-Sammour as described in Erich *et al.*[120]. For homogeneity analysis 1000 different, randomly chosen, combinations of spectra were compared for $R^2$ and fold-change values. To assess repeatability, 3000 different and randomly chosen spectra were compared.

Fold-change calculations on endogenous digest experiments were performed on mean spectra and intensities extracted from SCiLS Lab software. Respective datasets were converted in SCiLS Lab, common peak-lists were calculated, and respective intensities were exported into Excel. Further calculations were performed in Excel and Tableau.

# 4   RESULTS

## 4.1   Part I – Visualisation of tissue protease activity using MALDI MSI

### 4.1.1   Development of a score for ideal application of the substrate

The homogeneous application of a substrate is essential for spatial evaluation by MALDI MSI. Furthermore, the delocalisation of molecules in the tissue needs to be minimised. The next Figure 7 shows an innovative way to measure those factors. Applying water on the yellow Water- sensitive paper WSP (Syngenta) turns it blue. It is used in agriculture to check spray distribution, droplet density and droplet sizing of spray applications on fields[121]. It allows the visual inspection of spot density (spot/cm$^2$) and the automated analysis for spot size parameter, the number of spots and area coverage percentage[122]. So far, it has not been used in MALDI MSI or related spatially resolved methods. Spraying an aqueous solution with a sprayer system as the SunCollect (SunChrom) on the WSP revealed the droplet distribution (Figure 7 A). Using a bigger distance from the spray head to the WSP (25.3 mm) showed a deeper blue compared to the sparkled layer with a distance of 45.3 mm. The distance in millimetre represented the ascended spray head, thus a higher value meant a lower distance to the WSP. Although the visual inspection of the blue layer already indicated the advantage of the higher spray distance, an unbiased quantitative analysis is more valuable. Therefore, the WSP was scanned, the image converted into grey-scale and mean grey values were exported for three randomly chosen squares (ImageJ-software, Maryland) N=3. The mean grey values for three individual spray experiments were plotted in bar charts (Figure 7 B) showing that the higher distance ensured more stable and reproducible values.

The next important prerequisite for an ideal spray condition is a minimal delocalization of molecules in the tissue. A Rhodamine B – test was developed to check for delocalization. Here, three spots of 1 mg/mL Rhodamine B in water were pipetted on the tissue and dried prior to the spray application. With a distance of 45.3 mm the spots were spread and the dye was spread over the tissue, whereas with a distance of 25.3 mm the integrity of the spots was preserved (Figure 7 C). The endogenous digest experiments were performed with the optimized setting of 25.3 mm spray distance for three layers of 15 µL/mm flow.

**A** Water sensitive paper test



45.3 mm          25.3 mm

**B**



**C** Rhodamine B test for delocalisation
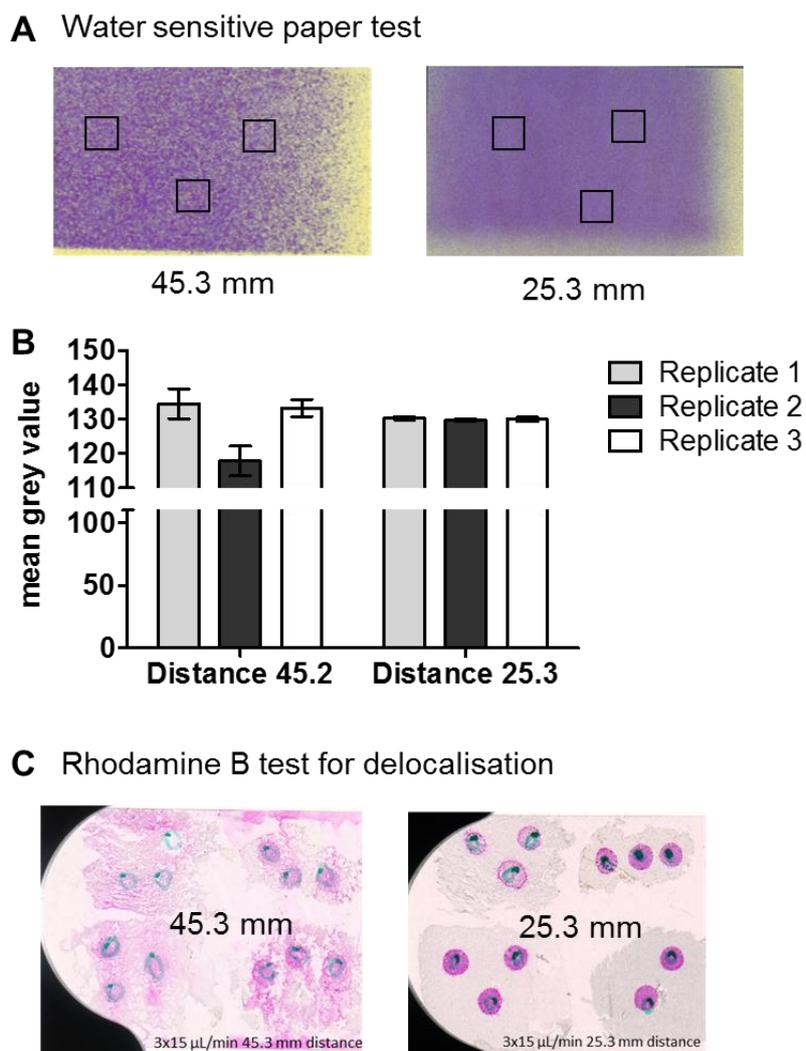


**Figure 7: Spray distance optimization using water sensitive paper (WSP) and the Rhodamin B test** Both tests were developed for testing spray homogeneity and delocalization, respectively. The yellow water sensitive paper (WSP) turns blue when getting into contact with water. **A** By spraying the solvent on WSP the difference in droplet composition was visually inspected. Lower distance to the WSP (45.3 mm) revealed more sparkled spray distribution. A higher distance (25.3mm) produced a denser and homogeneous blue colour. **B** Mean grey values were extracted from the blue colour using ImageJ (ImageJ, Maryland) for three randomly chosen squares (summed in one bar) and three technical replicates. **C** For testing delocalization rhodamine B was spotted on the tissue, then dried and the tissue was sprayed with solvent. The integrity of the rhodamine B spots was observed visually. (N=3)

### 4.1.2  Evaluation of substance P as a universal substrate

In this study substance P has been chosen as substrate. This assumption was evaluated by a database search based on 'MEROPS – the peptidase database'[e], which confirmed that several protease classes can cleave substance P (Figure 8)[25]. Proteases from organisms like *fish*, *plant*, or *fungi* could cleave substance P. When looking into the mammalian species, most MEROPS entries are from *Homo sapiens* (Figure 8 A). For mammals the found proteases belonged to different protease classes,

---

[e] http://merops.sanger.ac.uk

namely peptidylpeptidases, cysteine endopeptidases, aspartic endo-peptidases, dipeptidyl peptidases, serine endopeptidases, and metallo-endopeptidases, of which the latter two were listed most often (Figure 8 B). A detailed analysis of the recorded produced peptides (Figure 11) revealed that SubP(1-7), SubP(1-6) and SubP(1-9), referring to *m/z* 900.5, 753.4 and 104.6, respectively, might be produced predominantly by metalloendopeptidases, (Figure 8 C). Indeed, there might be proteases that do not cleave substance P. Based on this analysis, however, it seemed far away from being a specific substrate, and its use as overall tissue protease activity tracer is reasonable.
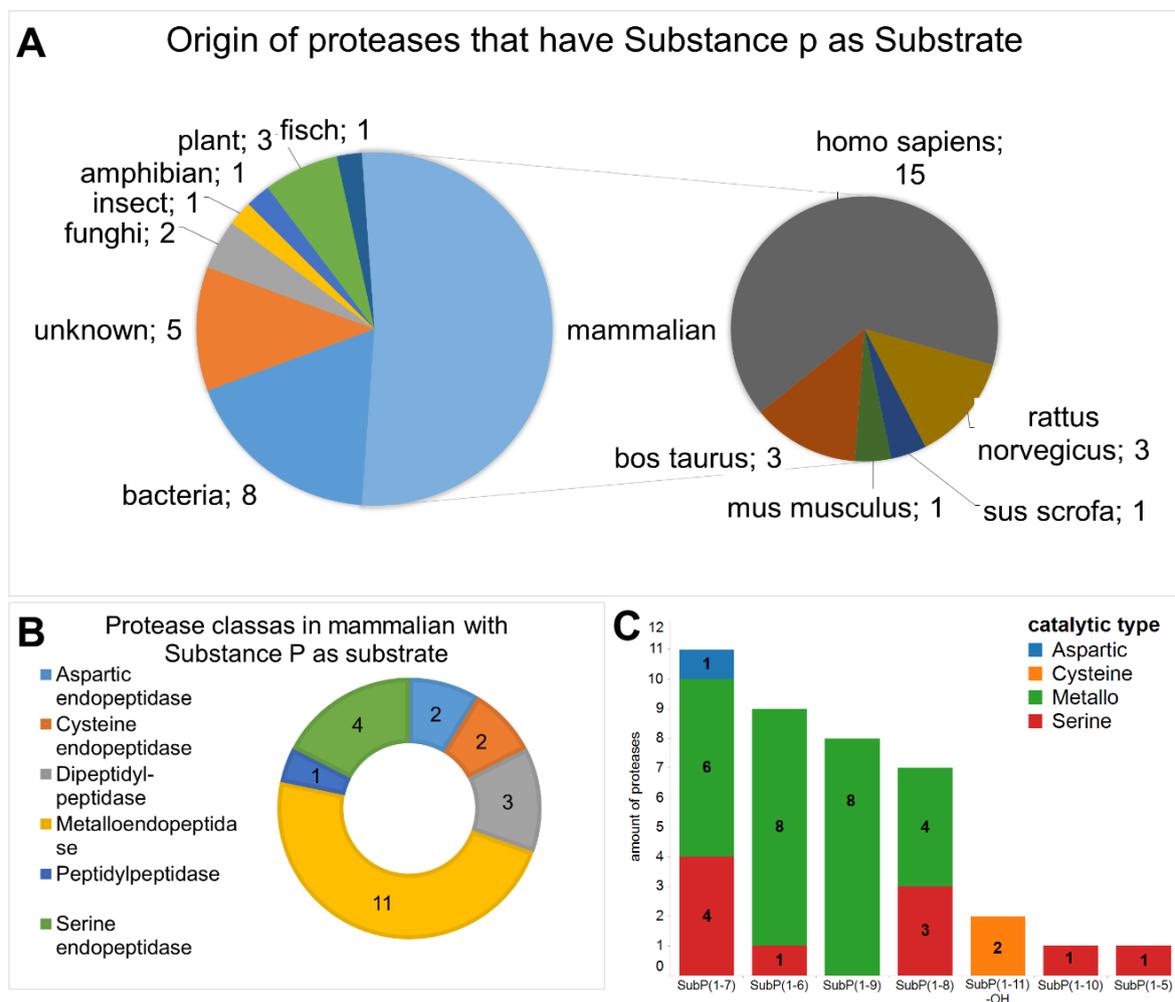


**Figure 8: MEROPS database analysis for substrate substance P A** When analysing MEROPS database for proteases that could use substance P as a substrate, 44 proteases were found and can be grouped for different characteristics like their origin. **B** Interesting for us are the 23 mammalian proteases grouped for their protease class. Most of these are metalloendopeptidases (11 proteases, shown in yellow) **C** Shown here is the number of proteases and their classes sorted by their substance P product specificity. The sorting was based on the described substance P – fragments and the related proteolytic class. The most proteases slice substance P at position 7 (phenylalanine) to the fragment SubP(1-7). This fragment has the *m/z* value 900.5. The next most abundant fragment SubP(1-6) corresponds to the observed *m/z* value 753.4 and finally SubP(1-9) has an *m/z* value of 1104.6. According to our data and this analysis, we observe the three most abundantly produced substance P fragments. Further, they may be produced mainly by metalloproteases (green colour).

### 4.1.3  Time-course of substance P digestion by endogenous tissue proteases

For a systematic analysis of tissue protease activity using MALDI MSI the undecapeptide substance P (RPKPQQFFGLM; [M+H]$^+$ = $m/z$ 1347.7354) was selected as tracer substrate. Porcine tissues (brain, kidney, liver, pancreas, spleen and muscle) were tested with if for unspecific whole-tissue protease activity.

**Homogeneity assessment of porcine tissue**

H&E stains or representative tissue slices reveal the inhomogeneity of brain tissue (Figure 9). Inhomogeneity can be problematic for the spatial analysis of the experimental setup. The homogeneity of all other tissues is a prerequisite for the topically applied inhibitor spots in the following experimental setup.
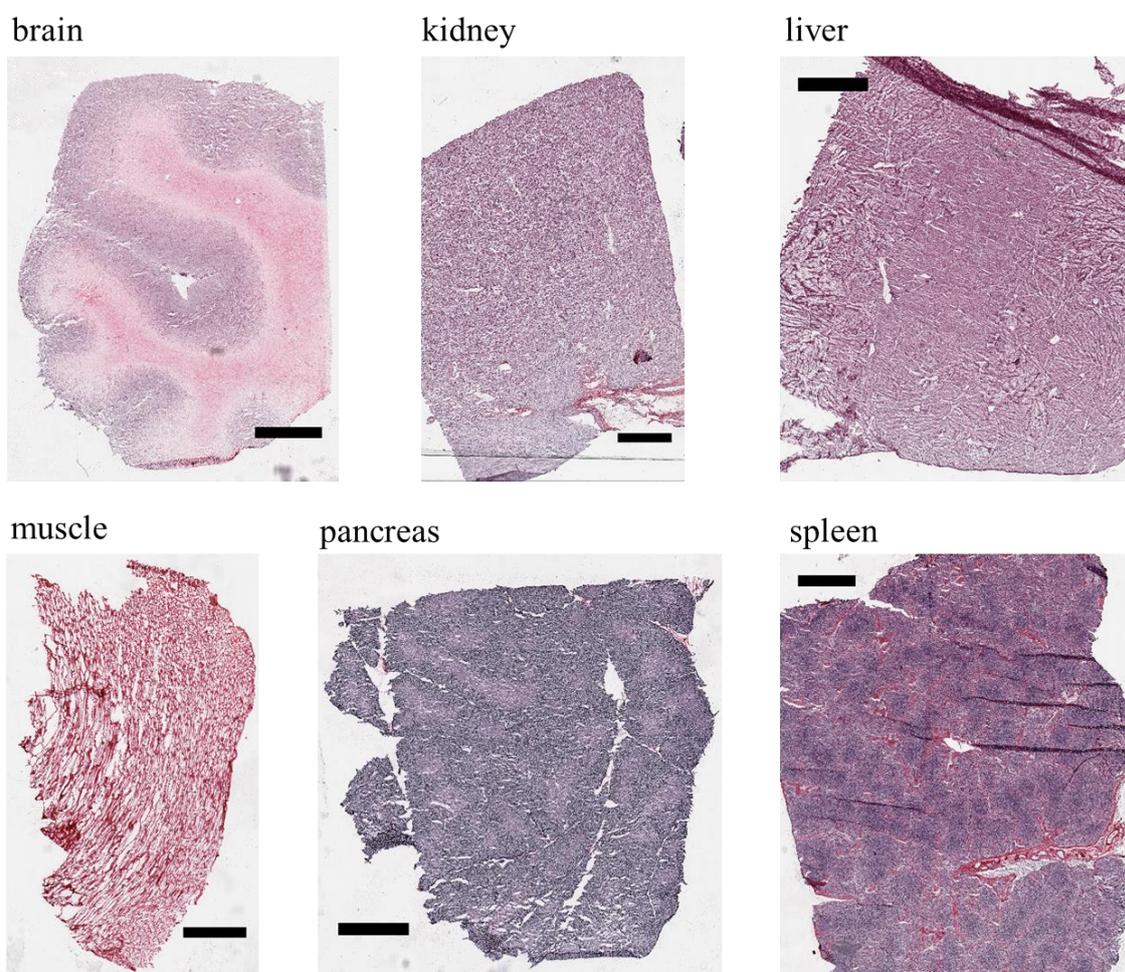


**Figure 9: H&E stain for porcine tissue** All porcine tissue were H&E stained according to standard staining protocol. The slides were scanned with high resolution using the Aperio CS2 (Leica Biosystems) scanner. Morphology of the tissue showed inhomogeneity for brain tissue, represented by white and grey matter. The other tissue blocks showed good homogeneity.

**Specificity analysis for the tracer peptide and related ions on porcine tissue**

It is another prerequisite that specificity of substance P signals is given for all tissues. All porcine tissues were measured using MALDI-TOF MS instrument (UltrafleXtreme, Bruker Daltonics) without any application of substance P. The tissue mean spectra did not show any signal that potentially could interfere with substance P or substance P–related signals (Figure 10).
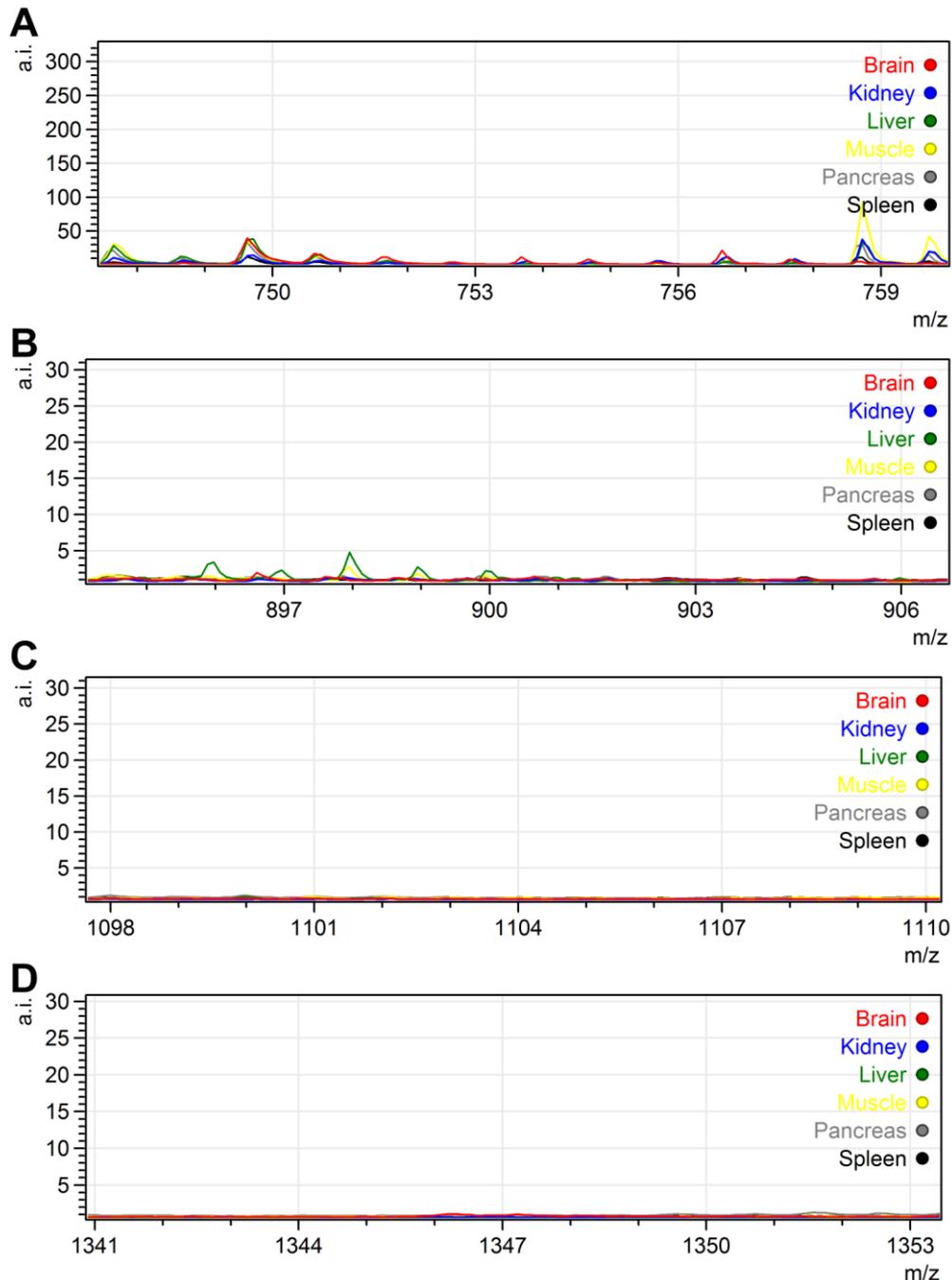


**Figure 10: Specificity of *m/z* values of substance P and its related peptides on porcine tissue** Shown are MALDI-TOF mean mass spectra of porcine tissues (brain=red, kidney=blue, liver=green, muscle=yellow, pancreas=grey, spleen=black) without trypsin-coating. No endogenous signals interfere with substance P signal at *m/z* 1347.7 (**D**) nor with potential resulting peptides at *m/z* 1104.6 (**C**), *m/z* 900.5 (**B**) or *m/z* 753.4 (**A**).

## **MALDI MSI time course visualising tissue protease activity of porcine tissues**

By spray coating, porcine liver tissue with substance P and further incubation at 37 °C and with 95% humidity (in SunDigest Incubation chamber) for 30 min a consistent decrease of the substance P signal and an increase in substance P-related peptide signals were observed (Figure 11), compared to a control without incubation. The experiment was designed by myself and conducted by Kevin Reinle in the context of his masterthesis[f]. The detected increasing masses could be assigned to the C-terminal cleavage products of substance P (Table 6). This first result led to the hypothesis, that the digestion of the tracer substance P by endogenous proteases, preserved in frozen tissue, could be visualised.

**Table 6: Substance P related peptides C-terminally cleaved**

| Substance P | 1347.7 *m/z* | RPKPQ QFFGL M |
|---|---|---|
| SubP(1-10) | 1217.7 *m/z* | RPKPQ QFFGL |
| SubP(1-9) | 1104.6 *m/z* | RPKPQ QFFG |
| SubP(1-8) | 1047.6 *m/z* | RPKPQ QFF |
| SubP(1-7) | 900.5 *m/z* | RPKPQ QF |
| SubP(1-6) | 753.4 *m/z* | RPKPQ Q |
| SubP(1-5) | 625.4 *m/z* | RPKPQ |

To verify this hypothesis, an experimental setup for all six porcine tissues was developed, where time-dependency of the digestion could be observed with MALDI MSI. Further, a protease inhibitor mix (PIM) was pipetted (4 x 1 µL in 1x working solution, concentrations of single inhibitors according to Table 3) on the tissue, to indicate a protease-related change of signal intensity (Figure 4). Incubation was performed in the SunDigest incubation chamber.

---

[f] Masterthesis Kevin Reinle, *Visualising endogeneous protease activity by MALDI Mass Spectrometry Imaging*, 2017
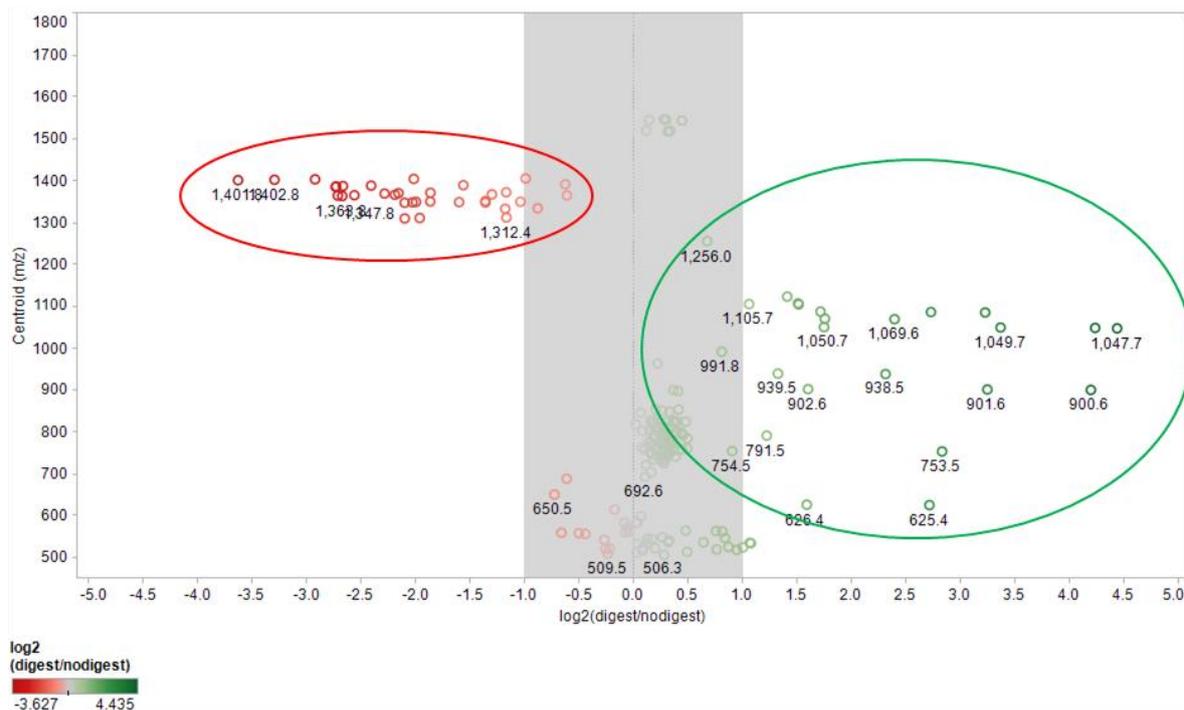
**Figure 11: Comparison spectra digest/no digest show increased fragments of substance P** In an initial experiment substance P was sprayed on pancreas tissue – one prior to incubation at 37 °C and 95% humidity, for 30 min (digest), the other after this incubation (no digest). The fold-change plot revealed that the digested tissue showed decreased substance P signals (in red) compared to no-digest tissue. The set of substance P signals consist of the protonated form, adducts with sodium and potassium, as well as their respective isotopologues. Further, *m/z* values increased in the digested tissue (green) that might correspond to cleaved products of substance P.

The first observation was that on muscle tissue there was no difference between substance P signal distribution on no digest- and digest-slide. This means that no reduction of the substance P – signal, thus no digestion could be observed (Figure 12). Further, the spotted PIM did not have an impact on the substance P signal distribution in both conditions.

There was a difference in the absolute intensity scale when measuring the time points on different days. To normalise this variability, the no digest control was always measured with the digest slide. This makes a comparison of the different time-points possible. Nevertheless, when the no digest control visually did not show a homogeneous distribution of the substance P signal, the data set was excluded for further analysis.
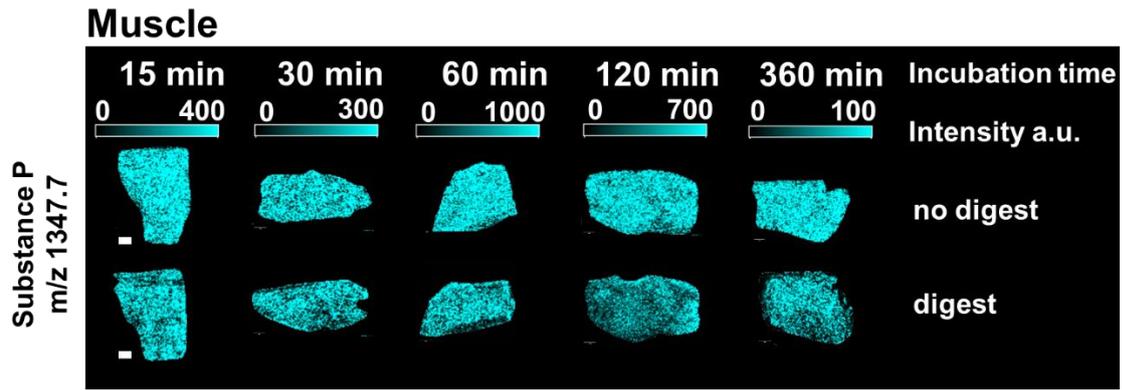
**Figure 12: MALDI MSI of substance P and resulting peptides on porcine muscle** Muscle tissue cryosections of 10 μm were mounted on two ITO-slides. Protease inhibitor mix was pipetted onto each tissue (4x 1 μL). The "digest" and "no-digest" slides were spray-coated with substance P before and after incubation (15, 30, 60, 120, 360 min), respectively. After coating with DHB, MALDI-TOF MSI was performed at 200 μm spatial resolution. For muscle tissue the ion intensity distribution of substance P ($m/z$ 1347.7) on the "digest" slide did not change over time. Scale bar is 2 mm.
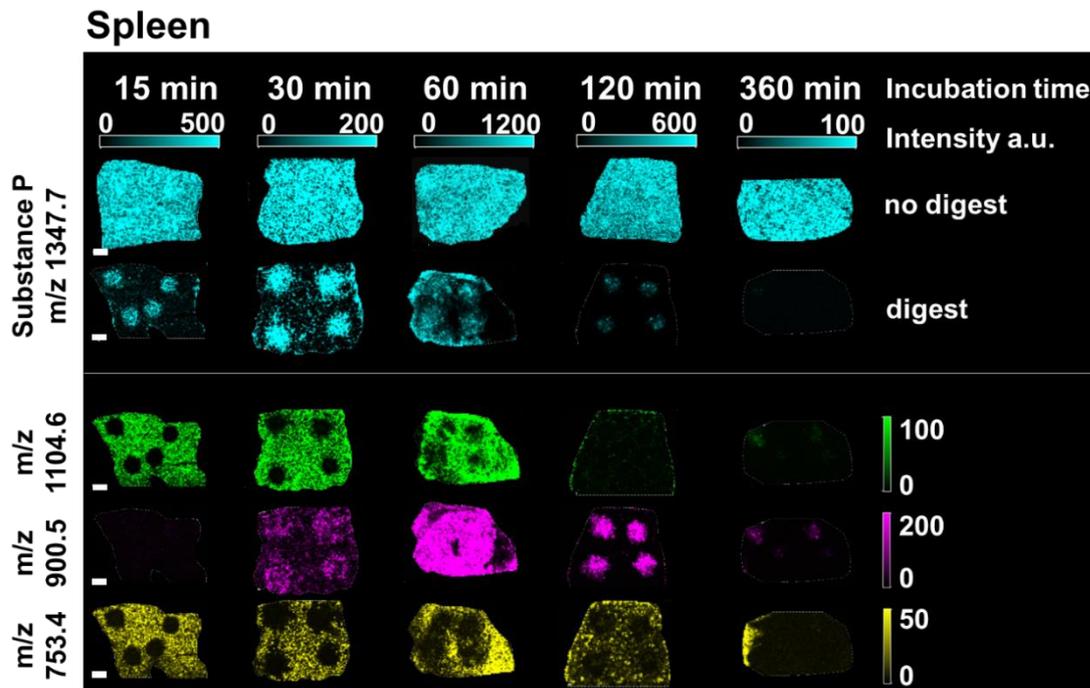


**Figure 13: MALDI MSI of substance P and resulting peptides on spleen** Tissue was sliced in 10 μm sections and placed on two ITO-slides ("digest"-slide and "no-digest"-slide). Protease-Inhibitor-Mix was pipetted onto each tissue (4x 1 μL). The "digest"-slide was spray-coated with substance P before and the "no-digest"-slide after incubation at 37 °C, 95 % humidity (incubation times: 15, 30, 60, 120, 360 minutes). After coating with MALDI matrix, the acquisition was performed on a MALDI-TOF MS (UltrafleXtreme, Bruker Daltonics) with 200 μm spatial resolution. MALDI-TOF MS images of the "no-digest"-slide showed a homogeneous distribution of substance P. This description holds true for the following figures. On the "digest" slide, the spots with inhibitor showed higher substance P signals than the surrounding tissue without inhibitor. Where low substance P signal intensity was detected, peptides corresponding to $m/z$ values 1104.6, 900.5 and 753.4 are visible. In the case of $m/z$ 900.5 the inhibition retained the decrease of the signal at 120 min incubation. Scale bar is 2 mm.

The porcine tissues spleen, liver, pancreas and kidney (Figure 13 to Figure 16) showed a time-dependent reduction and a homogeneous distribution of the substance P signal on the no digest controls. The spots, where PIM was pipetted, were clearly visible and displayed a higher substance P signal compared to the non-inhibited surrounding tissue. In detail, when looking at the MALDI MSI of substance P signal distribution on spleen after 15 min incubation, very low signal intensity (represented in blue colour) could be seen in the non-inhibited regions. In contrast in the PIM spots the intensity was preserved. After 120 min of incubation the substance P signal was decreased in the PIM spots also, until it was gone after 360 min incubation. The absolute depletion of substance P signal holds true for all tissue, apart from muscle.
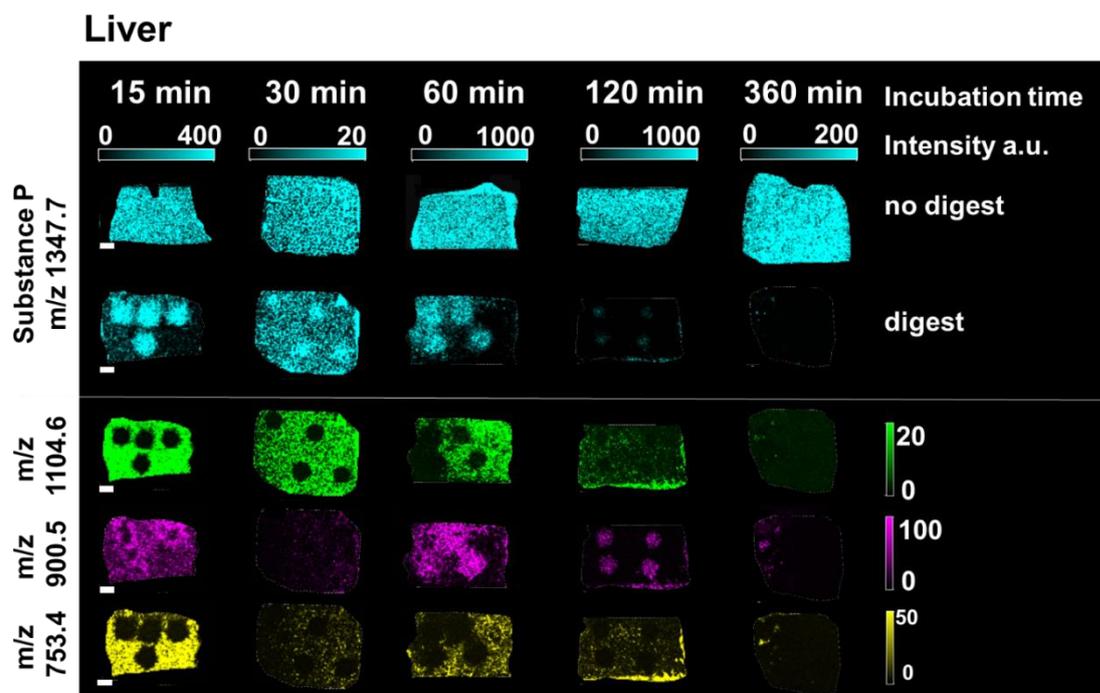


**Figure 14: MALDI MSI of substance P and resulting peptides on liver** See description of Figure 13. On the "digest" slide, the spots with inhibitor showed higher substance P signals than the surrounding tissue without inhibitor. Where low substance P signal intensity was detected, peptides corresponding to *m/z* values 1104.6, 900.5 and 753.4 are visible. In case of *m/z* 900.5 the inhibition retained the decrease of the signal at 120 min incubation. Scale bar is 2 mm.
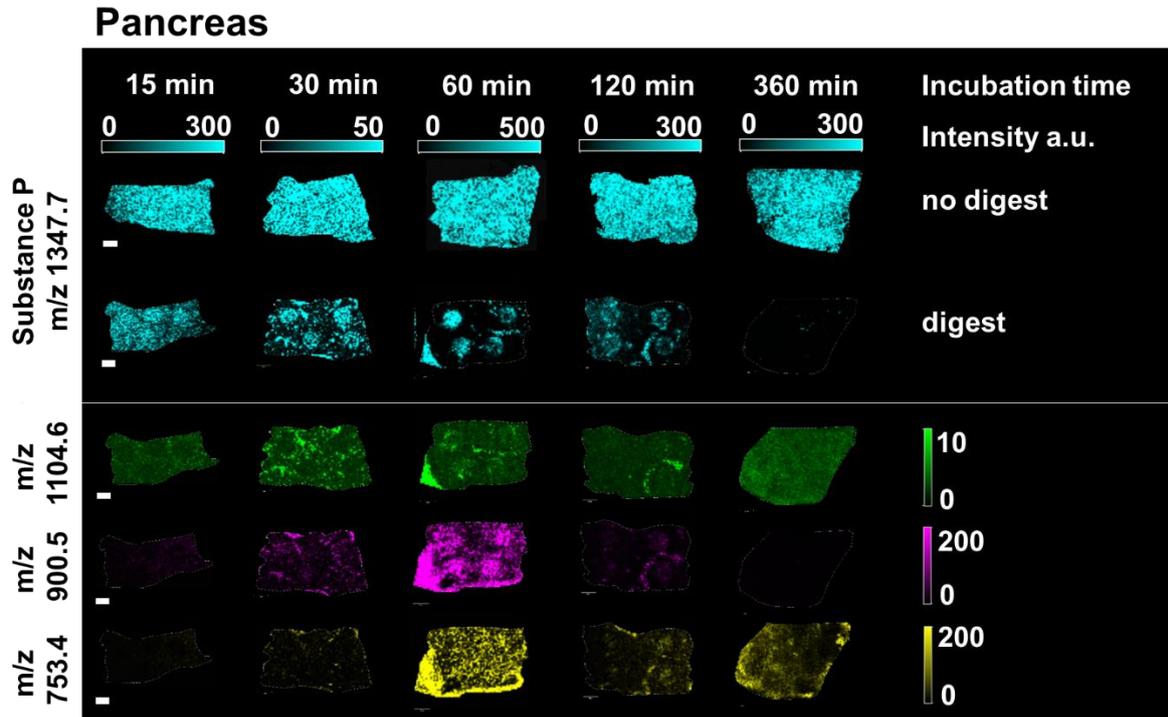
## Pancreas



**Figure 15: MALDI MSI of substance P and resulting peptides on pancreas** See description of Figure 13. On the "digest" slide spots with inhibitor showed higher substance P signals than the surrounding tissue without inhibitor. Where low substance P signal intensity was detected, peptides corresponding to *m/z* values 1104.6, 900.5 and 753.4 are visible. Pancreas seemingly shows a poor reaction on the spotted inhibitor. Scale bar is 2 mm.
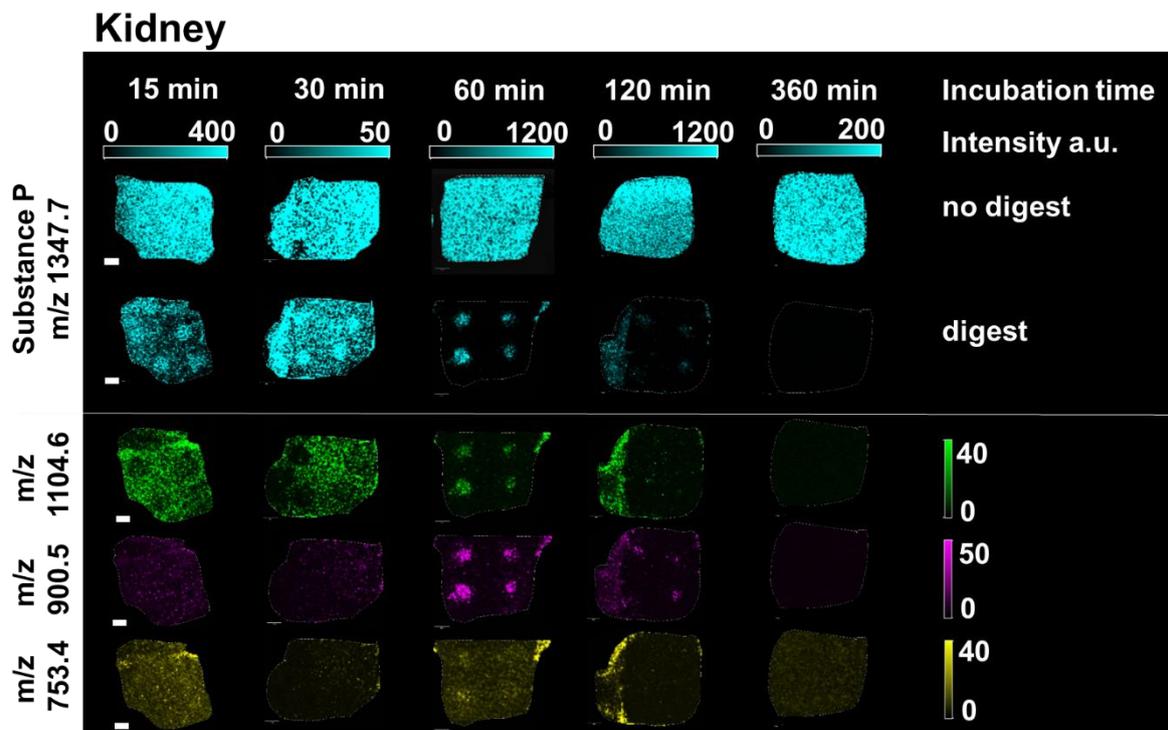
## Kidney



**Figure 16: MALDI MSI of substance P and resulting peptides on kidney** See description of Figure 13. On the "digest" slide spots with inhibitor showed higher substance P signals than the surrounding tissue without inhibitor. Where low substance P signal intensity was detected the *m/z* values 1104.6, 900.5 and 753.4 are visible. The inhibition retains the decrease of the signal *m/z* 900.5 at 120 min incubation. Scale bar is 2 mm

47

As previously mentioned homogeneous distribution of substance P on the no-digest control is the prerequisite for a proper statistical analysis. According to the H&E stain of brain tissue (Figure 9), the brain sample consists of white and grey matter. This inhomogeneity resulted in inhomogeneous distribution of the signal, most likely due to different ionisation and suppression effects in the two tissue types[123]. This generated very unreliable and unstable results for this dataset.
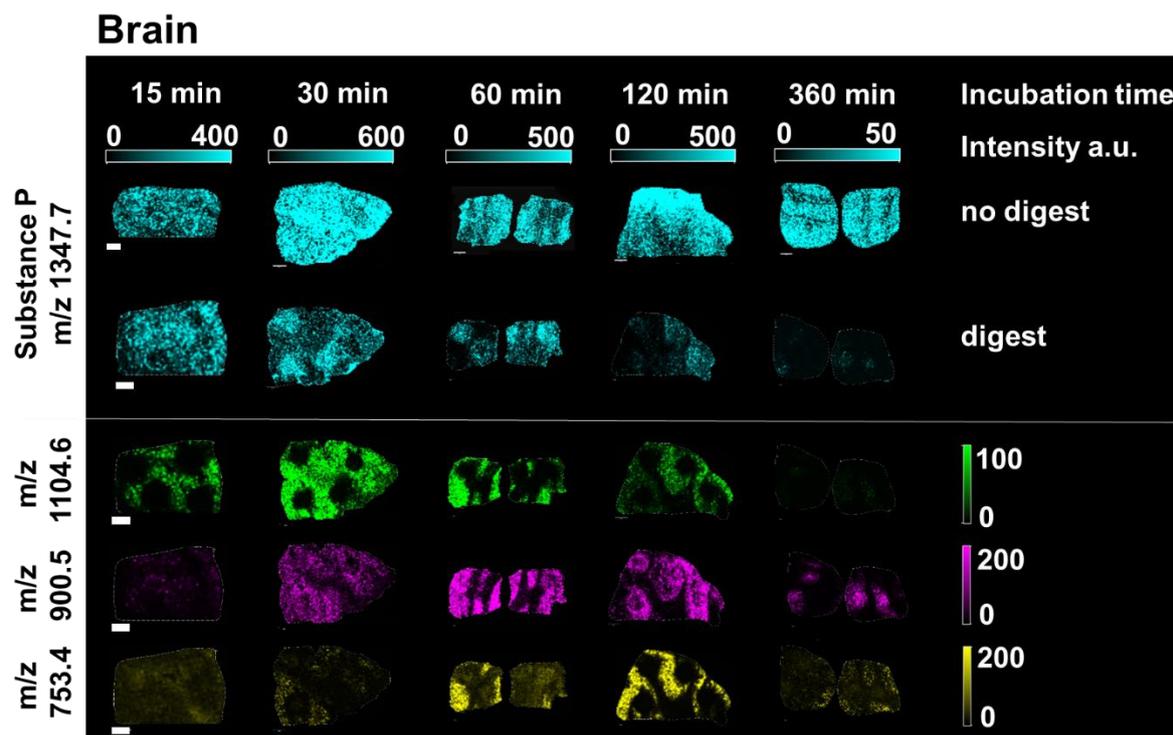


**Figure 17: MALDI MSI of substance P and resulting peptides on brain** See description of Figure 13**.** MALDI MSI of the "no-digest"-slide showed inhomogeneous distribution of substance P, due to morphological differences in brain tissue.

The MALDI MSI of the time-curve experiment did not only reveal the protease-dependent decrease of substance P signal (as PIM retains the decrease), but also the time-dependent occurrence of substance P-related peptides. The most intense were SubP(1-5) *m/z* 753.4, SubP(1-7) *m/z* 900.5 and SubP(1-9) *m/z* 1104.6. With *m/z* 1104.6 and 753.4 being dominantly produced in the non-inhibited tissue, *m/z* 900.5 is produced in the PIM spots. This could be optimally observed on spleen (Figure 13). Here, after 360 min incubation no difference between inhibited and non-inhibited regions was detectable anymore. The time-dependent production of peptides suggests that substance P is truly digested rather than sequestered into the tissue.

## Digest efficiency calculation in the time course experiments

An absolute analysis of the MALDI MS Images is difficult. All time-points and tissue relative digest efficiencies (DE%) were calculated according to equation (2). Mean spectra were extracted from the four PIM spots (+ inhibitor) and from tissue without PIM (- inhibitor). The substance P intensity for no digest and digest slide were also extracted. The time-curve experiments were performed a second time under slightly varied conditions: The incubation was done in a standard cell-culture oven at 37 °C (Figure 18) instead of the SunDigest incubation chamber[g] (Figure 19)
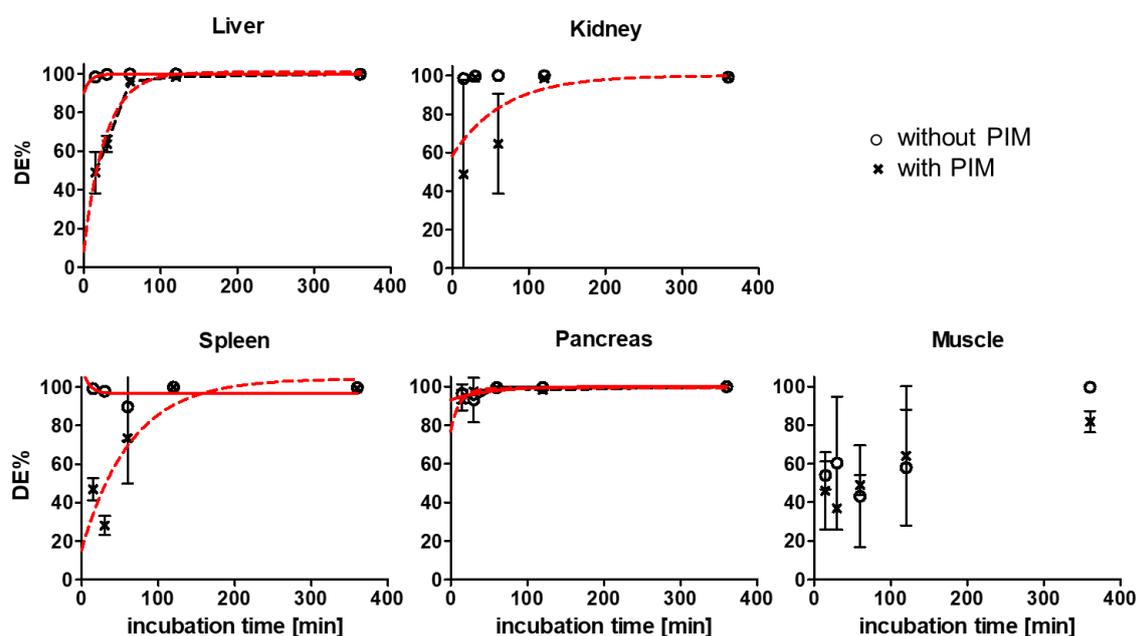


**Figure 18: Time-curves of digest efficiency of porcine tissues in a cell culture incubator** All tissue showed a very fast increase of DE% when no inhibitor was used (continuous line). The Protease Inhibitor Mix (PIM) slowed down the digestion process (broken line). Pancreas did not react on the PIM and showed a very fast digestion process. Muscle tissue showed no decrease in substance p signal and was thus used as negative control.

---

[g] Experiments in SunDigest chamber were designed by myself and conducted by Kevin Reinle in the framework of his Masterthesis: *Visualising endogeneous protease activity by MALDI Mass Spectrometry Imaging*, 2017
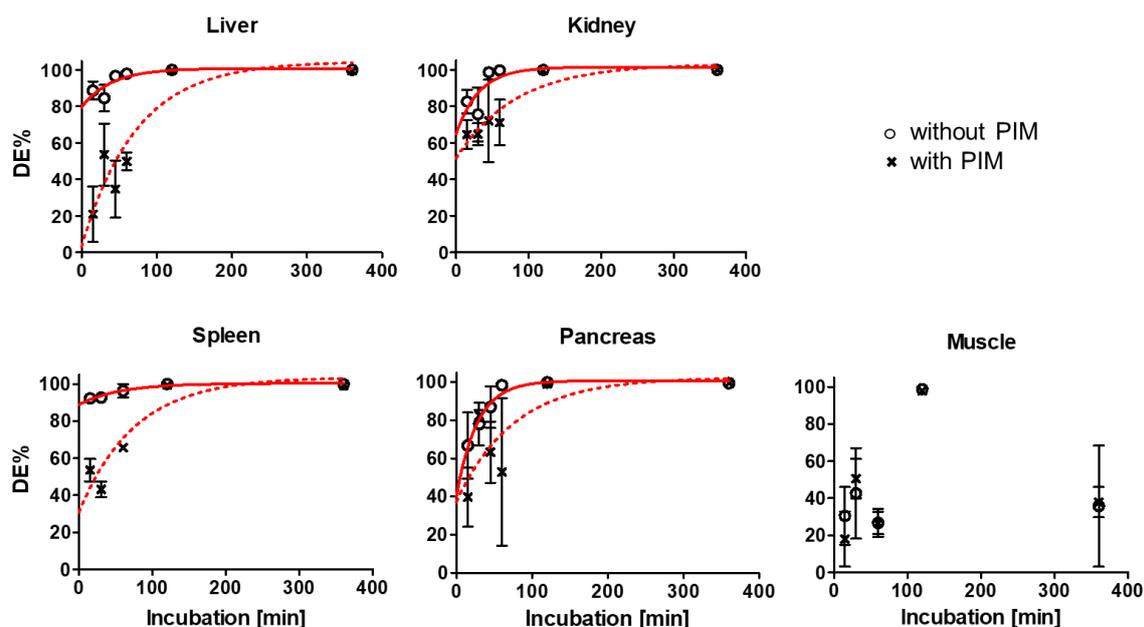
**Figure 19: Time-courses of digest efficiency of porcine tissues in the incubation chamber** All tissue showed a very fast increase of DE% when no inhibitor was used (continuous line). The Protease Inhibitor Mix (PIM) retarded the digestion process (broken line). Pancreas did not react on the PIM and showed a very fast digestion process. Muscle tissue showed no decrease in substance p signal and was thus used as negative control.

The calculated DE% in the cell culture incubator showed already 100% digestion of the substance P signal after 15 min incubation, lasting on this level in all tissues (instead of muscle) (Figure 18). In the SunDigest chamber a nearly 100% digestion for all tissues (instead of muscle) was reached after 60 min incubation time (Figure 19). It seemed that the conditions in the SunDigest chamber favoured a slow progress of the proteolytic activity. Both experiments showed decreased DE% when PIM was applied to the tissue. Further, brain showed a high standard deviation according to its tissue heterogeneity (data not shown). Porcine pancreas showed no effect on PIM and high variance (< 1 h), regardless of the incubation condition. This was possibly due to the complexity of protease constitution in this highly active digestive tissue[124]. In spleen and liver tissue PIM-induced retardation of substance P degradation was highly significant. Muscle tissue showed no reduction of the substance P signal in both conditions, so the calculation of DE% did not show an increase.

**Generation of substance P cleavage products in time course experiment**
It was observed that substance P related peptides occurred transiently during the time course. Ion intensities for *m/z* 1104.6, *m/z* 900.5 and *m/z* 753.4 were extracted in analogy to the ion intensity extraction of substance P. The TIC-normalised intensities from ROIs with and without inhibitor were plotted. In line with the observation from

MALDI MSI (Figure 12 to Figure 17) the *m/z* value 900.5 was predominantly produced in inhibited regions (blue line, Figure 20). The other two fragments were produced predominantly without inhibitor. This finding suggested that different sets of proteases are responsible:

1. Without PIM: *m/z* 1347.7 → 1104.6 → 753.4 → X
2. With PIM: *m/z* 1347.7 → 900.5 → X

In brain, the standard deviations were very high, so no difference could be observed.
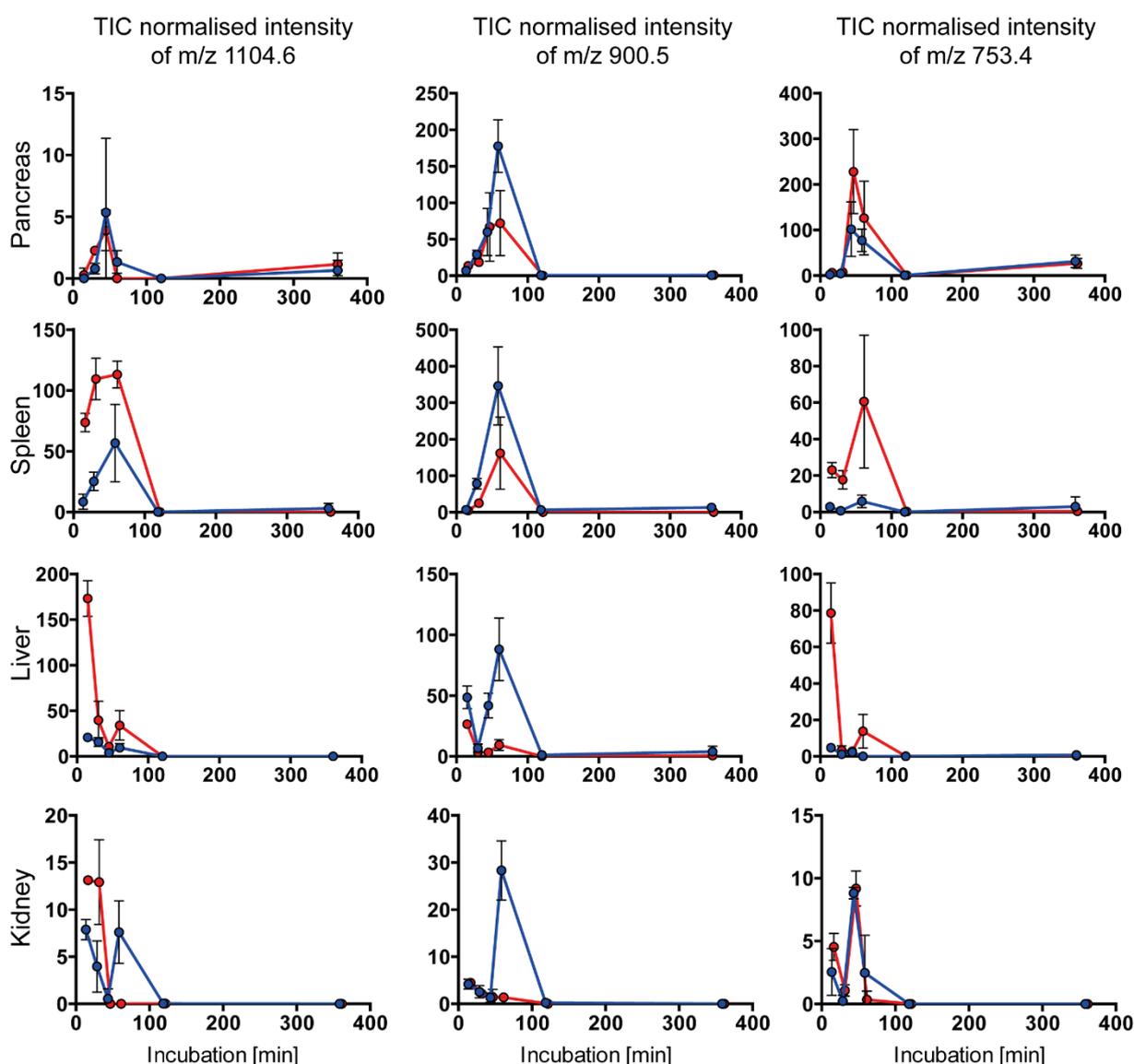


**Figure 20: Transient presence of substance P cleavage products is modulated with PIM** TIC-normalised ion intensities were extracted from mean spectra of porcine tissue of the areas without (orange line) and with (blue line) protease inhibitor mix (PIM) (S/N>5). The intensities of putative substance P cleavage products *m/z* 1104.6, 900.5 and 753.4 that are generated transiently are plotted versus the incubation time. Note that *m/z* 900.5 was recorded with higher intensity in PIM containing regions.

The effect of PIM indicated that the reduction of substance P signal was not due to uncontrolled effects like sequestering or adsorption of substance P into the tissue, but rather was related to real protease-driven digestion.

### 4.1.4 Inhibitor-concentration dependency of proteolytic activity in porcine tissue

An inhibitor-concentration-dependency of substance P cleavage would be a further confirmation of true protease reaction. Different working concentrations of PIM stock (10 x, 2.5 x, 1.0 x, 0.5 x, 0.25 x and 0.1 x) were pipetted onto porcine tissue. Tissue protease activity was measured using MALDI MSI after 60 min incubation in SunDigest incubation chamber (N=2). Mean ion intensities per PIM region were extracted for substance P, and DE% was calculated according to equation (2) (Figure 22). Non-inhibited tissue showed very high DE% values, and muscle displayed essentially no protease activity, in line with the time-course results (Figure 19). In analogy with previous results and possibly due to heterogeneity brain tissue showed high variance (Figure 9). All other tissues showed non-linear decrease of DE% with increasing PIM concentration. The final DE% (highest PIM concentrations) are listed in Table 7 in ascending order. The tissue with the highest survival potency is pancreas, followed by spleen, kidney and liver.

**Table 7: DE% values with the highest PIM concentration and survival potency**

| tissue | DE% (N=2) | | survival potency |
|---|---|---|---|
| muscle | No activity | | |
| liver | 0 | 2 | |
| kidney | 2 | 7 | |
| spleen | 37 | 30 | |
| pancreas | 57 | 59 | |
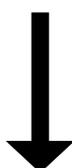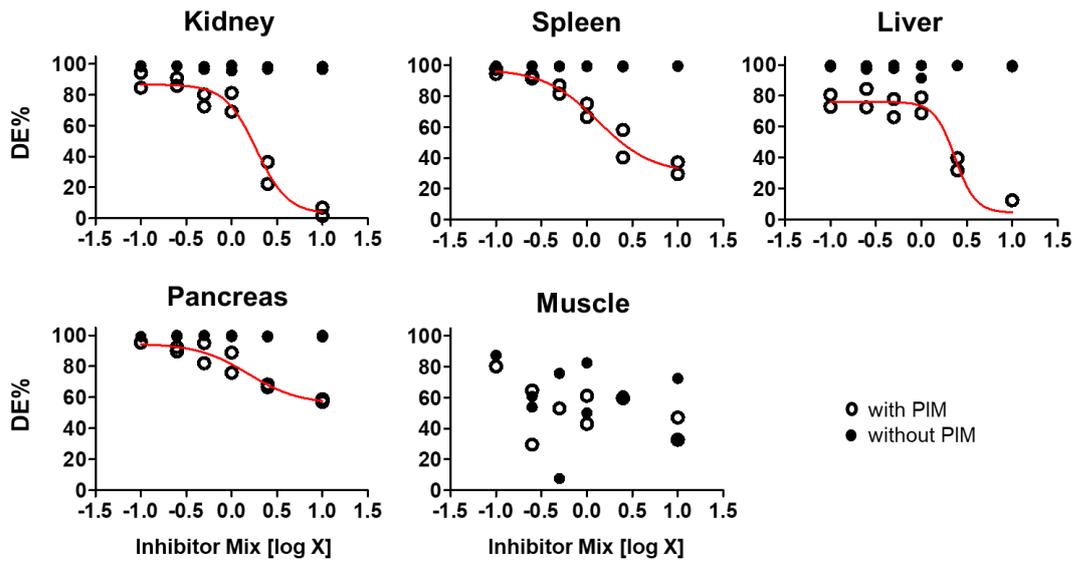
**Figure 21: Increasing dilutions of PIM promote a concentration-dependent decrease in DE%** Protease inhibitor mix (PIM) was diluted and pipetted onto each tissue (10 x, 2.5 x, 1.0 x, 0.5 x, 0.25 x, 0.1 x). "Digest" slide and "no-digest" slide were prepared and incubated for 60 min (N=2). The calculated DE% was plotted for inhibited (filled circles) and non-inhibited (empty circles) regions. Non-linear curve fitting with variable slope and four parameters were used.
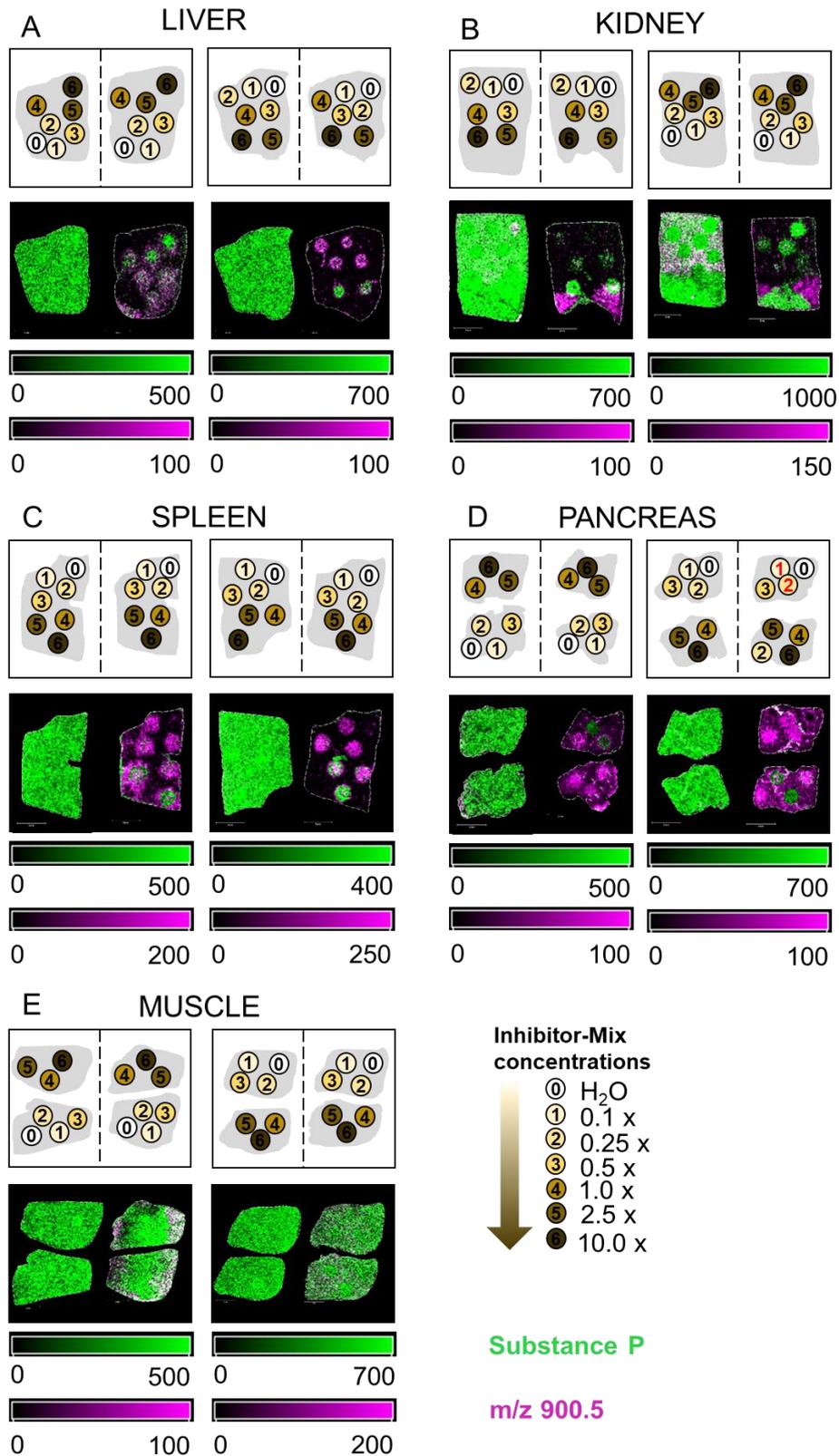
**Figure 22: Concentration-dependent attenuation of substance P cleavage by protease inhibitor mix dilution series** Protease-Inhibitor-Mix was diluted and pipetted on porcine tissue (**A – E**) according to the dilution scheme in the figure. "Digest"- and "no-digest"-slides were prepared, followed by incubation for 60 min at 37 °C and 95% humidity. The experiment was performed two times and both replicates were shown. MALDI-TOF MS ion images of substance P (*m/z* 1347.7 (green)) and a related peptide *m/z* 900.5 (purple) distribution was shown. The no-digest slides showed homogeneous distribution. A solvent spot ($H_2O$) showed no effect on the ionization. PIM on muscle (**E**) showed again no effect, which was consistent with the previous results.

### 4.1.5  Development of a photometric tissue-protease activity assay (TPPA)

It is one scientific aim to verify gained results with a comparable method. As no method for visualising overall protease activity was known, an in-solution method based on C. Cupp-Enyard's 'universal protease activity assay: casein as substrate' was adapted[113].

In the first run, the extraction of global proteases from tissue was necessary. For that a Tissue Protease Extraction Reagent T-PER (Thermo Scientific) was used. The reagent was described as a reagent for total protein extraction from tissue. It is mild as it contains a minimal amount of detergent for cell lysis and is suitable for kinase assays, suggesting that enzymes are in their native form. For the TPAA a total volume of 100 µL T-PER containing extracted proteins was required. T-PER in its normal form is a clear solution, not absorbing in the required wavelength of 660 nm. After the blank processing (no tissue extracted) high absorption values were observed. A dilution series of T-PER was used to define, if a lower amount of the reagent reduces the interfering absorption. The absorption of T-PER could be reduced to 0.1 with a high dilution (1 µL T-PER and 99 µL $H_2O$). With this dilution, the amount of extracted proteins was too small for the TPAA and thus not suitable.

With this information tissue extraction, using a buffer consisting of PBS containing 1% (w/v) Triton-X-100 and 0.05% (w/v) SDS (at pH 7.5 and 3.2), was compared to T-PER extraction. Spleen tissue was used and extracted, the protein amount was quantified using a standard Bradford assay. The results of the extraction buffer at pH 7.5 were comparable to T-PER extraction (Figure 23 A). Extracting the proteins from porcine tissue showed that most proteins were extracted from liver and the fewest from muscle tissue (Figure 23 B). The protein amount (in mg/mL) was used to normalise the calculated protease activity values.

In the TPAA the protein casein was used as substrate and released tyrosines were photometrically quantified ($\lambda$= 660 nm). Substance P could not be used as a substrate because it does not contain the amino acid tyrosine. The calibration curve of L-tyrosine (0.0055 – 0.11 µmol) was very reproducible and showed good linearity (N=3) (Figure 24 B). Pancreatin is an extract of active proteases from bovine pancreas. It was used for positive control resulting in a protease activity of 0.78 ± 0.12 unit/mL (1 mg/mL in H2O). For negative control, this solution was heat denatured (20 min, 95 °C) and a low protease activity of 0.02 ± 0.01 unit/mL was calculated (Figure 24 C).
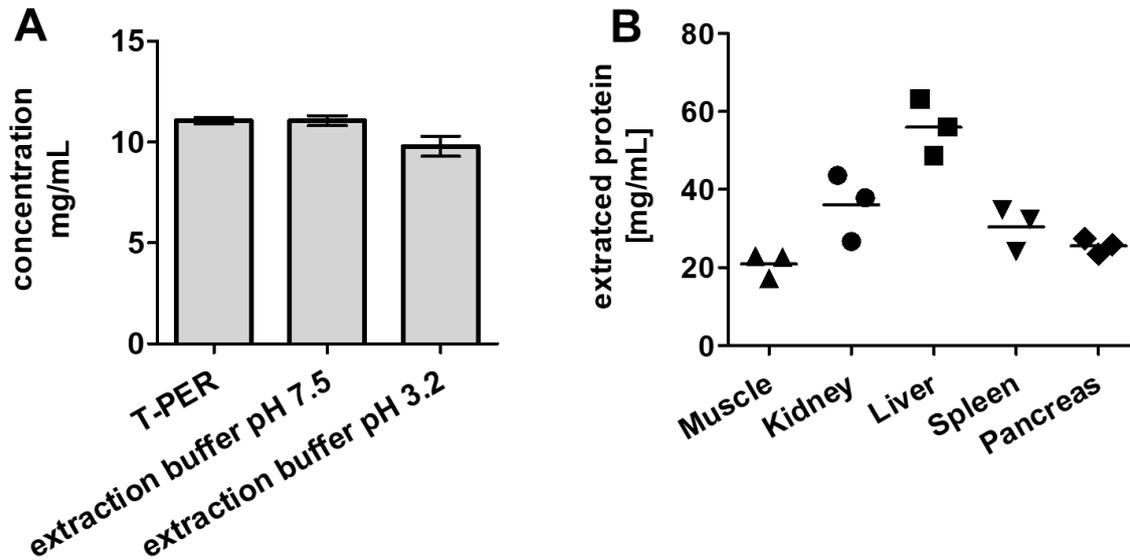
**Figure 23: Use of extraction buffer in comparison to T-PER** Tissue Protein Extraction Reagent T-PER (Thermo Scientific) is described to extract protein mildly and totally, in their active form **A** Extraction efficiency of suitable extraction puffer consisting of (PBS / 1% (w/v) Triton-X-100 / 0.05% (w/v) SDS) at pH 7.5 and 3.2 was tested. The extracted protein concentration is shown in the graph and showed good comparability for the 7.5 pH extraction buffer (N=3) **B** Frozen porcine tissues were cut into 30 µm slices, and six slices were collected for one extraction. Extraction was performed in 500 mg/mL wet tissue. Samples underwent five cycles of sonication and cooling on ice. The mixture was centrifuged, supernatant was collected and placed on ice. Protein quantification was done by Bradford assay. The extraction of the tissues resulted in differing protein concentrations, with the highest amounts for liver tissue, followed by kidney, spleen, pancreas and muscle (N=3).

For protein extraction frozen porcine tissue was cut into 30 µm slices. Six of them were used for one extraction. Using the extraction buffer (500 mg/mL amount of wet tissue/volume of extraction buffer) and the developed TPAA method, tissue protease activities of porcine tissue were quantified based on absorption values (equation (1)). The highest activity was found for pancreas tissue (8.1 ± 0.8 U/mg, N=3) followed by tissue from spleen, liver, kidney and muscle (Figure 24 A). One has to note that the activity per mL (U/mL) did not show this order, as different amounts of protein were extracted from the tissue. The results confirmed the MALDI MSI observation that muscle showed low to no protease activity and pancreas the highest. The ranking of protease activity spleen > liver > kidney was also confirmed, compared to the survival potencies of the inhibitor-concentration experiment (Table 7).

**A**

| | Muscle | Kidney | Liver | Spleen | Pancreas |
|---|---|---|---|---|---|
| **Activity [U/mL]** | 0.040 ± 0.007 | 0.107 ± 0.002 | 0.0305 ± 0.017 | 0.174 ± 0.003 | 0.779 ± 0.116 |
| **Protein amount [mg/mL]** | 21.0 ± 3.22 | 36.1 ± 8.64 | 56.0 ± 7.29 | 30.4 ± 5.55 | 25.6 ± 1.99 |
| **Activity [U/g]** | 2.0 ± 0.7 | 3.1 ± 0.9 | 5.5 ± 0.6 | 5.9 ± 1.1 | 8.1 ± 0.8 |

**B** calibration curve

$y = 7.27x + 0.00973$
$R^2 = 0.998$

**C** Positive control   Negative control
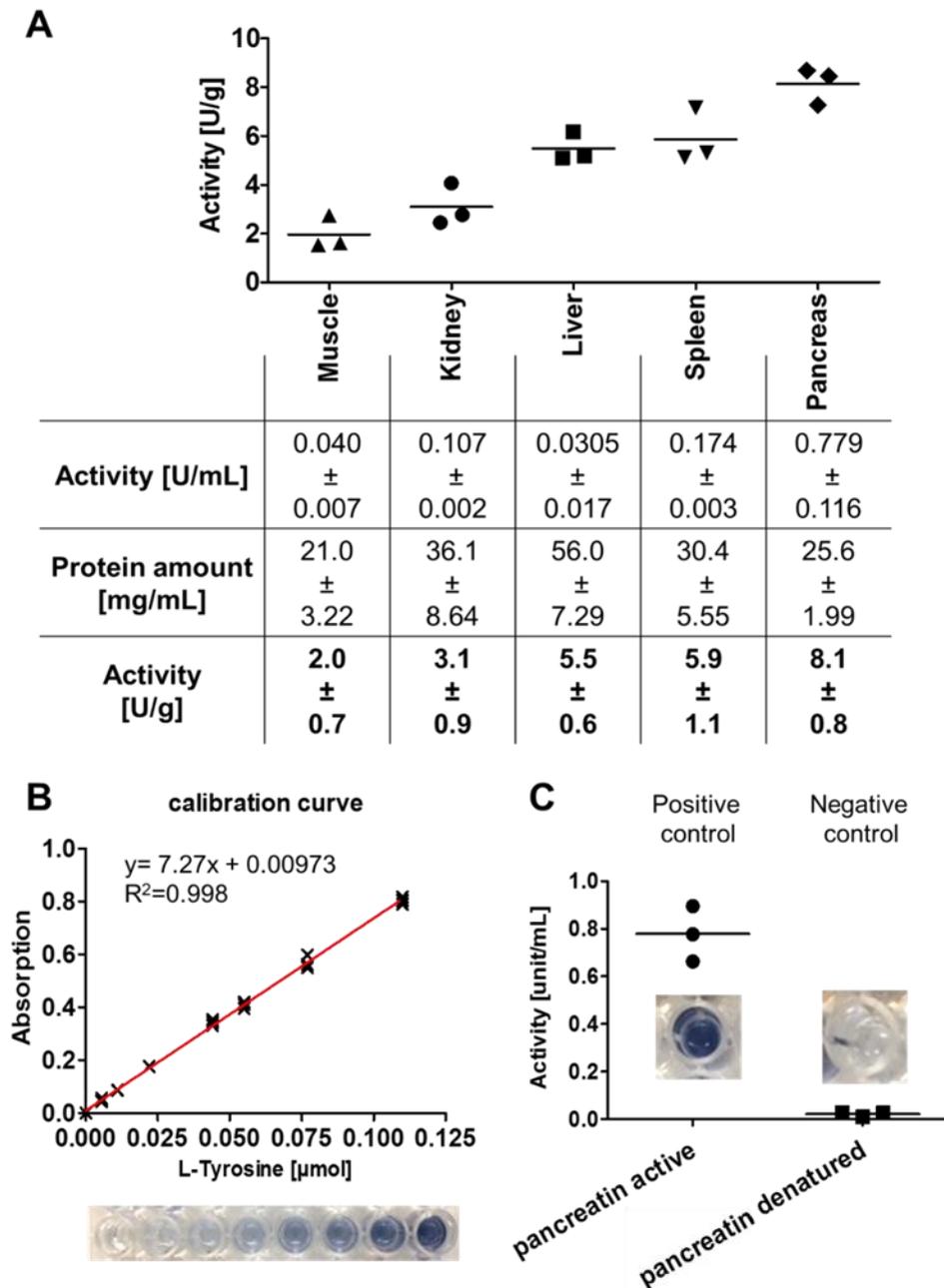
**Figure 24: Tissue activities, calibration curve and controls of TPAA** To assess protease activity of the extracted proteins casein was placed at 37 °C. Then protein extract was added and incubated at 37 °C. The reaction was stopped by adding TCA and further incubated. Protein precipitate was separated by centrifugation. Finally, sodium carbonate and Folin & Ciocalteau's phenol reagent were added to the supernatant and again incubated. For detailed volumes, concentrations and incubation times see method section 3.2.3. **A** The calculated activity values based on casein conversion to free tyrosine were shown in the table. When activity in U/mL was normalized on the extracted protein amount, the activity in U/g of the tissue showed same ranking of high activity in pancreatic tissue to low activity in muscle tissue. **B** The released tyrosine concentration was calibrated with high correlation coefficient. **C** As positive control native pancreatin solution (1 mg/mL in $H_2O$), which is a protease extract from porcine pancreas, was used. Heat-denatured pancreatin solution was used as negative control. Both solutions were used in the TPAA and showed reproducible results. (N=3)

## 4.1.6  Proteolytic activity of tumorous and non-tumorous tissue

In the next step the methodology should be transferred to visualise endogenous protease activity to preclinical studies. Transgenic CEA424-SV40 Tag C57BL/6 J mice

develop spontaneous gastric carcinoma[110,125]. Earlier studies showed that the potassium adduct of the lipid PC(34:1) [M+K]$^+$ = 798.54 is enriched in the tumour tissue[114,126]. Wild-type and tumour bearing tissue were first tested for selectivity (0 min, red spectra in Figure 25 A) in the mass ranges of substance P and its related peptides. Additionally, the tissue was checked for aging-related changes at RT (after 5, 10, 15 and 60 min), as it is known that protease activity changes the peptidome of tissues[124,127]. None of the spectra showed interfering peaks for TCEA positive or WT tissues (Figure 25 A). Some signals could be observed in the vicinity of *m/z* 753.4, as most lipid signals occurred in the range of *m/z* 600 to 1100.
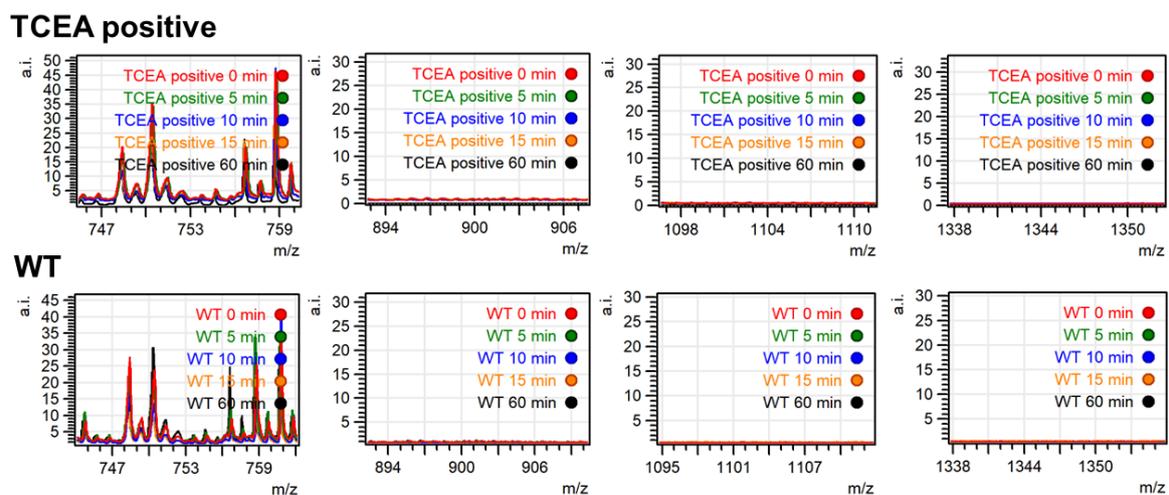


**Figure 25: Aging-related changes on TCEA positive mouse stomach could not be observed** TCEA positive and wild-type tissue was kept at RT (spectra colour: green 5min, blue 10min, orange 15min, black 60min) prior to MALDI matrix application compared to immediately used tissue (red spectra, 0min at RT). Shown are mean spectra of MALDI MSI. In the observed mass ranges for the resulting peptides (*m/z* 753.4, 900.5, 1104.6) and substance P (*m/z* 1347.7) itself no interfering signal was observed.

For visualising endogenous tissue protease activity in mouse tissue, the incubation time was reduced to 30 min, as the fragments of substance P could be measured with higher intensity (Figure 26). Substance P distribution was shown in blue, the lipid signal PC(34:1)+K$^+$ in red. The overlay on the left side showed that no substance P signal is left after 60 min of incubation. In addition, the signal intensities of the produced peptides were very low. With 30 min of incubation, all peptides could be visualised. Note that the intensity of substance P was reduced in regions were the tumour lipid marker was increased. With this reduced incubation time all further experiments were performed.
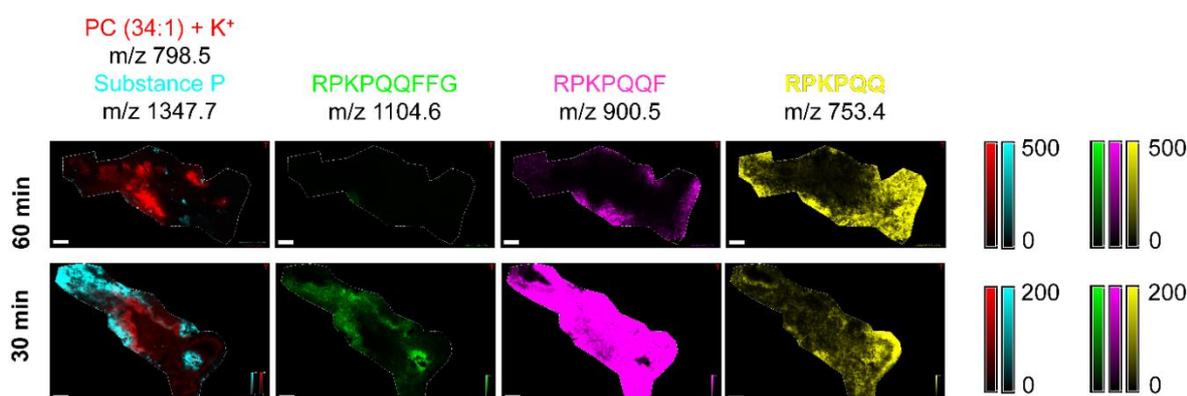
**Figure 26: Incubation time optimisation for mouse stomach endogenous protease activity** When stomach tissues were incubated for 60 min during sample -preparation, no substance P signal was measured. The resulting peptides *m/z* 1104.6, 900.5 and 753.4 showed very low signal intensity. When incubating a consecutive slice for 30 min we were able to monitor the residual substance P signal. Further, the related peptide signals were visible as seen in the lower panel.

## Evaluation of tissue protease activity in TCEA-positive mouse stomach

Tissue protease activity of TCEA positive mouse stomachs was first imaged on a MALDI TOF MS instrument, the rapifleX (Bruker Daltonics) (N=3). On one slice protease inhibitor mix was applied and results with and without PIM were compared. MALDI MSI ion distributions of the lipid tumour marker PC(34:1)+K$^+$ [114], substance P, and its related peptides were shown for one representative replicate (Figure 27 A). The second replicate (replicate 2) was measured additionally using MALDI FT-ICR mass spectrometry. For statistical analysis of the ion distribution, spatially-aware shrunken centroid clustering was performed by D. Abu-Sammour[h]. By reducing the mass range for the calculation to *m/z* 798.54 ± 5 (798.54 ± 0.05 for MALDI-FT-ICR data) and restricting the cluster to r=2, two segments (tumour (T) and non-tumour (NT)) were calculated (Figure 27 B). The segments correlated well with the H&E annotation of tumour tissue and tumour-mucosa transition zone in all replicates, regardless of PIM application. Annotated muscularis and mucosa correlated with NT segment (Figure 28 B). When segmentation was performed with the FT-ICR mass spectrometry data, the segmentation was sharper, probably due to higher mass resolution (Figure 28 A).

For statistical analysis intensities of *m/z* 1347.73, 1104.59, 900.50 and 753.43 were extracted for each pixel of the segments T and NT (Figure 28 C) for both conditions +PIM (+) and –PIM (-). The intensities were log$_{10}$ transformed for visualisation because of a wide spread of intensities. In the NT segment higher ion intensities of substance

---

[h] The spatially-aware shrunken centroid clustering analysis had been performed by D. Abu-Sammour as described in Erich *et al.* (2019)[115]

P were found then in the T segment, regardless of PIM addition. Further, *m/z* 1104.6 was increased in T segments, *m/z* 900.5 showed nearly no difference and *m/z* 753.4 was increased in inhibited T+ segments (Figure 28 C). Regarding the segmentation, higher mass accuracy and resolving power improves the result, as less scattering was visible. FT-ICR MS CID fragmentation was used on the tissue to confirm the identity of the observed peptides. The intense signals *m/z* 1347.735, 900.504 and 753.435 were fragmented, and b-ion series in the MS/MS spectra indicate their origin from substance P (Figure 29). For *m/z* 1104.6 the accumulated intensity was below the required intensity for successful CID. These results substantiated the interpretation that tissue protease activity monitored by MALDI MSI showed differentially distributed activity. The activity seems to be higher in tumorous tissue and susceptible to PIM inhibition.
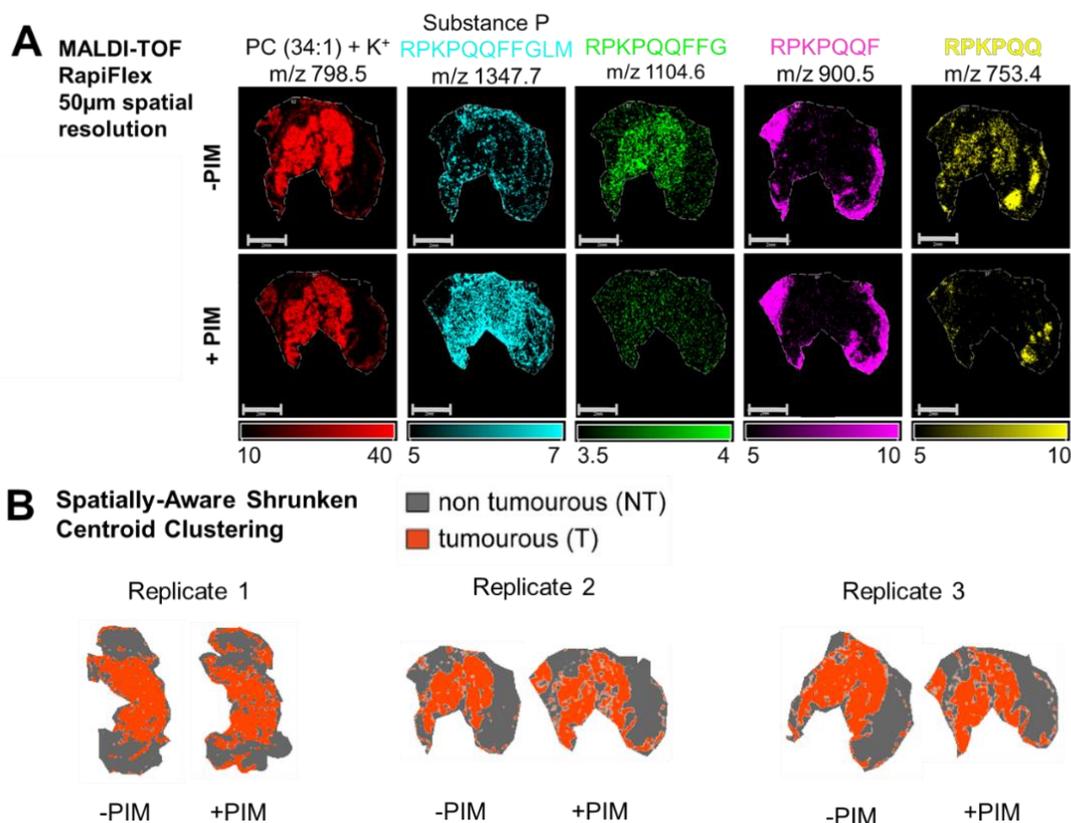


**Figure 27: MALDI-TOF data of TCEA-positive mouse stomachs** Two cryosections of CEA424-SV40 Tag-positive stomachs were melted onto ITO slides, one of which was covered with protease inhibitor mix (+PIM). All tissues were covered with substance P and incubated for 30 min at 37 °C. **A** For one representative tissue the MALDI MS ion images of the tumour lipid *m/z* 798.5 (PC (34:1) + K⁺), *m/z* 1347.7 (substance P), and peptides cleavage products (*m/z* 1104.6, 900.5, 753.4) were shown. Note that areas of highest concentration of *m/z* 753.4 represent peptide wash-out outside the tissue. **B** The images showed an automated identification of tumorous (T) and non-tumorous (NT) tissue by segmentation with spatially aware shrunken centroid clustering for all three replicates[i]

---

[i] The spatially-aware shrunken centroid clustering analysis had been performed by D. Abu-Sammour as described in K. Erich et al[115]
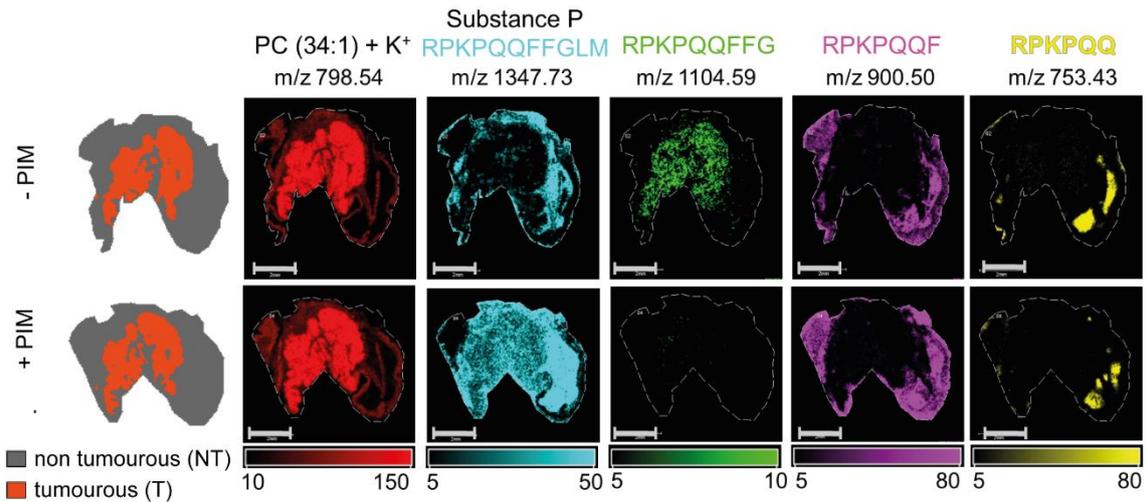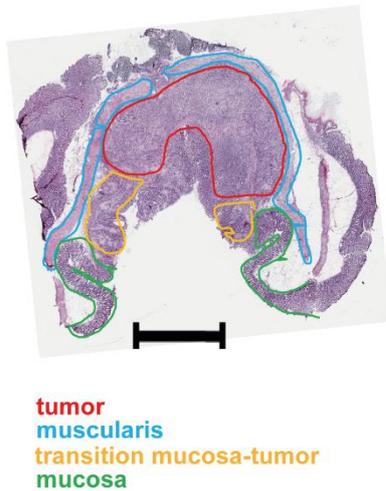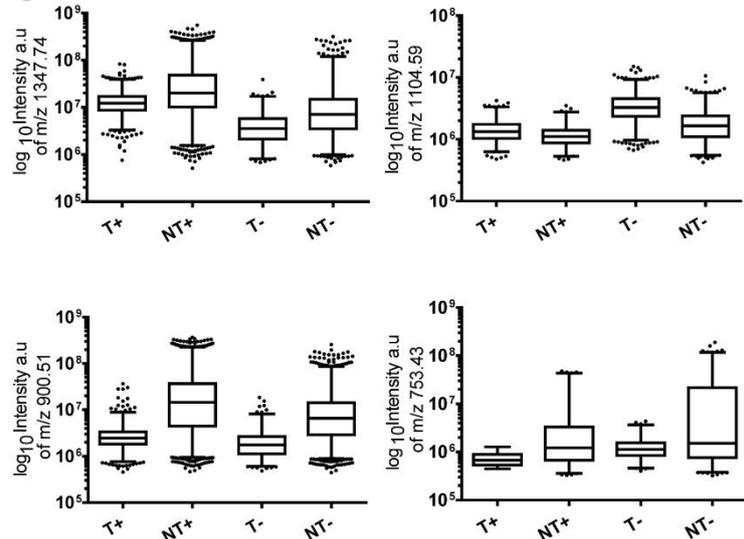
**Figure 28: MALDI-FT-ICR of TCEA positive mouse stomach** The stomach of transgenic CEA424-SV40 Tag-positive tumour-bearing mouse was dissected and immediately frozen. Two cryosections were melted onto an ITO slide, one which was covered with protease inhibitor mix (+PIM). All tissues were covered with substance P and incubated for 30 min at 37 °C. MALDI MSI was acquired with 50 µm spatial resolution on a SolariX FT-ICR instrument. **A** Showen on the left is the automated identification of tumorous (T) and non-tumorous (NT) by segmentation with spatially aware shrunken centroid clustering[j]. The MALDI MS ion images of the lipid *m/z* 798.54 (PC (34:1) + K^{+}), *m/z* 1347.73 (substance P) and peptides cleavage products (*m/z* 1104.59, 900.50, 753.43) are shown. Note that areas of highest concentration of *m/z* 753.43 represent peptide wash-out outside the tissue. MALDI-FT-ICR ion images have higher mass accuracy and sharper segmentation results than MALDI-TOF images and also show the inhibitor mix' effect on substance P cleavage and the production of truncated peptides. **B** After data acquisition slides were H&E stained, and tumour, mucosa, tumour transition tissue and muscularis were annotated. **D** For pixel-wise statistical analysis, intensities for *m/z* of substance P and resulting peptides were plotted for all pixels on a logarithmic scale. Scale bar is 2 mm.

---

[j] The spatially-aware shrunken centroid clustering analysis and pixel-wise intensity extraction had been performed by D. Abu-Sammour as described in K. Erich et al[115]
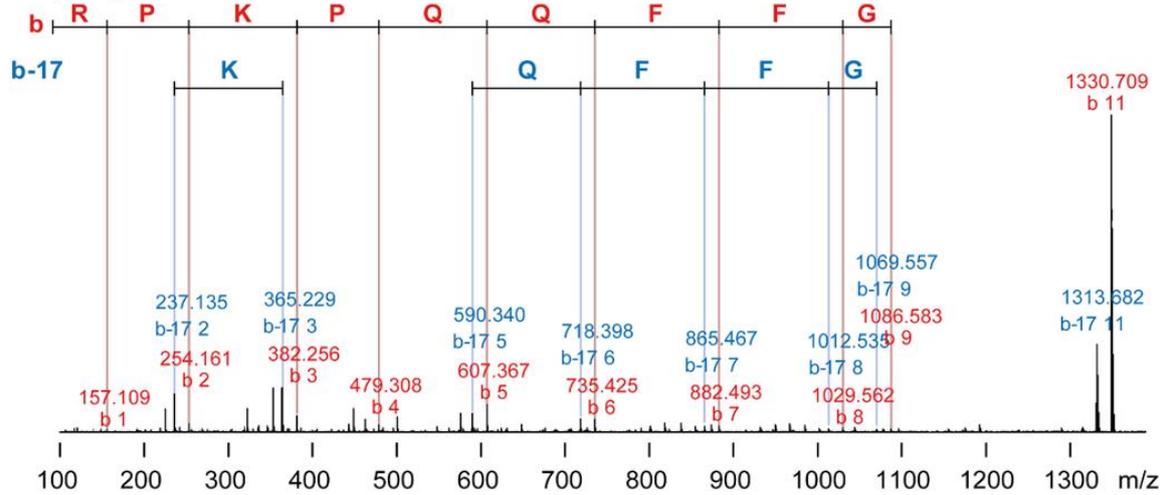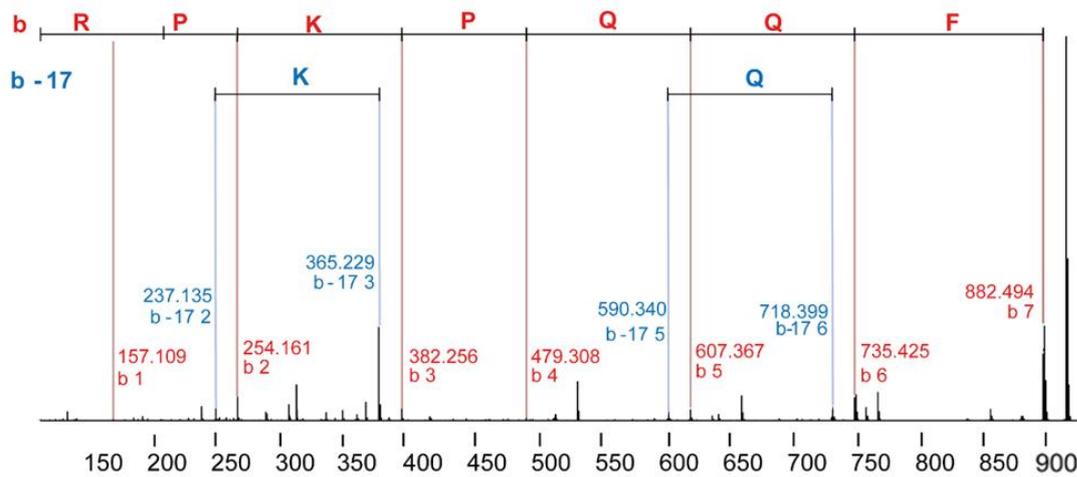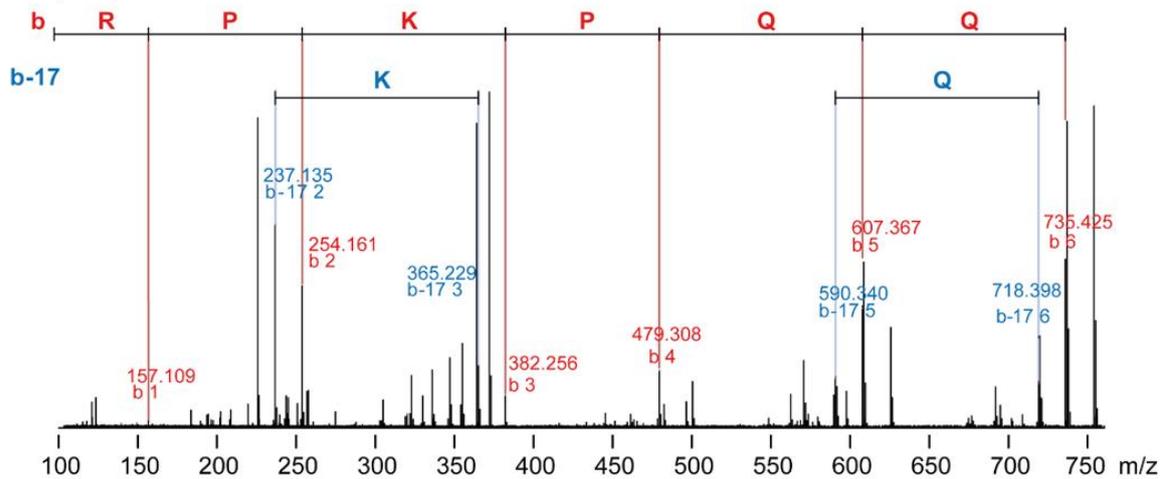
**Figure 29: B-ion series in MS/MS spectra of fragmented highly abundant peptides reveal stretches of substance P sequence** Using MALDI-FT-ICR tandem MS of those *m/z* was performed with optimised CID energies on tissue samples. The sequence of substance P (*m/z* 1347.735) RPKPQQ (*m/z* 753.435) and RPKPQQF (*m/z* 900.505) were fully sequenced and verified.

## Influence of pH on tissue protease activity in gastric mouse tumour tissue

As protease activity is prone to environmental tissue conditions like salt-concentration, pH and other co-factors, tissue protease activity was tested for its reaction to altered tissue pH. Tumour containing mouse stomachs were washed with ammonium formate (pH 3 and pH 7), and tissue protease activity was measured by MALDI MSI (N=3). Washing was performed by rinsing the tissue two times with 1 mL of the respective buffer[128]. It effectively removed potassium adducts of PC(34:1), as only the hydrogen adduct represented the tumour after washing (Figure 30 C). Its distribution was less confined, and more background signal in non-tumorous tissue was visible (Figure 30 A). Regarding tissue protease activity higher signals of residual substance P were found, when tissue was washed with ammonium formate at pH 7 (Figure 30 B). It seems that the proteases responsible for the digestion of substance P required acidic pH, whereas the digestion was reduced with neutral pH. Intensity comparison of tissue without wash (std) and wash with ammonium formate pH 3 showed similar results. However, the spatial distribution of the substance P signal was indeed different. By washing the tissue, more substance P could be found in the tumorous tissue.
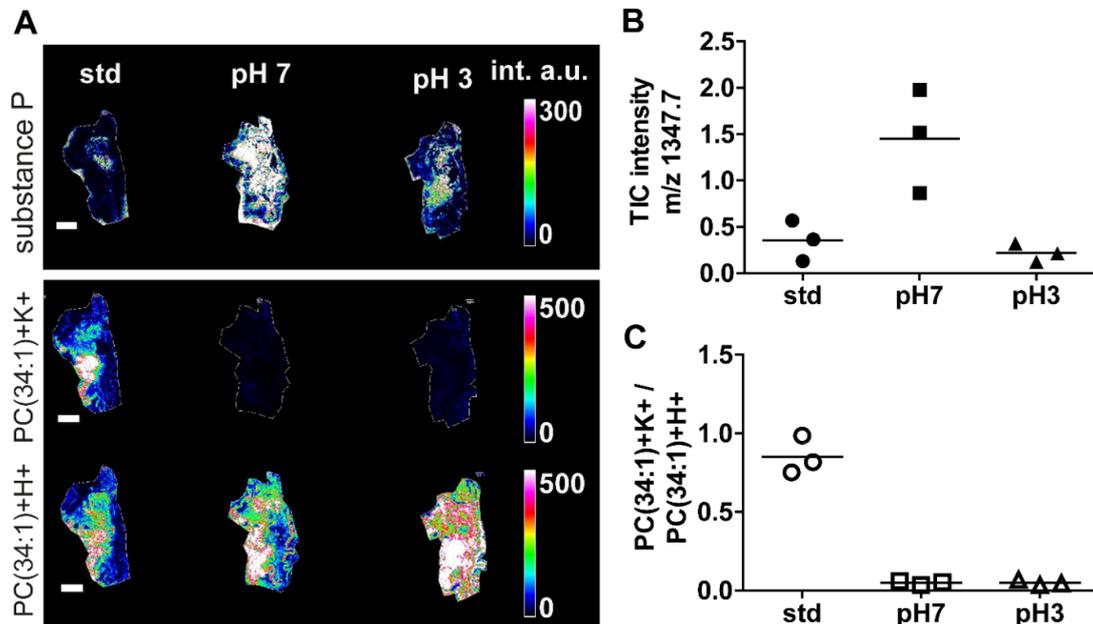


**Figure 30: pH changed the proteolytic activity of TCEA positive mouse stomach** . Stomach tissue samples were washed with ammonium formate (pH 3, pH 7), dried under vacuum, and proteolytic activity was assessed **A** MALDI MSI of one representative tissue slice was shown. Ion distributions refer to substance P PC(34:1) + K$^+$ in the upper panel, +H$^+$ in the lower panel. **B** The experiment was performed in triplicates and the TIC normed intensities of substance P were shown in the scatter plot. Substance P had the highest intensity in the tissue washed with ammonium format pH7. When washed with ammonium formate pH 3 the intensity of substance P was reduced as the standard procedure without washing. **C** The ratio of PC(34:1)+K$^+$/PC(34:1)+H$^+$ confirmed, that washing reduced the adduct formation. In addition, in the MALDI MSI, it was clearly visible, that the potassium adduct was only present in the unwashed tissue slice. Scale bar 2 mm; N=3.

**Proteomics study of mouse gastric cancer tissue with focus on peptidases**

A proteomic study was performed to further investigate the difference of protease expression between tumourous and non-tumorous tissue. The first obstacle was the accessibility of pure tumour and non-tumour tissue. Therefore, TCEA positive mouse stomachs (N=3) were sliced on the cryostat. The whole slice was stored in vials labelled as TS (tumour-stomach). Further, MALDI MSI was acquired to localise the tumour (Figure 31). According to these results, the tissue was further sliced manually (white line, Figure 31). Tumour samples (T) and non-tumour samples (NT) were manually excised and used for quantitative proteomic analysis[k]. This preparation was not ideal for gaining pure tumour tissue, but suitable for low sample amounts as in mouse stomach. In addition, WT stomachs were sliced and used as reference tissue (N=3).
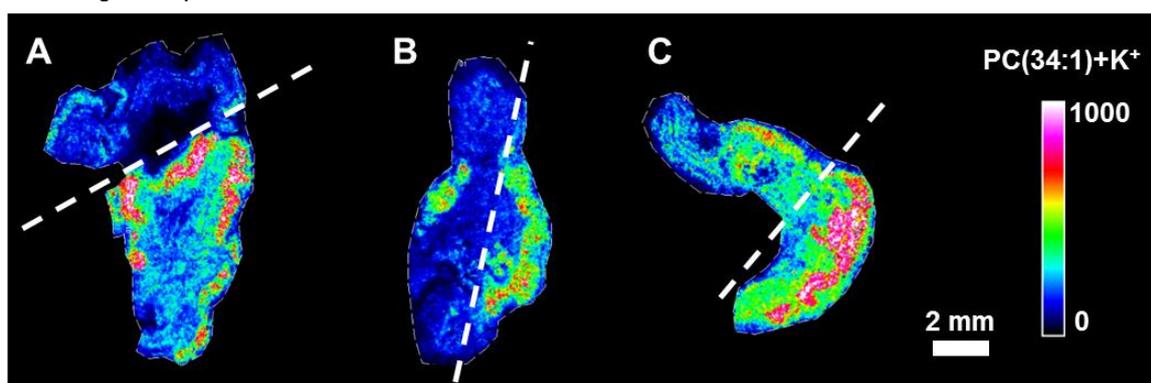


**Figure 31: MALDI MSI of TCEA positive mouse stomachs to localise the tumour** The MALDI MSI has been performed prior to the separation of the tissue to locate the tumour tissue. The signal of PC(34:1)+K+ is highly enriched in the tumour. Shown are the three biological replicates used in the proteomics study (**A, B, C**). The white line shows the separation of tissue to gain tumour (T) and non-tumour (NT) samples.

In total 3394 proteins were identified and quantified using label-free quantification (LFQ). By filtering the UniProt database search (organism:mouse, reviewed:yes, gene ontology:proteolysis GO:0006508) for enzymes with "enzyme class" of peptidases (EC3.4.-.-), 537 proteases were found. From all identified proteins 104 were thus identified to be peptidases. Principal component analysis (PCA) and hierarchical

---

[k] Bottom-up proteomics experiments were performed by Torsten Müller at the German Cancer Research Center (DKFZ) in the group of Prof. Dr. Jeroen Kriijgsveld as described in K. Erich *et al.* (2019)[115]

clustering (HC) were accomplished for all identified proteins[I] (Figure 32). When statistical analysis was performed on all identified peptidases, the PCA showed independent groups for WT, NT and T tissue. Component 1, which describes the biggest difference in the samples, showed the highest variance between WT and T sample. NT data points were spread in between those two. HC showed grouping of WT and NT tissue, with one origin. A second group consisted of T was found. Therefore, the NT sample displayed more similarities to WT tissue, as to tumour and tumour-containing tissue.
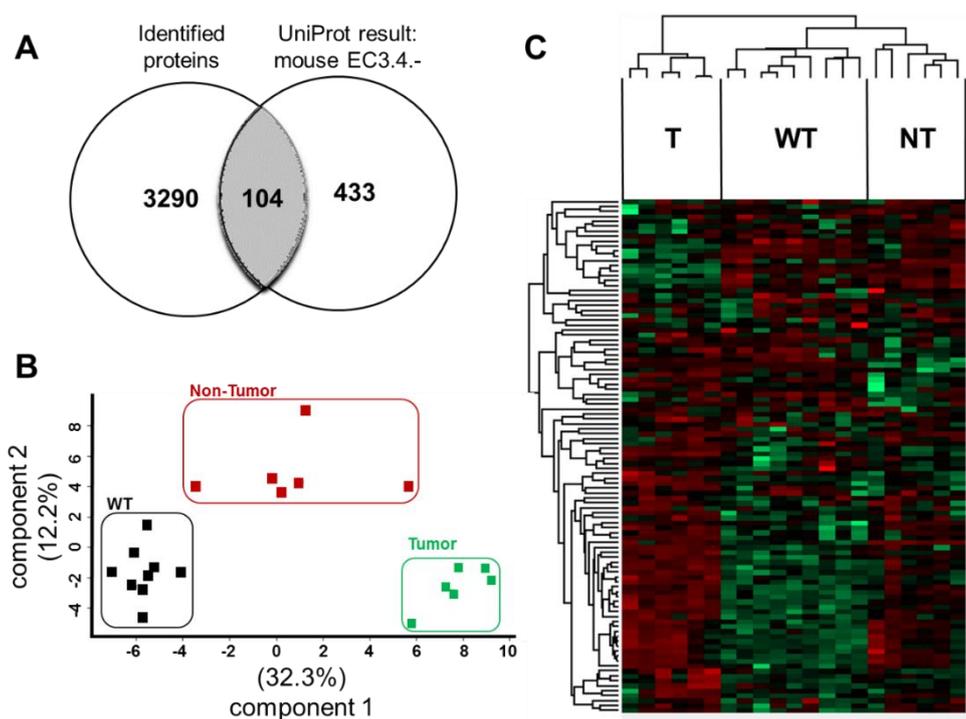


**Figure 32: Statistical analysis of proteomic results for all identified peptidases without TS samples A** In the proteomic analysis of wild-type stomach (WT), separated tumour (T) and non-tumour (NT) tissue samples 3394 proteins were identified. In the UniProt database there are 537 hits for proteins in the organism: mouse having the GO-term: proteolysis (GO:0006508) and an EC number of 3.4.-.-, representing peptidases. The comparison showed that 104 peptidases were identified. **B, C** Using the information of all identified proteins and their (label-free quantified) LFQ intensity for hierarchical-clustering (HC) and principal-component-analysis (PCA) the three tissue groups can clearly be separated.

Statistical analysis based on the identified proteases showed also a separation in PCA space and in HC analysis. In sum, these results indicated that the expression levels of proteases are different between tumour and non-tumorous tissue, with some uncertainty about the state of the non-tumorous tissue.

---

[I] Statistical analysis were performed by Torsten Müller at the German Cancer Research Center (DKFZ) in the group of Prof. Dr. Jeroen Krijgsveld as described in K. Erich *et al.* (2019)[115]

Using limma statistics[129] the fold-change values were used to identify peptidases that differ significantly between T and NT[m] (Table 8). The most dominant differently expressed protease was the proteasome subunit beta type-10 (EC 3.4.25.1). Further, comparison of T and WT was performed. Here, two differentially expressed proteases were found: Caspase 7 (EC 3.4.22.60) and Endoplasmic reticulum aminopeptidase 1 (Q9EQH2) (Table 9).

**Table 8: List of significantly changed proteases comparing tumour and non-tumour-tissue** In the statistical analysis of T against NT samples two peptidases were identified to be weakly but significantly changed (fold-change >1.5 or <-1.5 and p-value <0.05).

| UniProt | Protein name | Nb. of identified peptides | Sequence coverage % | EC number | MEROPS ID |
|---|---|---|---|---|---|
| Q9EQH2 | Endoplasmatic reticulum aminopeptidase 1 | 11 | 14 | 3.4.11.- | M01.018 |
| P97864 | Caspase-7 | 4 | 17.5 | 3.4.22.60 | C14.004 |

**Table 9: List of significantly changed peptidases comparing tumour and wild-type-tissue** In the statistical analysis of T against WT samples 22 proteases were identified to be significantly changed (fold-change >1.5 or <-1.5 and p-value <0.05). From those 22 identified proteases, 14 are described as peptidases with EC 3.4.-.-. Further enzymes belong to the class of Hydrolases, Acetyltransferase and Glycosyltransferase.

| UniProt | Protein name | Nb. of identified peptides | Sequence coverage % | EC number | MEROPS ID |
|---|---|---|---|---|---|
| O35955 | Proteasome subunit beta type-10 | 3 | 18.7 | 3.4.25.1 | T01.014 |
| O55234 | Proteasome subunit beta type-5 | 8 | 28.8 | 3.4.25.1 | T01.012 |
| P07146 | Anionic trypsin-2 | 2 | 12.2 | 3.4.21.4 | S01.064 |
| P18242 | Cathepsin D | 11 | 31.7 | 3.4.23.5 | A01.009 |
| P20918 | Plasminogen | 9 | 13.5 | 3.4.21.7 | S01.233 |
| P28076 | Proteasome subunit beta type-9 | 2 | 8.7 | 3.4.25.1 | T01.013 |
| P70398 | Probable ubiquitin carboxyl-terminal hydrolase FAF-X | 16 | 7.2 | 3.4.19.12 | C19.017 |
| P97864 | Caspase-7 | 4 | 17.5 | 3.4.22.60 | C14.004 |
| Q6A4J8 | Ubiquitin carboxyl-terminal hydrolase 7 | 10 | 11.2 | 3.4.19.12 | C19.016 |
| Q6P1B1 | Xaa-Pro aminopeptidase 1 | 6 | 11.2 | 3.4.11.9 | M24.009 |
| Q80W54 | CAAX prenyl protease 1 homolog | 5 | 15.8 | 3.4.24.84 | M48.003 |
| Q9CR35 | Chymotrypsinogen B | 6 | 31.6 | 3.4.21.1 | S01.152 |
| Q9CYN2 | Signal peptidase complex subunit 2 | 13 | 53.5 | 3.4.-.- | - |
| Q9D7R7 | Gastricsin | 7 | 18.4 | 3.4.23.3 | A01.003 |

---

[m] Statistical analysis were performed by Torsten Müller at the German Cancer Research Center (DKFZ) in the group of Prof. Dr. Jeroen Kriijgsveld as described in K. Erich *et al.* (2019)[115]

### 4.1.7 Proteolytic activity of human gastric biopsy samples

**Tissue protease activity in human gastric biopsy**

To conclude this proof-of-concept study the potential of the method was evaluated for its translation into clinical research. Sections of gastric biopsy with substance P were incubated for 30 min and MALDI-TOF MSI (resolving power R ~10,000; mass accuracy < 30 ppm) as well as MALDI-FT-ICR MS images (resolving power R ~100,000; mass accuracy < 3 ppm) at 20 µm spatial resolution were acquired. Notably, low protease activity in muscular tissue was consistently found in porcine skeletal muscle (Figure 12), mouse *muscularis mucosae* and muscle in human gastric adenoma (Figure 33). In analogy with the mouse tumour-mucosa transition zone after 30 min of incubation the substance P cleavage product *m/z* 753.4 was enriched in a similar zone in the human adenoma. The same was true for the transient accumulation of *m/z* 900.5 in glandular gastric mucosa (Figure 33). These results were obtained by MALDI-TOF and MALDI-FT-ICR mass spectrometers. With higher spatial and mass resolution the image quality was improved.
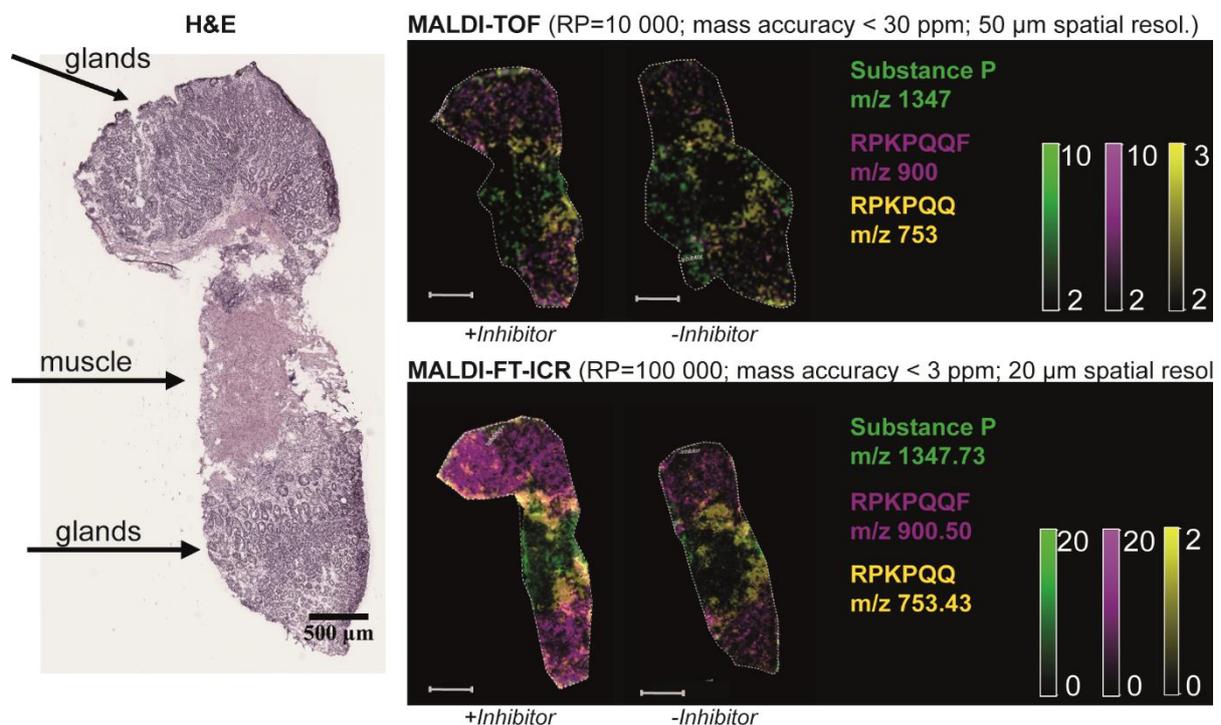


**Figure 33: Human gastric adenoma biopsy showed lower protease activity in muscularis than surrounding glandular tissue** Gastroscopic biopsy was taken and immediately frozen to -80 °C. Two cryosections were prepared, of which one was immediately covered with protease inhibitor mix. Further two tissue slices were covered with substance P and incubated for 30 min at 37 °C. MALDI MS images were acquired using MALDI-TOF instrument (50 µm spatial resolution, RP=10 000, mass accuracy < 30 ppm) and MALDI-FT-ICR instrument (20 µm spatial resolution, RP=100 000, mass accuracy <3 ppm). H&E staining was performed on an adjacent section. Substance P signal (green) was still visible after 30 min in muscle tissue, whereas the glandular tissue prominently displayed the cleavage product at *m/z* 900.5 (purple). The same distribution was found in FT-ICR MS measurement, albeit with higher mass accuracy. White scale bar = 1 mm

## Comparison of proteolytic activity of human adenoma and normal gastric biopsies

It was now the idea to test human biopsies of gastric tumour tissue and normal gastric tissue for their tissue protease activity. Two patients who underwent gastroscopy were chosen by our partner Dr. Tobias Gropp (Department of Medicine II, Medical Faculty Mannheim, Heidelberg University). Multiple biopsies (Ø about 5 mm) were taken from tumorous tissues (adenoma) and from tissue far away from tumorous tissue (normal). Biopsies were immediately frozen to -80 °C and further processed in our lab. Each biopsy was sliced for H&E staining and histological annotation performed by Tobias Gutting (Department of Medicine II, Medical Faculty Mannheim, Heidelberg University). Only samples with confirmed tissue type (adenoma or normal mucosa tissue) were selected for further analysis. Three slices of each biopsy were placed on an ITO-glass slide for MALDI MSI. One slice was used for selectivity assessment and therefore not further processed (native). The second tissue slice was covered with PIM and substance P, whereas the last slice was only covered with substance P. The experiments were performed two times with two different incubation times (30 min and 15 min). Using DHB MALDI matrix acquisition was performed on MALDI-TOF MS rapifleX (Bruker Daltonics). The distribution of the substance P signal and the resulting peptide signal $m/z$ 900.5 was shown in Figure 33. Other resulting peptides were below the sensitivity level of the instrument. It was observed that no interfering signals were present in the native tissues regarding the mass range of substance P and $m/z$ 900.5. For patient 1 no clear difference in signal intensities for adenoma and normal tissue can be found. In patient 2, a difference was observed. Further, the ion distribution was consistent in the groups of tissue type and patients.

With 15 min incubation few $m/z$ 900.5 signal intensity was present, whereas after 30 min incubation, the peptide was clearly present. This was in line with the dynamic production of this peptide on porcine tissue, where no significant difference with and without PIM could be found after 15 min (Figure 20). Furthermore, the signal is more intense without PIM application on normal tissue. White pixels represented the co-localisation of substance P (green) and $m/z$ 900.5 (pink), so both peptides were present in the same pixel. This was clearly visible in patient 2 and slightly in patient 1. In contrast, adenoma tissue did not show $m/z$ 900.5 without PIM application. There were two possible reasons for that: It might have been, that the proteases present in tumour

did not produce this peptide, or the proteases were highly active, and the peptide was already further degraded and not present any more.

During the 30 min incubation experiment, in normal tissue more $m/z$ 900.5 and less substance P signal were found. This could be interpreted as an ongoing tissue protease activity and ongoing digestion of substance P. Further, the peptide $m/z$ 900.5 was present in the adenoma samples of patient 1 without PIM, and also slightly in adenoma samples of patient 2. Concluding that the peptide was produced in adenoma tissue, but in a transient state, which is not ideally covered at 30 min of incubation time. Further, the two cases of adenoma (-PIM) were not operating similar, as in patient 1 intense signal of $m/z$ 900.5 can be found.

Overall, the expectation of different tissue protease activity of tumorous and normal biopsies was supported by these data. It was not answered, if high tissue protease activity could be correlated with a low presence of $m/z$ 900.5. It can be concluded, however, that on human biopsies the degradation of substance P and production of $m/z$ 900.5 was sensitive to PIM. Thus it was feasible that a dynamic proteolytic process can be observed. Studies with optimized and standardised workflows and higher patient numbers are required for answering clinical questions.

| | sample | H&E | 30 min | | | 15 min | | |
|---|---|---|---|---|---|---|---|---|
| | | | -PIM | +PIM | native | -PIM | +PIM | native |
| patient 1 | adenoma 1 | | | | | | | |
| | adenoma 3 | | | | | | | |
| | normal 6 | | | | | | | |
| patient 2 | adenoma 5 | | | | | | | |
| | adenoma 4 | | | | | | | |
| | normal 7 | | | | | | | |
| | normal 8 | | | | | | | |
| | normal 9 | | | | | | | |
| | normal 10 | | | | | | | |
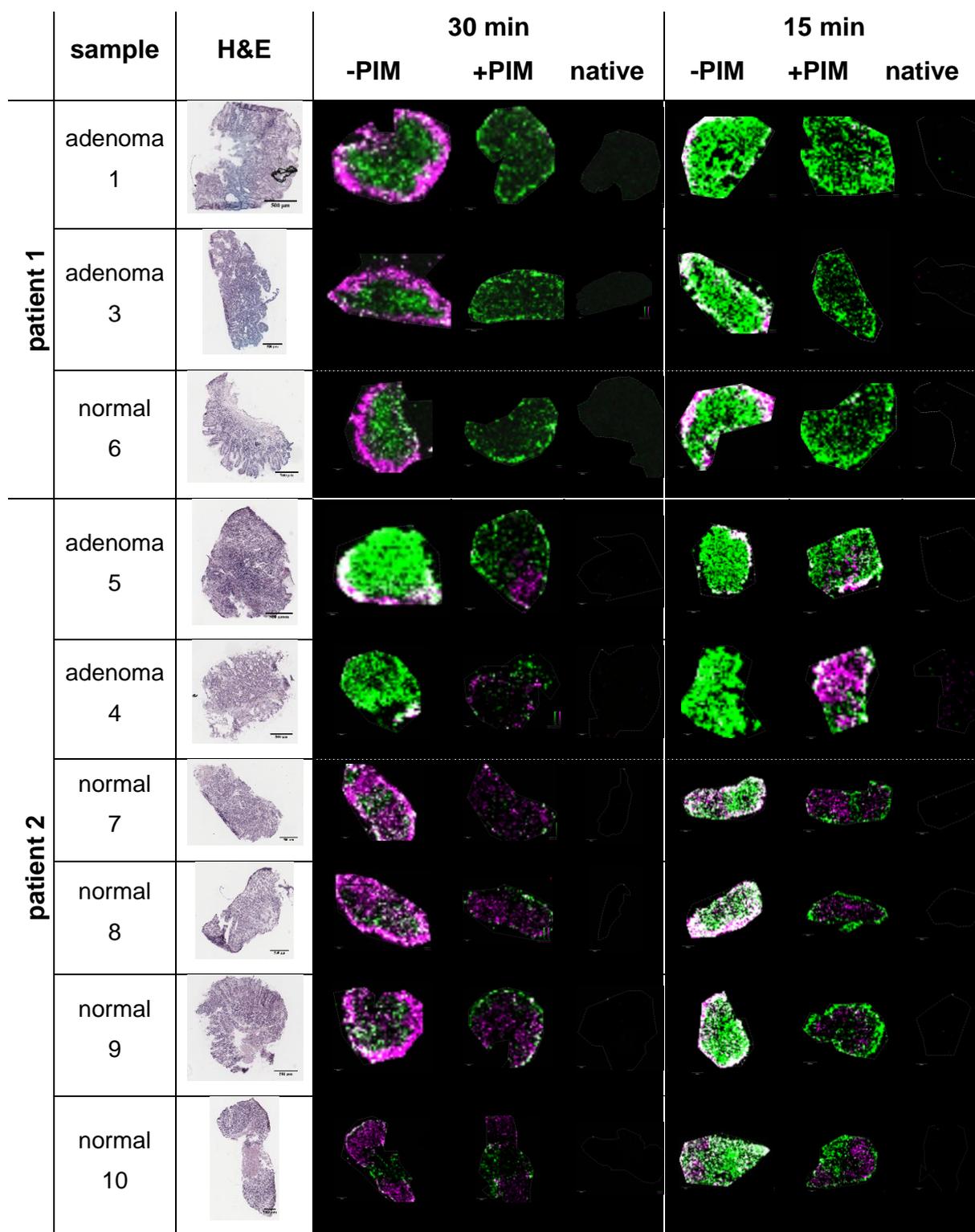
**Figure 34: Human gastric adenoma biopsy showed low protease activity in muscularis compared to surrounding glandular tissue** Gastroscopic biopsies were taken of two patients and immediately frozen to -80 °C. Three cryosections were prepared, of which one was immediately covered with protease inhibitor mix (+PIM). This and one more slice were covered with substance P. One slice was not covered at all (native). This setup was prepared two times and incubated for 30 min and 15 min (37 °C, 95% humidity). MALDI MS images were acquired using MALDI-TOF instrument at 50 µm spatial resolution. H&E staining was performed on the same section after washing away the MALDI matrix. Tissues were annotated based on the H&E stain into normal and adenoma tissue. Ion distributions of substance P (green) and *m/z* 900.5 (pink) are shown. If the masses co-localise the colour turned white. After 15 min incubation higher intensity of residual substance P was detected, whereas after 30 min, the resulting peptide was more dominant. Adenoma tissue and normal tissue show different behaviour regarding the degradation of substance P.

## 4.2 Part II - Development of scores for the assessment of quality factors using FFPE tissue digest

A method that should finally be applied for diagnostics or prognostic evaluation in clinics requires high standardization with guaranteed reproducibility and repeatability. In addition, the use of quality parameters is a prerequisite for routine clinical application. Score-based method development in MALDI MSI is still a rare occasion. The use of MALDI MSI however, can increase the understanding of molecular basis of tissue and thus give insights into mechanisms of disease[62,130,131]. MALDI MSI is a method with great potential in drug development[126,132,133], disciplines like studying plant organism[134] or textile surfaces[135], but also in clinical pathology[62,64,136]. Present publications show the use of MALDI MSI for therapy response prediction[137–139], disease classification[140–142] and assessing tumour heterogeneity[143,144].

As the method is still young (initially developed for proteins in the late 1990s)[145,146], MALDI MSI has deficits of quality criteria and validation criteria compared to standard analytical methods[147–149]. Quantitative LC-MS/MS methods, for example, are defined as reliable, if specificity, selectivity, accuracy, precision, recovery and reproducibility are fulfilled. Even the accepted range is defined in CV%-values (< 10%)[150]. Further, the positive and negative controls as well as blanks are a prerequisite in LC-MS/MS and should be added to MALDI MSI workflows as well.

In general, MALDI MSI requires distinct sample preparation, namely the application of MALDI matrix on fresh frozen tissue. The sample condition itself defines which steps are required to make the tissue accessible for the matrix co-crystallisation. Frozen tissue is vulnerable to temperature changes during excision and sample storage. In contrast FFPE tissue is stable over long storage time periods at RT. The preparation of FFPE tissue for MALDI MS require the removal of paraffin and retrieval of tissue antigens. Further, a digestion steps is necessary to cut proteins into small pieces, as only molecules up to 20 kDa are accessible in MALDI MS[151]. Regarding the law of error propagation such multiple handling processes also introduce variability, which stresses even more the need for unbiased score-based method development for FFPE tissue digestion in MALDI MSI.

### 4.2.1 Score for digest efficiency DE%

The use of a positive control in analytical methods shows a high-quality standard. So far this was uncommon in MALDI MSI. Heijs *et al.* used an isotopically labelled peptide

71

in analogy to their target molecule to investigate the digestion of their target protein on frozen rat brain[95]. The use of a protein as a positive control is remarkably new. During the tests for a suitable candidate as positive control protein (myoglobin and cytochrome c) also the condition was tested. Both proteins have a molecular mass within the MALDI-assessable mass range <20 kDa ($MW_{myoglobin}$ = 16.7 kDa, $MW_{cytochrome\ c}$ = 12.4 kDa) and could be measured in linear positive mode. To simulate the digestion condition of endogenous proteins myoglobin and cytochrome c were pipetted (3x 1 µL of 100 µM protein in $H_2O$) on tissue and on an ITO glass slide before ("digest") and after incubation ("no-digest"). As digestion of the proteins with trypsin produces smaller peptides, the spots were additionally measured in reflector positive mode. In Figure 35 A and B, MALDI MSI and mean spectra of a representative spot were shown for myoglobin and cytochrome c on an ITO slide and on tissue, respectively. For cytochrome c pipetted on the ITO slide lower signal intensity of the protein was found in the digested spot compared to the not digested spot. For myoglobin this behaviour was not observed in a reproducible way (Figure 35 A). Looking at the mean spectra of cytochrome c, a high number of digested cytochrome c signals (see lower mass range) were present, and these signals were not visible in the undigested spots. When proteins were pipetted on the tissue (FFPE preserved human liver, processed as described in material and methods) a reverse effect was visible (Figure 35 B). By taking the mean intensity of the protein signals in the pipetted spots and calculating the DE% (according to equation (2)) it became obvious that cytochrome c on ITO slide gave most reproducible results and DE% about 95 % (Figure 35 C). As DE% was a new score sequence coverage and the number of matched peptides were also observed. These two values were commonly used to evaluate the efficiency of digestion procedures[152,153]. Cytochrome c pipetted on the ITO glass slide gave the best result with sequence coverage of about 60 % and the highest number of matched peptides (Figure 35 D).

In order to monitor the digestion procedure using trypsin in MALDI MSI cytochrome c (100 µM in $H_2O$) pipetted on ITO glass slides revealed as the most reliable positive control.
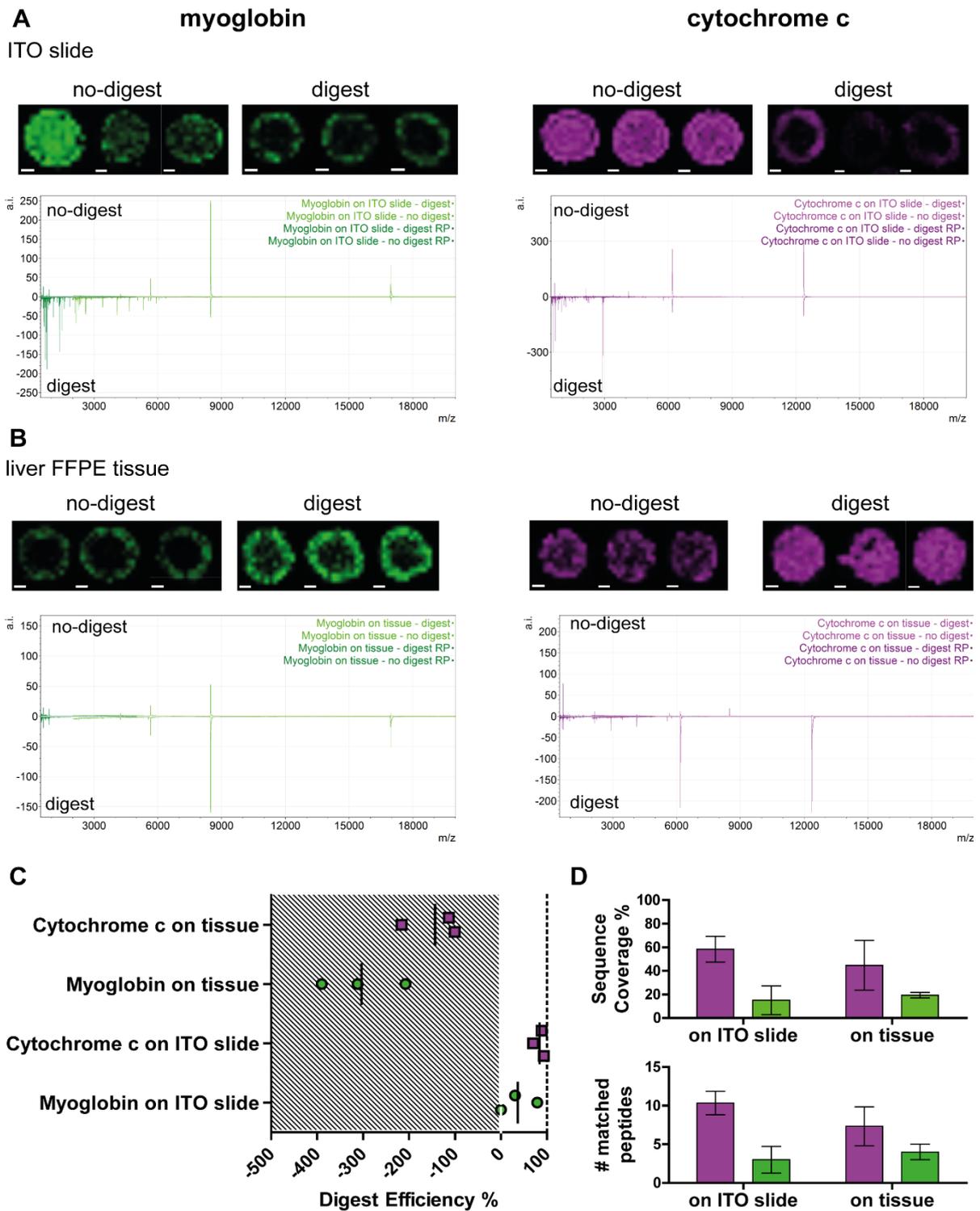
**Figure 35: Cytochrome c on ITO slide revealed best digestion results** The proteins myoglobin (green) and cytochrome c (purple) were tested for their use as positive control digestion spots (on ITO slide or on tissue). **A** MALDI MSI showed protein signal pipetted on ITO slide of three spots in undigested and digest condition. The spectra represent mean spectra of one spot. Signal intensity in the digested spots was reduced with better reproducibility for cytochrome c. **B** MALDI MSI showed protein signal pipetted on liver tissue of three spots in undigested and digest condition. The spectra represent mean spectra of one spot. The intensity in the digested spots was not reduced. **C** The graph shows the calculated DE% values for both proteins and conditions. **D** Sequence matches and peptide coverages were calculated by using BioTools (Bruker Daltonics).

73

In the comparison of the described five methods (see Figure 6) for FFPE tissue digestion the score DE% of cytochrome c could only be calculated for three of them. Those were method I, III and V, as these are the ones using DHB as MALDI matrix. A measurement of the native protein was not possible with the MALDI matrix HCCA. Comparing the achieved DE% values revealed that method III has the highest value with the lowest standard deviation (Figure 36).
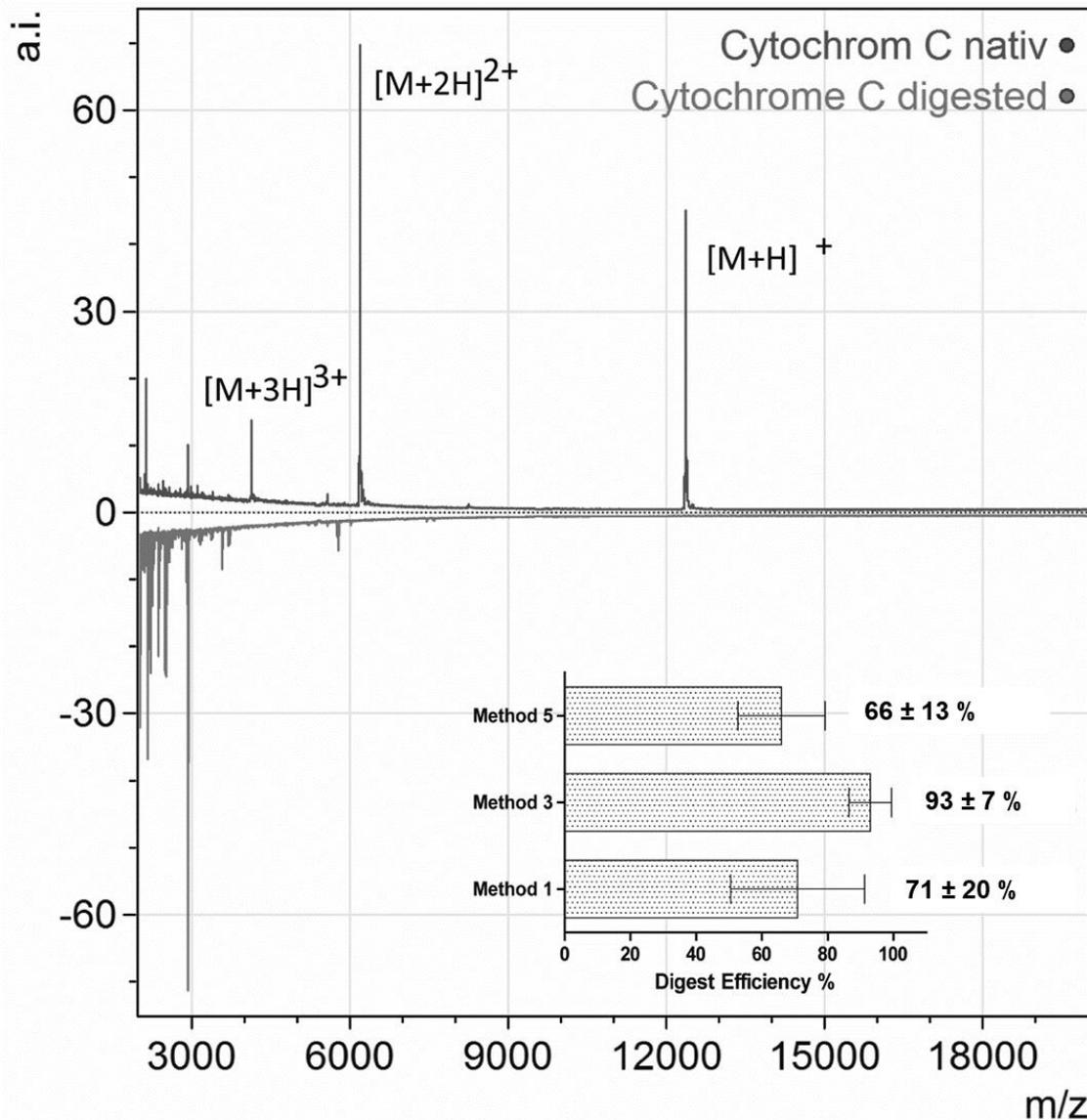


**Figure 36: Decrease of cytochrome c molecular ions is used to calculate digest efficiency (DE%)** This calculation was possible only for methods 1, 3 and 5 that use 2,5-dihydroxybenzoic acid (DHB) matrix which enables measurement of cytochrome c molecular ions $[M+H^+]^+$, $[M+2H^+]^{2+}$ and $[M+3H+]^{3+}$. As shown in the bar chart, method 3 resulted in the highest DE% and the lowest variability. The spectrum shows cytochrome c molecular ions of method 3 replicate 1 as an example - with the undigested measurement region in the upper spectrum and the digested region in the flipped spectrum. None of the three cytochrome c molecular ions could be detected in the digest, which corresponds with full digestion.

### 4.2.2 Scores for repeatability and homogeneity

Repeatability or reproducibility in MALDI mass spectrometry has been analysed very rarely with the focus on MALDI matrix application[103,154,155] or protein profiling in body fluids (reviewed by Albrethsen *et al.*[156]). Few studies evaluated their method for repeatability in tissue digestion experiments. De Sio *et al.* and Heijs *et al.* used peak counting to identify a highly repeatable method for digestion of human FFPE brain and frozen rat brain, respectively[93,95]. Diehl *et al.* used visual inspection of PCA and manual organ-structure counting (by different independent researchers) to find the best method for digestion of FFPE and frozen rat brain tissue[96]. To identify the preparation steps that induce variance and to develop an SOP Oetjen *et al.* used fractional factoring design of experiments (DoE) and the measure of spatial chaos[98].

When applying the commonly used peak-counting (picking peaks with S/N >3) to our dataset of five different methods on two individual FFPE tissues (human GIST and liver) for all three replicates, we were not able to distinguish which method gave the best result (Figure 38 and Figure 39). By adding a colour-coded grouping of the picked peaks to three mass ranges (small 500-700 Da, medium 700-2000 Da, big 2000-5000 Da) it became visible that in the small mass range the number of peaks was very stable and ranged from 7 to 13 peaks. The most peaks were discovered in the medium mass range which covered the resulting peptide size after tryptic digest[157]. The highest variance was visible in the big mass range. Neither peak counting nor the applied mass range grouping revealed a method being highly repeatable. Therefore, it was our declared aim to develop easily computing and user-independent scores for evaluating repeatability. To accomplish that comparison of mean spectra within one tissue (judged to be >98% homogeneous) for **homogeneity analysis** and between replicate runs for **repeatability analysis** had been performed. The comparison was performed by introducing the novel use of correlation coefficient $R^2$ and $\log_2$-fold-changes calculated by merged peak lists of mean spectra. All mean-spectra analysis were performed with commercially available software. Depicted in Figure 37 is the derivation of the extracted values for homogeneity analysis. The intensities for three mean spectra were compared pair-wise (a/b, b/c, c/a), and three $R^2$ values calculated. In the same way comparison and fold-change calculations for each *m/z* value were done. Because of the use of homogeneous tissue the variability could only be introduced by the preparation of each method. In a homogeneous method the fold-change spread

(*natFC*, equation (3)) is expected to be very small. To sum that, a high $R^2$ and a low *natFC* value accounted for a homogeneous tissue preparation.
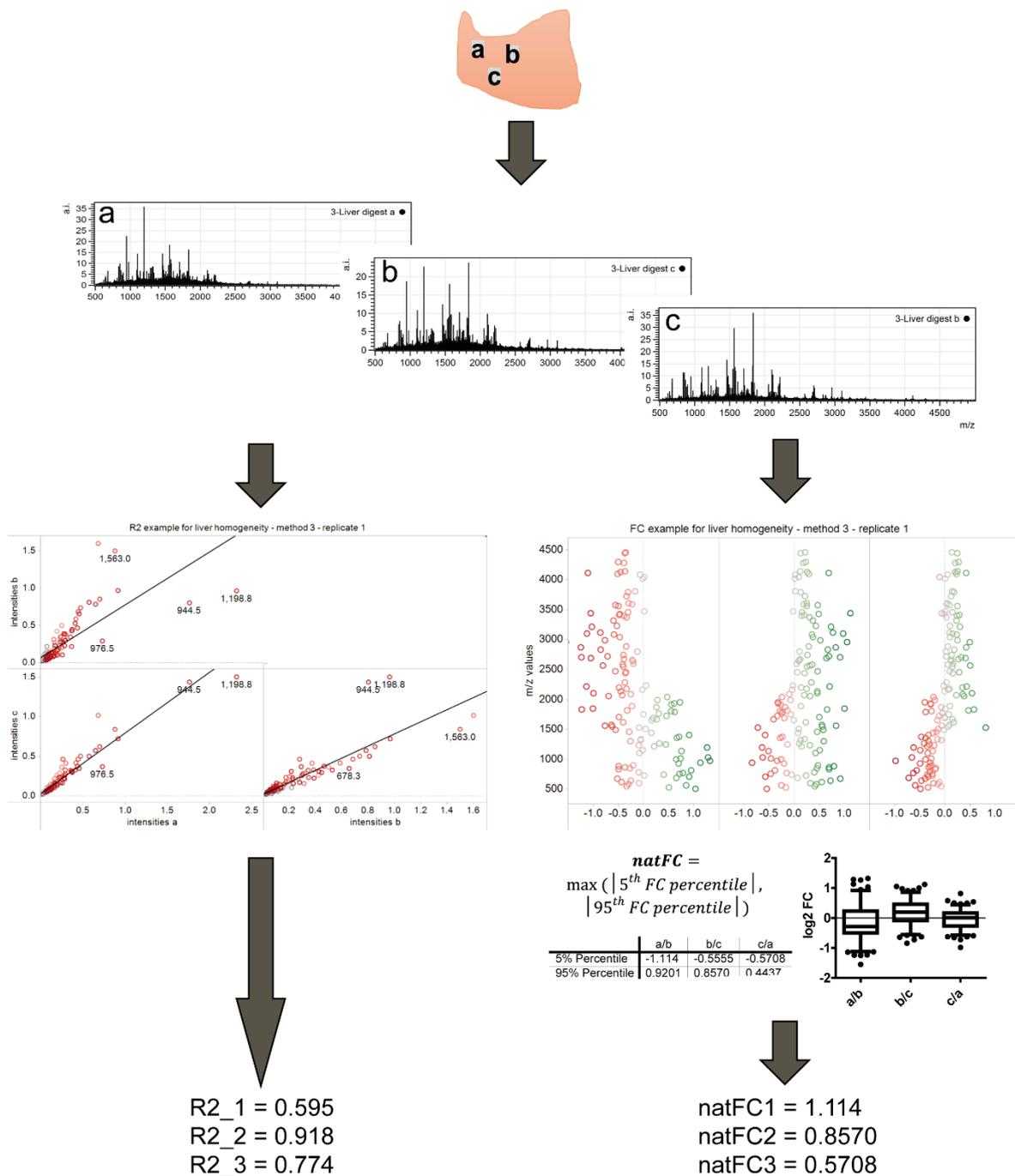


**Figure 37: Derivation of natFC and $R^2$ for homogeneity analysis** For the homogeneity analysis mean spectra of three ROIs in one tissue are extracted using mMass software. Based on one common peak list intensities are exported by using Scils Lab. Fold-change calculations and correlation analysis were performed in Excel. This analysis resulted in three values for one tissue, which were all considered for the judgement of the homogeneity. If tissue homogeneity was high, $R^2$ was also high and natFC was low.
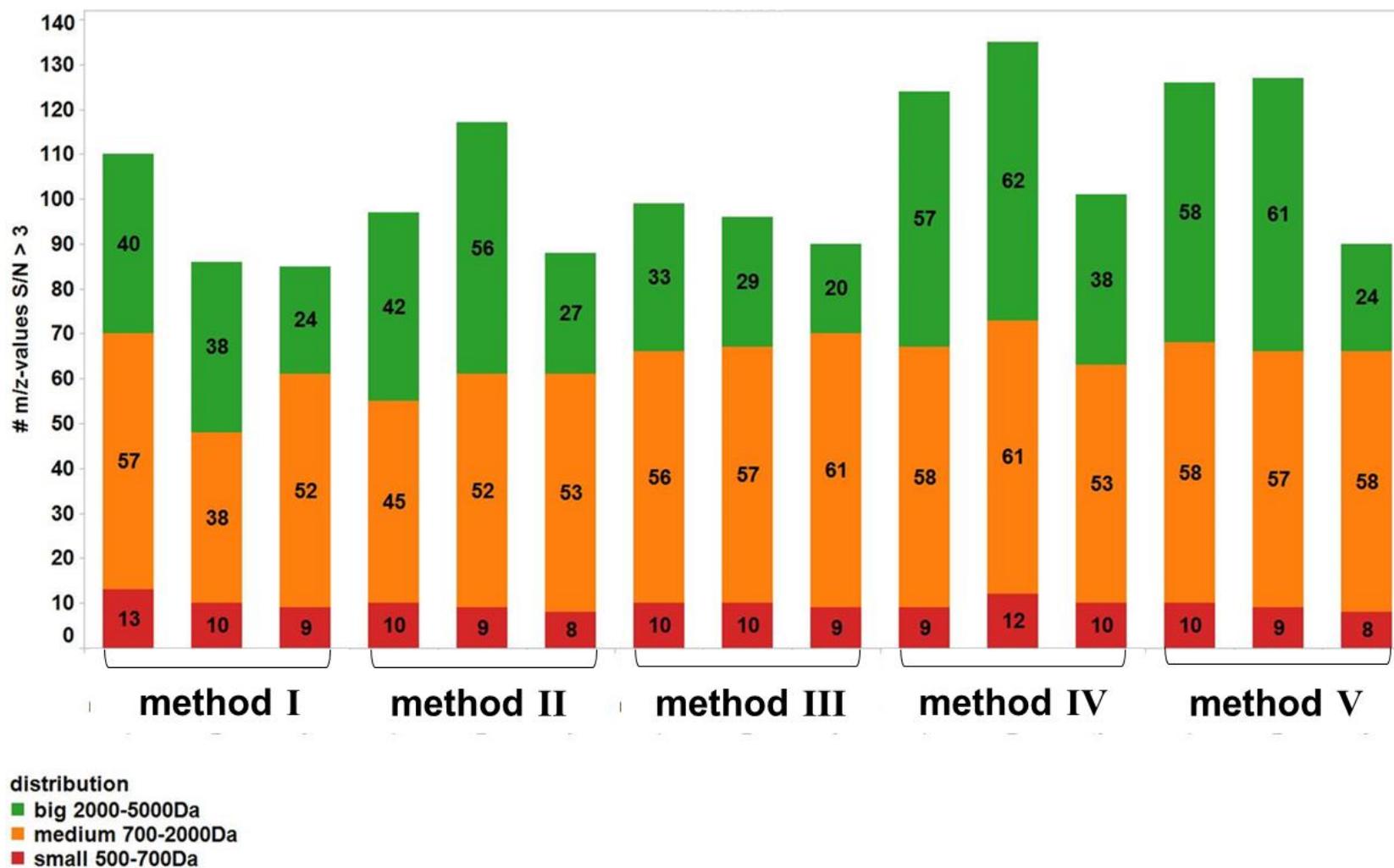
**Figure 38: Number of picked *m/z*-values for each method and each replicate on GIST** Peaks were picked based on finding local maxima and compared to the noise baseline, which was estimated using the Supersmoother algorithm as implemented in the "MALDIquant" R package with $S/N > 3$. Furthermore, columns are split into three parts: red representing the signals from 500-700 Da, orange from 700-2000 Da and green from 2000-5000 Da
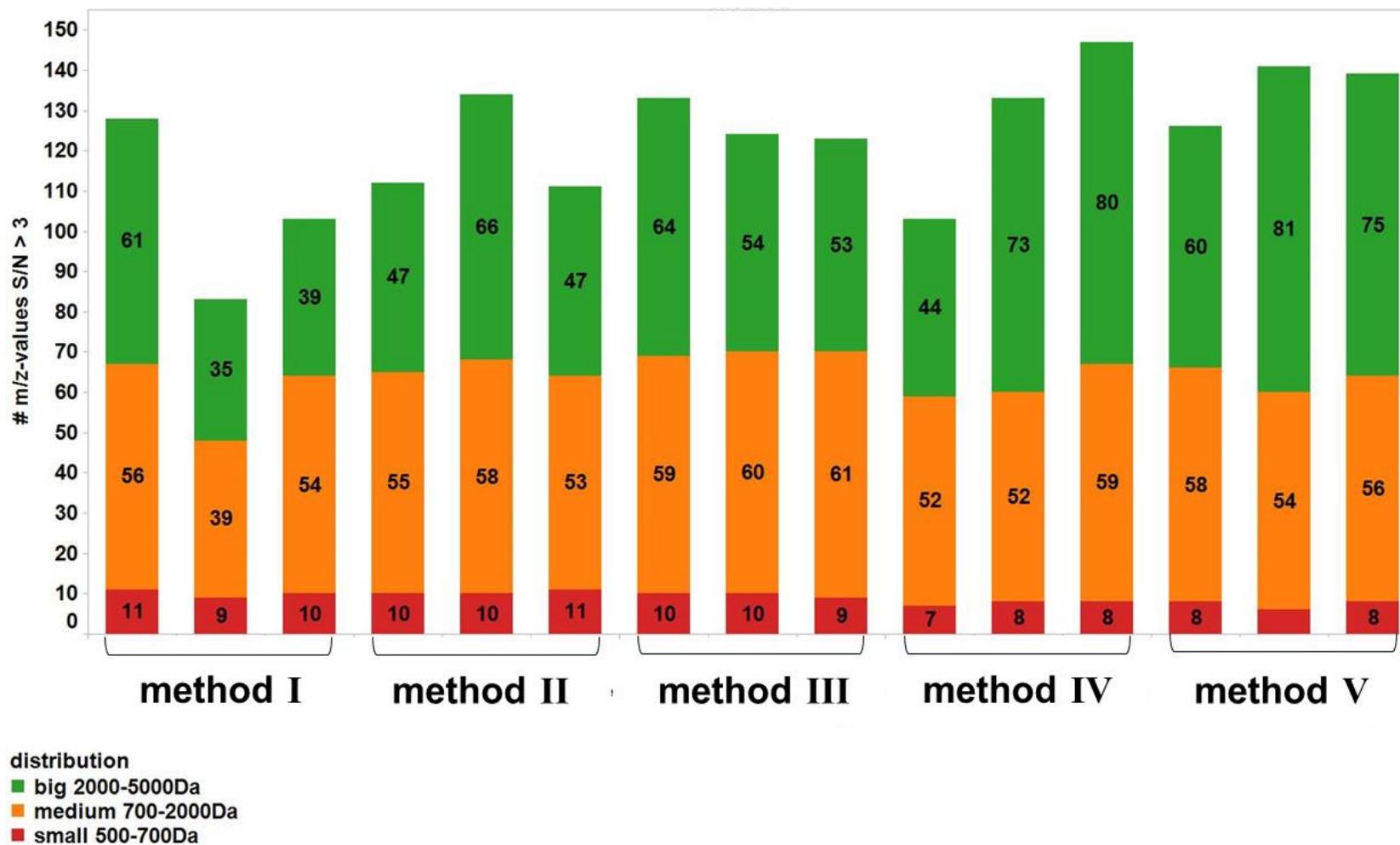
**Figure 39: Number of picked *m/z*-values for each method and each replicate on LIVER** Peaks were picked based on finding local maxima and comparedto the noise baseline, which was estimated using the Supersmoother algorithm as implemented in the "MALDIquant" R package with $S/N > 3$. Furthermore, columns are split into three parts: red representing the signals from 500-700 Da, orange from 700-2000 Da and green from 2000-5000 Da.

When comparing the $R^2$ and *natFC* for homogeneity analysis between the five compared methods, it was obvious, that method III and IV have high $R^2$ and low *natFC* values with the lowest variability between the three performed replicates (Figure 40). On GIST tissue (Figure 40 A), the difference to the other methods is more obvious than on liver tissue (Figure 40 B).
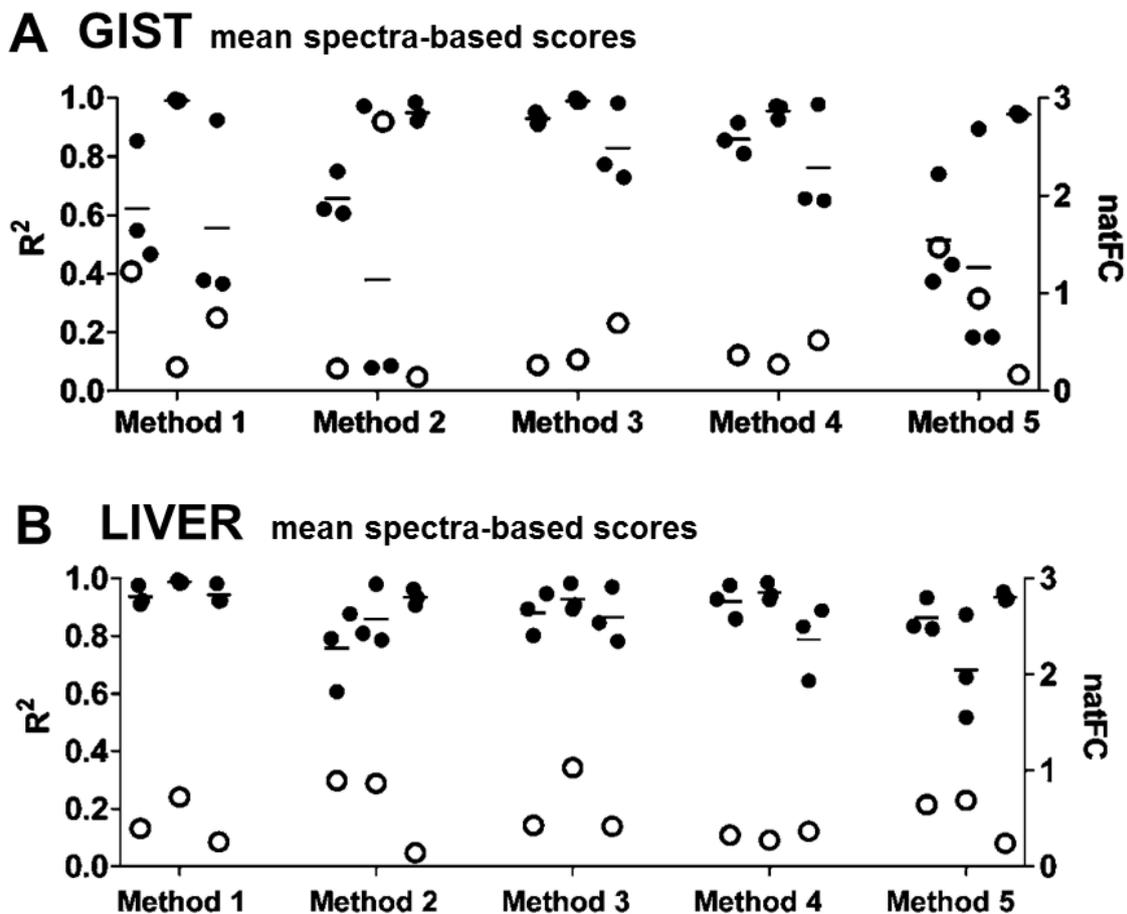


**Figure 40: Scores for statistical analysis of homogeneity of FFPE tissue processing and sample preparation** Histomorphologically homogeneous GIST and liver FFPE tissue was processed and analysed by MSI according to five different methods [N=3 replicates]. Three regions of interest (ROI; ~110 pixels each) per tissue section were selected and statistically evaluated using SCiLS lab and R software. **A, B** (**A**, GIST FFPE tissue; **B**, liver FFPE tissue) Coefficients of determination $R^2$ (filled circles) were calculated for all *m/z* with *S/N* > 3 extracted from mean spectra of the three ROIs (1 versus 2, 2 versus 3, and 3 versus 1) for all replicates with all methods. Furthermore, $\log_2$ fold-changes for the identical *m/z* values between the same ROIs (1 versus 2, 2 versus 3, and 3 versus 1) were calculated for all replicates and all methods. The natural fold-change value (*natFC;* open circles) represents either the 95th or 5th-percentile of fold-changes in the box-and-whisker plot (whatever is higher). Prior to all calculations spectra were median-normalized and square root-transformed to minimize variability and the influence of highly intense signals. Please note that methods 3 and 4 resulted in consistently high $R^2$ and low *natFC* for both tissues.

With a small adaptation, the same scores can be calculated to evaluate repeatability. Instead of comparing three ROIs within one tissue (Figure 37), three ROIs from three individual experiments were compared (Figure 41). For GIST tissue again, method III

and IV displayed high $R^2$ and low *natFC* values (Figure 41 A). In the case of liver tissue only method III showed high $R^2$ values (Figure 41 B). These results suggest that method III showed the best repeatability and homogeneity behaviour.
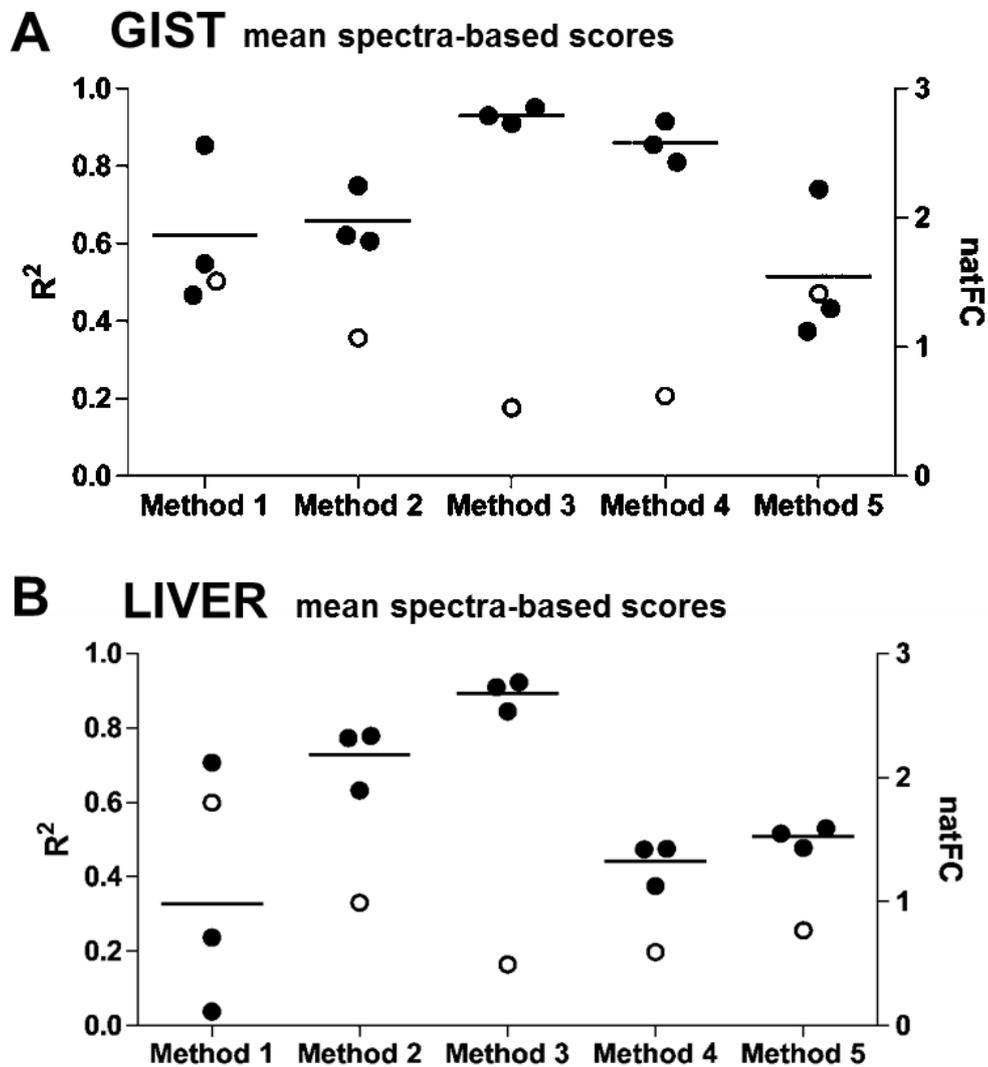


**Figure 41: Score-based analysis of inter-day repeatability indicates that prolonged incubation time minimizes variation** Histomorphologically homogeneous GIST or liver FFPE tissue was processed and analysed by MSI according to five different methods. For assessment of inter-day repeatability, three full technical replicates with three selected ROIs each were analysed per tissue. **A, B** (**A**, GIST FFPE tissue; **B**, liver FFPE tissue) Coefficients of determination $R^2$ (filled circles) and a single *natFC* value (open circles) were calculated for all *m/z* with *S/N* > 3 extracted from mean spectra of the three replicates (1 versus 2, 2 versus 3, and 3 versus 1) for all methods. The single *natFC* value is the highest absolute value of all 95th and 5th percentile fold-changes for the three replicates. Note that the most consistent and highest $R^2$ and lowest *natFC* were observed for method 3 (with prolonged incubation time) in both tissues.

So far, all results were obtained on mean spectra. For confirmation computationally intensive pixel-wise-analysis (comparing 1000 pixels for homogeneity analysis and 3000 pixels for repeatability analysis) was done by my college Denis Abu-Sammour. The results are summarised in Erich *et al.* (2016) and they confirmed the mean-spectra

analysis (Figure 42). The mean of $R^2$ values was the highest in method III (close to 1), and additionally the spread of the values, reflected by the inter-quartile-range IQR, was small. Additionally, this reflected a high similarity between the compared pixels. The scatter-plot of fold-change values now comprised all the calculated fold-changes (instead of *natFC*). Here IQR reflected the similarity of the intensities. A small IQR accounted for similar fold-change values (scattered around 0) and thus similar intensities in the compared spectra.
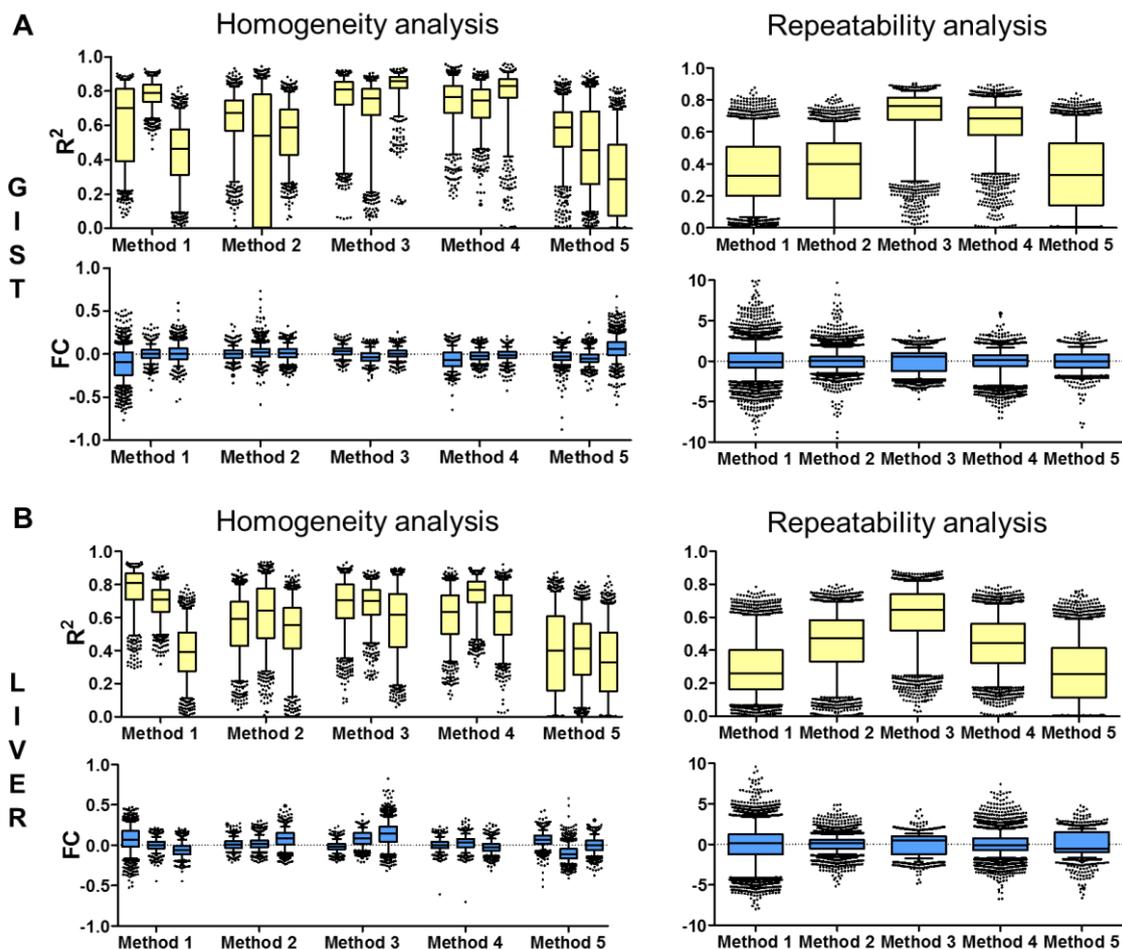


**Figure 42: Scores calculated on pixel-wise comparison for homogeneity and repeatability analysis** (**A**, GIST FFPE tissue; **B**, liver FFPE tissue) In pixel-wise analysis using R statistical computing language, individual spectra belonging to a given tissue, replicate and method (all 3 ROIs) were pooled together and the boxplots were generated by finding $R^2$ and fold-changes (FC). For homogeneity analysis 1000, and for repeatability analysis 3000 different and randomly chosen combinations of the pooled spectra were used. Hence, good homogeneity were attributed to samples that had a small interquartile range (IQR), that showed consistency between the replicates and that had high $R^2$ and low FC. The pixel-wise homogeneity analysis indicated superior homogeneity with methods III and IV for $R^2$, whereas all methods showed similar behavior with FC. Again, the pixel-wise repeatability analysis indicated the superiority of method III for $R^2$ and FC[n].

---

[n] Calculations for pixel-wise comparison had been performed by D. Abu-Sammour as described in Erich *et al.* (2017)[120]

# 5 DISCUSSION

## 5.1 Optimised substrate application with water sensitive paper test

It has been discussed several times that the homogeneous application of MALDI matrix followed by effective extraction and co-crystal formation is the most important step to assure good spatial resolution and high-quality spectra[146,154,158]. This fact holds true for any deposition of liquid on tissue, in our case the application of the tracer substrate substance P. For matrix applications the overall CV% of pixel-wise signal intensity and the mean intensity of the spectra were used as quality criteria for homogeneous application[154]. Further, the matrix crystal size is a measure of a good application, as smaller crystals assure lower spatial resolution. The size of the crystals can be measured by light or electron microscopy[159–161]. Smaller crystal sizes could be achieved by applying the matrix in dry sprays (low organic solvent amount and/or high temperature). This, however, has a negative effect on the extraction of the analytes from tissue and therewith results in poorer sensitivity. Mean ion intensity, CV% of pixel intensity or crystal size cannot be used with the application of an aqueous solution that contains a small molecule/peptide/lipid for normalisation[162–164] or monitoring tissue digest[95]. For proper method optimisation an easily accessible and MALDI-acquisition-independent measure for the solvent application is necessary. With the use of WSP the spray quality of aqueous solutions can easily be accessed and quantified by the mean grey value. The method has good potential to be used in quantitative MALDI MSI, when internal standards being structural analogues (e.g. deuterated molecule) of the substance of interest are sprayed to allow for relative quantitation[165]. The use of internal standards is one way to overcome ion suppression that is varying in different tissue regions and is also varying between different tissue types/organs[166,167]. WSP can additionally be used to routinely check for instrument performance, as spray devices often consist of capillaries and screw fittings that are prone to constipate. The dye rhodamine B is not universally suitable to test delocalisation effects. Note, that rhodamine B is soluble in water and alcohol and so does not represent all molecules in a tissue slice. One can assume that immobilised or lipid-soluble molecules are not affected by the application of an aqueous solution. It thus would have an effect on water-soluble molecules that are easily accessible in tissue compartments. For this

scenario rhodamine B represents the affected subgroup of molecules and can be used for optimising spray parameter in favour of lateral diffusion.

## 5.2 Mean spectra analysis is restricted to homogeneous tissue

Latest literature from Taylor *et al.* showed that heterogeneous tissue can be responsible for differing ionisation and suppression effects in MALDI MSI. The suppression of olanzapine sprayed on brain tissue was evaluated calculating a tissue extinction coefficient. This calculation includes removal of peaks, segmentation, and clustering, thus is computationally intense and not calculable with commercially available software[123]. In contrast, ROI based analysis is feasible without much computational effort[120]. In this study brain tissue was initially included, but the morphology led to an inhomogeneous distribution of substance P signal in the control slide. As homogeneity was the prerequisite for a ROI based analysis of mean spectra, brain data has been excluded in further analysis. All other tissues showed a homogeneous distribution of the substance P signal in the control slide. The use of this control tissue for each time point enabled the comparison of the incubation time points. MALDI MSI acquisition settings require the adjustment of laser intensity and detector gain, optimised prior to each run[168]. The values depend on the current condition of the instrument (clean status of the ion source and detector), and on the preparation quality (tissue quality, matrix amount and crystallisation). Further, the instrument settings are directly related to the absolute value of intensity (a.u.), which makes the comparison of absolute values nearly impossible. That is the reason for the differing intensity scales between the time points in the MALDI MSI. Proper controls are required for a validated comparison of these values. For tissue protease activity the control signal intensity was undigested and therefore used as 0% DE%. Commonly used TIC or median normalisation does not serve the purpose of inter-day comparability. For that reason, in quantification studies internal standard is sprayed on tissues to make quantification possible[162,165]. In this study, the monitoring of several *m/z* values was intended, and so several internal standards would be required for absolute quantification. Further, there is no consensus which preparation technique is the best for absolute quantification, and this was beyond the scope of this study[169]. Relative quantification related to the control tissue slices is the most elegant solution for the verification of tissue protease activity.

## 5.3 Observation of C-terminally cleaved substance P peptides

Starting with the tracer substrate substance P (undecapeptide), only C-terminally cleaved peptides were observed, dominated by the hexa-, hepta- and octapeptide (Table 6). The digestion process is a first order sequential multi-step reaction, especially, when the peptide products of exopeptidases activity was observed[170]. The transient production and further degradation could be a reason for low intense signals of the decapeptide and nonapeptide, while the further digestion products were dominant. Yi *et al.* spiced isotopically labelled peptides into human plasma and serum samples. The researchers observed their digestion of the peptide and a final decreased of the digestion products in a four hours timeframe[170]. The study at hand covers a larger time frame, but also showed a decrease of the digestion products down to complete disappearance. Due to the fact that substance P is a unique peptide, there seems to be no biological explanation, why the active exopeptidases should cleave only from C-terminus. It is far more likely that MALDI ionisation process favoured the C-terminally cleaved peptides. It is known that the gas-phase basicity of amino acids is a requirement for ionisation[171,172]. The amino acids arginine (R) and lysine (K) fulfil this requirement. Peptides containing these basic amino acids can thus be protonated and measured in positive mode. In an ionisation comparison of MALDI to ESI, Nadler *et al.* showed that MALDI favoured a C-terminal arginine, while ESI prefered lysine as C-terminal amino acid. Both methods disfavoured cysteine (C), methionine (M) and tryptophan (W) containing peptides[173]. Now, looking at the amino acid sequence of substance P (RPKPQQFFGLM), the removal of the first N-terminal amino acid (R) already leads to a disfavoured amino acid composition for detection. A protonation, required for detection in MS, is then limited to the lysine in the peptide. Furthermore, the amino acid methionine is still present in the peptide chain. This could additionally explain the negative bias for the detection of N-terminally cleaved substance P peptides.

## 5.4 Development of tissue protease activity assay

An analogue method to measure tissue protease activity photometrically (TPAA) was developed to verify the results of MALDI MS tissue protease activity determination. With active protein extract from porcine tissues and casein as substrate, the released tyrosine was quantified and activity of the tissue was calculated.

The critical point in the assay exists in the extraction of proteins in their active form. Many protein extraction buffers contain detergents for cell lysis that also denatures proteins and proteases. Therefore, some effort was put in the extraction of active proteins by comparing a commercially available tissue protein extraction reagent (T-PER) with a mild extraction buffer. According to supplier's information T-PER should be able to extract whole protein content in the active form. Although T-PER is a clear solution, for the TPAA it was not suitable, as it produces high and thus interfering absorption values. T-PER consists of 25 mM bicine, 150 mM sodium chloride and a proprietary detergent. As Folin & Ciocalteu's Phenol reagent is not selective for tyrosine, but rather react with total phenols and further non-phenolic reducing substances. The interfering absorbance might be produced by the reaction of Folin & Ciocalteu's Phenol reagent with the unknown detergent[174]. The component bicine, an organic compound used as a buffering agent, could also react as a reducing agent and thus possibly reacts with the Folin & Ciocalteu's Phenol reagent. The low detergent extraction buffer was therefore used for extracting active total amounts of proteins from tissue. The total amount will always be an approximation, as this non-selective extraction will still miss some proteins. Integral and peripheral membrane proteins, for example, required specialised extraction procedures[175,176]. For this study the activity of proteases was of interest, which are mostly secreted and present in the extracellular matrix (ECM)[177,178] or expressed ubiquitously in lysosome[179].

## 5.5 Imaging of endogenous tissue protease activity by MALDI MSI in clinical routine

So far high effort has been put on the development of photonic probes to monitor tissue protease activity[45,180]. Besides the requirements of a narrow excitation/emission spectrum, high chemical and photostability, non-toxicity, biocompatibility, biodegradability, and excretability[181], specificity to an enzyme is also of high interest[182,183]. Now several lines of evidence suggested, that overall tissue protease activity can be measured with MALDI MSI:

- ✓ Endogenous tissue protease activity was found to be time-dependent
- ✓ A protease inhibitor mix (PIM) decreased tissue protease activity in a concentration-dependent manner
- ✓ Not only the decrease of the tracer substrate but also increases of defined peptide products could be measured

Fluorescent chemical probes underwent great development in clinical applications with the goal of cancer imaging[184]. In future optical chemical probes should be used for diagnostics and pre-operative planning. They should be injected intravenously to find the location of tumorous tissue. To achieve this, dyes with enhanced properties and sensitive detection methods are required. Pre-operative images are made so far by positron emission tomography (PET) in combination with PET tracers. Garland *et al.* envision the use of one agent that has a PET tracer (for pre-operative planning) and can be used as an optical probe (for intraoperative decision making)[185]. As MALDI MSI required the use of tissue sections it cannot be used for in vivo surgical guidance. Another important clinical field, where optical chemical probes were of interest is the *ex vivo* surgical guidance. Cutter *et al.* were the first to apply activity-based probes topically on tumour tissue to identify the boundaries between tumour and healthy surrounding tissue in glioblastoma multiforme[186]. A recent study showed that 19% of women who underwent breast-conserving surgery received a re-excision[187]. Re-excisions are required when post-residual cancer is found. During surgery intraoperative consultation (frozen section) of a pathologist is required to evaluate the excised specimen and give a preliminary result about the tumour margin. The pathologist will judge the tissue to be normal or indeed a tumour and, if the tissue is primary or metastatic. This procedure interrupts the surgery at the minimum of half an hour but also guides the surgeon to the complete tumour resection[188]. In addition, optical imaging probes and MALDI MSI could help to visualise tumorous tissue. Withana *et al.* developed a protocol for topical application of activity-based probes. This enables the imaging of enzyme activity on a cellular level[50]. The study in hand shows the ability to visualise protease activity using MALDI MSI. For both methods additional requirements need to be fulfilled to be evolved into a clinical application. (1) One next step for MALDI MSI is to study the **specificity** of the method by using specific protease substrates and their targets. It has already been measured by MALDI MS that proteolytic enzymes in brain tissue convert synthetic dynorphin B (neuropeptide) to N-terminal fragments[189]. In 1962 Gross & Lapiere showed collagenolytic activity in tissue[190] which later was referred to the enzyme family of matrix metalloproteinases[191]. Latest literature reviews the role of matrix metalloproteinases in invasion and metastasis of cancer[192]. Matrix metalloproteases degrade the extracellular matrix (and therewith allow cancer cells to invade surrounding tissue and enable tumour growth. Therewith the visualisation of MMPs activity can be of high interest for the analysis of

tumour surrounding tissue. Using a specific MMP substrate applied on a suitable tissue sample (containing an invading tumour and surrounding normal tissue) and by performing protease activity MALDI MSI could show the conversion products in a spatially resolved manner. As there are already developed ABPs for MMP activity the result should be compared to an optical image of a serial tissue section. This would show that MALDI MSI could also be used for targeted analysis, in contrast to the here shown universal protease activity analysis. (2) Further, it is absolutely required that **large scale studies** are performed where real patient tissue is analysed for protease activity using MALDI MSI and the gold-standard method for frozen sections[193]. This critical step will show how accurate MALDI MSI is to detect the tumour margins. (3) To bring this method to the clinics MALDI MSI **equipment** needs to be installed, specifically trained employee need to be hired and finally, the method needs to be covered by health insurance. All-in-all there is a long way to go. In the near future, the visualisation of protease activity with MALDI MSI will be restricted to basic clinical research and preclinical animal studies.

## Reduction of proteolytic activity due to post-mortem degradation of proteins

Although in a preclinical experimental setup sampling storage conditions can be highly controlled, in a clinical setting this is hard to achieve. Scholz *et al.* analysed the impact of temperature on proteome and peptidome in liver and pancreas[124]. It showed that the post-mortem degraded proteins in the pancreas were, for example, Peptidyl-prolyl cis-trans isomerase (Q9DCY1), type II cytoskeletal keratin 8 (P11679) and several regulation-related proteins. The dominant peptides that were digested were for example from insulin I and II C-peptides, glucagon and somatostatin. In brain tissue, the post-mortem degradation is dominated by cytoskeletal associated proteins[194,195]. For the developed visualisation of tissue activity using MALDI MSI, a post-mortem degradation of proteases would lead to reduced tissue protease activity. With respect to the results of the mentioned studies, it is very unlikely, that proteases are highly affected in post-mortem degradation. Still, in clinical setup it is highly recommended to set up sample logistics comprising cooled tissue transport and fast tissue evaluation, to minimise possible post-mortem degradation Further, it is recommended to perform such stability test when different tissue material is used, as the post-mortem degradome differs in various tissues[124].

**The use of students t-test in pixel-wise analysis**

For comparing complex and data-intense scenarios like for MALDI MSI an intensity box plot can help but has some drawbacks. When high amounts of pixels are used for comparison, also empty noise-containing pixels are included, which contain overall a very low TIC. Depending on the preparation, the tissue condition and the selected measurement region, this could massively influence the mean-calculation in a box plot and therewith the interpretation. Ideally, a threshold would be used to exclude such pixels from the analysis, as proposed by my colleague Denis Abu-Sammour[120]. A second pitfall is exposed to the number of data points, in such a pixel-wise analysis. It is the nature of MALDI MSI to produce high spatially resolved data, that contains thousands of pixels for one tissue slice (depending on the size of the tissue). If all pixels are included in the statistical analysis, as commonly performed with a Student's t-test, the number of values is very high (= number of pixel). Of course, having a low number of values would make a statistical analysis unreliable. With a very high number of values, nearly all mean-differences generated statistically significant results, even if the absolute difference of the mean is very low. Talking about significance then is problematic and the biological context of the values needs to be taken into account. To compare intensities statistically with segmentation, excluding-criteria and proper statistics[196] are required and is far not implemented in commercially available software.

## 5.6 A first idea of active proteases

The pH test on protease activity showed that activity is preserved when wash with buffer at pH 3 was done. So one might conclude that acidic proteases are highly active in the analysed tissue. A protease-rich and acidic cell organelle is the lysosome, whose function is protein degradation. Lysosomal proteases are mainly aspartic-, cysteine, or serine- proteases, which are mostly ubiquitously expressed[179]. Still, the difference in intensity could result from the MALDI MSI pitfall of ion suppression in heterogeneous tissue[123]. The identity of varying protease expression between a tumour and non-tumour could be clarified by using bottom-up proteomics. Therefore, forces were joint with researchers from the German Cancer Research Centre (DKFZ, Prof. Dr. Jeroen Krijgsveld). In a statistical comparison of expressed peptidases in T against NT, the most dominant differently expressed protease is the proteasome subunit beta type-10 (EC 3.4.25.1). It is part of the proteasome and therewith an important part in protein degradation. Already 2002 the proteasome became a target for cancer treatment[197].

Inhibitors like bortezomib were approved for cancer therapy of myeloma[198]. As non-tumorous tissue is already impacted by the tumour cells the comparison of T and WT has been performed (Table 9). One differently expressed protease is Caspase 7 (EC 3.4.22.60). Caspase-7 is a cysteine-protease involved in the cascade for apoptosis execution. Several caspases and their deregulated proteolytic activity direct to tumour growth[18]. To balance growth and degradation of cells, caspases are also targets for anticancer strategies[199]. Interestingly also Cathepsin D, which is located in the lysosome and ECM is differentially expressed in tumour and wild-type tissue. The other peptidases are located in nuclei, ECM or cytoplasm of cells. Further, the peptidases belong to catalytic classes of threonine-, serine-, aspartic-, cysteine-, and metallo-proteases. The identification of the expressed peptidases does not reveal the identity of the proteases, that might be responsible for the degradation of substance P, as it is rather a combination of several proteases. But the analysis shows, that there are differentially expressed peptidases, that might be responsible for the different activities visualized in MALDI MSI. Note that the expression of a protein is not equal to its activity, rather confirms its presence. Especially for proteases the activation process from the inactive zymogens is a highly regulated process[200,201].

## 5.7 Assessment of the proteolytic tissue analysis in human gastric tumour

For diagnosing gastric carcinoma, the standard procedure involves gastroscopy with collecting multiple biopsies, already when patients suffer from suspicious symptoms[31]. Although there are several non-invasive methods for diagnosing and staging of gastric cancer like confocal endomicroscopy[202], NBI-magnifying endoscopy[203] and endocytoscopy[204], a histological study of biopsies is the current gold standard for histopathological examination of biopsies. However, biopsy seizing is time-consuming, bears the risk of bleeding and can cause submucosal fibrosis. As advanced gastric cancer has a poor prognosis, and early detection of resectable gastric cancer detection is of high interest[205]. To achieve this, proteases were targets of research as they are involved in early cancer development. The tumour microenvironment is extensively remodelled by proteases and change cell-cell and cell-ECM interaction, in favour of tumour growth angiogenesis and metastasis[206]. It has already been shown that in human gastric cancer cell lines the expression of cathepsin B, H and MMP2 is

elevated. Further, cathepsins and MMPs are described as potential biomarkers for early gastric cancer in mouse models[42].

In our analysis, slight differences in tissue protease activity of normal mucosa versus adenoma tissue could be visualised (Figure 34). The experimental preparation bared some problems. The slicing of such tiny tissue blocks (5-7 mm in diameter) requires high expertise with a cryostat. Additionally, two incubation times were prepared on different days. As between each preparation day, the tissue was kept at -80° and freshly frozen on metal tissue holder using CMC, the cutting angle differs. In the scenario of a tissue block (3 Dimensions) without a fixed orientation, this potentially results in different tissue compositions in the tissue slice. Therefore, differences in incubation times could also be related to differing slicing angles and therewith tissue composition (and size/form of the slice). Ideally, sequential sections are prepared with the same angle, to avoid this. It is not recommended to store already prepared ITO slides, as the tissue is melted on the slide and uncontrolled tissue changes could be introduced.

Our study comprises two patients, which is of course not enough to solve a clinical question, but already shows experimental requirements, that need to be fulfilled for a bigger study. The observed difference in tissue protease activity of tumour and normal tissue is not consistent between the two patients. The normal mucosa tissue of patient 1 showed a similar pattern as the adenoma tissue of that patient. As mentioned, also tissue in the vicinity of a tumour suffer from tumour induced changes, that are histologically inconspicuous[22,207]. In the case of gastric tumour the non-tumour cells include stromal cells, and the stromal content is associated with poor prognosis for the patient[208,209]. This could be the reason, why the histologically declared normal tissue showed a tissue protease activity comparable to adenoma tissue. So how should normality or healthiness of the normal tissue be defined? The surgeon decides on basis of his expertise where to take the tumorous and normal tissue. Indeed, there are two definitions of normal tissue: nearby the tumour ("Tumor-nah") and distant to the tumour ("Tumor-fern"). For bigger studies this should be defined. Ideally a healthy person should be the donor for the normal tissue, to circumvent the possible changes due to tumour-initiated changes. This leads to an ethical problem, as gastroscopy and taking biopsies without any medical incidence is not approved. Further, the location where the biopsies were taken are based on the stomach anatomy (cardia, fundus, body –

lesser or greater curvature, antrum or pyloric canal)[210], and should be defined and noted.

Apart from the inconsistency in normal and tumour-tissue it is also possible, that adenomas of different patients might have different protease content and therefore activity. Based on molecular classification gastric cancer is a very heterogeneous disease[211]. Personalised medicine takes not only the common phenotypes of adenoma, but also the individual genetic profile into account. This together defines clinical decisions regarding diagnosis, prognosis and therapeutics. Especially in cancer treatment, the effectiveness of the chemotherapeutics in hand with the minimised toxicity aims from individual predictive biomarkers. For gastric cancer there is a need for better methods to identify molecular targets, that look the same in conventional pathology, to clear the way for the development of specific drugs[212]. Proteases can be targets for the different states of gastric cancer and are insensitive in standard histological analysis. With more effort in the development of clinical studies based on MALDI MSI tissue protease activity monitoring such targets could be revealed. The spatially resolved monitoring of protease activity could potentially reveal also small local differences (<5 µm) which were not detected in methods that require homogenisation of the biopsy (expression analysis or protein extraction).

## 5.8 Scores for FFPE tissue digests and evaluation of the best FFPE on-tissue digestion method

Many studies showed the great potential of MALDI MSI in clinical pathology, reviewed by J. Kriegsmann in 2015[213]. But already there, the need for optimisation and standardisation of sample handling and preparation to minimise variability was claimed. Further M. Aichler and A. Walch postulated the need for high-quality studies in cooperation with pathological institutes to gain clinical relevance and improve tissue quality[64]. Due to the fact that the analysis of frozen material is prone to variability (simply due to temperature changes during transport or storage), MALDI MSI with on-tissue digestion of FFPE tissue has been used for this initial studies on repeatability. **Repeatability** is defined as the variability that is induced when the same person repeats a measurement. The study in hand and two further studies evaluated the variability of FFPE conserved tissue preparation methods for MALDI MSI, and conclude that the multistep process is prone to introduce variability[98,120,214]. With this background latest research focussed on the translation of FFPE tissue preparation for

MALDI MSI into clinical studies and diagnostic/prognostic testing, by evaluating multicentre reproducibility. **Reproducibility** includes the variability that occurs if a method is repeated by different operators[215]. Buck *et al.* used multi-organ tissue microarrays from wild-type mice to study the impact of inter- and intracenter technical variation on the MALDI MSI of peptides and metabolites from FFPE tissue[216]. Reproducibility was described as dependent on the molecular class (peptides or metabolites) and the tissue type. This observation goes in line with the results presented in this study, where human liver and GIST tissue showed slightly different repeatabilities. Both studies use the correlation coefficient which is insensitive to multiplicative effects between the observed spectra. Despite the fact that the round-robin study proposed first results that intercenter comparison improved multivariate classification, further explanations why peptide measurement is superior to metabolite measurement is required. In the study in hand, the most homogenous and repeatable preparation protocol for on-tissue digestion was identified. The main difference in preparative steps is a long incubation time of 18 h for the tryptic digestion, which has also been used by Buck et al resulting in surprisingly superior classification compared to the less complex metabolite preparation protocol[216]. It might be that the high reproducibility comes from a reached peptide limit, so all possible cutting sites are cleaved[217]. For specific applications in the future it needs to be clarified if the peptides of choice are still present. In plasma it is already shown, that different proteins have different optimum conditions for a full tryptic digest and these optimum conditions need to be defined for on-tissue digestion[218]. Note, that the maximum of detected peaks is not only limited by the amount of occurring peptides (=peptide limit), but also by the resolving power of the MALDI-TOF MS instrument (0.1 – 0.01 Da)[102]. After tryptic digestion with this mass resolution, a signal is present on nearly every mass, so the spectrum (700 – 2000 Da) is saturated. Peaks that occur here are most likely due to partial digestion, as fully tryptic peptides have a maximum mass of about 2000 Da. Each signal consists of several isotopic peptides, that cannot be resolved. Scherl *et al.* calculated that the *in silico* tryptic digest of human proteins (17 175 according to UniProt database, entered 2008) theoretically result in 2883 fully tryptic peptides in the mass range of 1200 – 1210 Da[219].

Contemporaneously to the round-robin study, Ly *et al.* performed a site-to-site study using ileum and jejunum from C57Bl/6 mice, human ovarian teratoma and TMA of six different human tumours prepared by on-tissue digestion for MALDI MSI. The on-tissue

digestion protocol was optimised in preparation time (reduced to 2 h at 50 °C with the use of saturated $K_2SO_4$ to maintain humidity[220]) but maintains spatial resolution. With the use of the standardised preparation protocol, the resulting segments were based on biological differences in the tissue, and not from the preparation centre, date of preparation or the initial location of the tissue. The authors claimed that trypsin deposition, digestion and matrix deposition cause preparation heterogeneity.

The effort that had been made to address reproducibility can increase the acceptance of MALDI MSI to the clinics. It is an absolute requirement in clinical applications for diagnostic and prognostic tests that sample preparation is highly reproducible. Acquired results need to be stable over days and years, and also between clinical centres or operating clinicians/technicians. Predictive models will be reliable when the input data is of high quality in terms of low variability. To achieve the goal of MALDI MSI based diagnostics there is still a long way to go including studies with high sample number to set up a training model, define not only standardised preparation methods but also standardised data evaluation methods and develop scores for quality control (matrix deposition and digestion). For frozen samples additional optimisation and standardisation is necessary to reduce temperature variance and thus minimise post-excision proteolytic activity. As long as those prerequisites are not fulfilled MALDI MSI will increasingly be used for pre-clinical and pharmaceutical research[221].

# 6 CONCLUSION

MALDI MSI provides unique advantages for analysing tissue specimen raising information that no other method can yield. Tissue-based research with MALDI MSI covers a broad spectrum of analytes like peptides and proteins, but also small molecules and lipids.

The development of a spatially resolved tissue protease activity assay using MALDI MSI adds another group of biological targets to the wide range of MALDI MS accessible target molecules. In this study, the method was proven to be reliable and reproducible on porcine tissue and on the specific mouse model for gastric cancer. Time- and inhibitor-concentration dependency, and tracer related resulting peptides suggested the successful visualisation of a digestive processes. As proof-of-concept, a gastric tumour mouse model was used to visualise different protease activity in tumour tissue compared to surrounding tissue. Here MALDI-FT-ICR MS data gives superior results over MALDI-TOF MS data, with respect to spatially aware cluster analysis and peptide identification. The transfer to human biopsies is possible but requires further clinical validation studies with a higher number of participants, statistical analysis and pathologist expertise to classify the tumour subtype. It can be envisioned that the visualisation of protease activity can aid tumour margin detection during surgery.

It is a final goal to improve MALDI MSI methods for the transfer to clinical applications, as it has been done for the 'MALDI Biotyper', which is already implemented in routine clinical use and provides the characterisation of bacteria. Molecular histology is so far in the field of pathology, where unique skills are required to identify tissue that represents patient's disease. To bring MALDI MSI in routine diagnostic two aspects are absolutely inevitable: High reproducible MALDI MSI methods need to be combined with the expertise of pathologist to gain high-quality clinical studies.

It was the second aim of this work to develop scores to assess repeatability and homogeneity, which are easy to compute, so scientists would be able to apply those without high computational effort during method development and as quality control. By using the scores *natFC* and $R^2$ the best repeatable and homogeneous method for FFPE tissue analysis was identified and presented a start for further reproducibility and method optimisation studies. Entering the field of FFPE tissue analysis opens a door to countless tissue amounts of the last decades stored in clinics.

# 7  SUMMARY

The enzyme class of proteases which hydrolyse proteins peptide bonds play a major role in tumour angiogenesis, invasion, and metastasis. Much effort was spent on the development of optical probes, in particular the use of fluorescently labelled probes. Although those probes can be administered *in vivo* and *in vitro*, there was only little research dealing with the topical application on frozen tissue slices. The design of photometric probes is challenging as it requires knowledge of the molecular target and chemical design to guarantee biocompatibility and specificity. Matrix-assisted laser desorption/ionization (MALDI) mass spectrometry imaging (MSI) comprises the advantages of mass spectrometry (the measure of mass-to-charge ratio *m/z*) with histological information. Several molecular classes like proteins, peptides, and lipids were measured with MALDI MSI in a spatially resolved way, but it was so far it has not been shown if tumour protease activity can be measured.

Therefore, this thesis had thus the following aims:

(1) To develop a method using MALDI MSI for monitoring tissue protease activity exemplarily on different porcine tissues.

(2) To validate the developed method by time- and concentration-dependency, as well as by the production of specific degradation products. Further, to compare protease activities of tumorous and non-tumourous tissue in a gastric tumour mouse model.

(3) To demonstrate the transferability of the developed MALDI MSI method to relevant clinical samples by analysing the proteolytic activity of human tissue biopsies from gastroscopy.

At the beginning a substrate application method was developed that fulfilled the requirements of a homogeneous application and minimised delocalisation. With that method porcine tissue was analysed for proteolytic activity on the tracer substance P, which was chosen as a universal protease substrate. A time course study covering six hours revealed the time-dependent decrease of the substance P signal with the fastest degradation in porcine pancreas tissue and no degradation in porcine muscle tissue. By applying a protease inhibitor mix the degradation process was decelerated to different extents in the tissues. Porcine pancreatic tissue proteases showed less inhibitory response than porcine liver tissue. In addition to the decrease of the substance P *m/z* value, a number of C-terminally cleaved peptides arose during the

incubation. Those peptides might result from the activity of exopeptidases and were transiently formed. In the next step, the method was used to visualise proteolytic activity in mouse stomachs developing a spontaneous gastric tumour. The degradation of substance P was indeed faster, thus the proteolytic activity was higher, in the tumour compared to the surrounding tissue. Here again the application of the protease inhibitor mix decelerated the reduction of the substance P signal and the production of the related proteolytic products. With the use of MALDI Fourier-transform ion cyclotron resonance (FT-ICR) MSI the segmentation of the tissue in tumorous and non-tumourous tissue based on the lipid tumour marker PC(34:1) + K$^+$ correlated well with the hematoxylin-eosin staining and its pathological annotation. Further analysis of human gastric tumour biopsies showed the applicability of the method, but lacked in significant evidence, as only samples of two patients were analysed. Nevertheless, it already showed the importance of good cooperation between the surgeon, pathologist, and mass spectrometrist to ensure a representative sample cohort. Although further validation for visualisation of specific proteolytic activity will be necessary, this method has high potential for being a successful application in pre-clinical studies.

To implement a MALDI MSI method in clinical routine a high degree of standardisation and reproducibility is required.

Therefore further aims for this study were defined:

(1) To develop scores suitable for standardisation (unbiased, low computational effort) of on-tissue digestion workflow for MALDI MSI by the use of clinical material processed methods already published.

(2) To detect the best on-tissue digestion method for FFPE tissue and MALDI MSI in terms of repeatability and homogeneity of the application system.

The best repeatable and homogeneous application has been identified by developing the *natFC* score and the $R^2$ in mean- and pixel-wise-comparison of FFPE on-tissue digest preparation methods. The significant difference between the best method and the others was the prolonged incubation time of 18 hours. In summary, additional studies covering reproducibility and standardised MALDI MS methods with score base evaluation and a multicenter set-up are required to gain acceptance of this technology in clinical application.

# 8 REFERENCES

1. Hirokawa G: Report of the Commission on Enzymes of the International Union of Biochemistry, I.U.B. Symposium Series Vol 2. 237: 979–981, 1961

2. Grisolia S: Enzyme Nomenclature. *Science* 133: 1672–1674, 1961

3. López-Otín C, Matrisian LM: Emerging roles of proteases in tumour suppression. *Nat. Rev. Cancer* 7: 800–808, 2007

4. Barrett AJ: Proteases. *Curr. Protoc. Protein Sci.* 21: 21.1.1-21.1.12, 2001

5. Davie EW, Neurath H: Identification of a peptide released during autocatalytic activation of trypsinogen. *J. Biol. Chem.* 212: 515–29, 1955

6. Jesty J, Spencer AK, Nemerson Y: The mechanism of activation of factor X. Kinetic control of alternative pathways leading to the formation of activated factor X. *J. Biol. Chem.* 249: 5614–22, 1974

7. Twining SS: Regulation of Proteolytic Activity in Tissues. *Crit. Rev. Biochem. Mol. Biol.* 29: 315–383, 1994

8. Jackson HW, Defamie V, Waterhouse P, Khokha R: TIMPs: versatile extracellular regulators in cancer. *Nat. Rev. Cancer* 17: 38–53, 2017

9. Mehta DP, Freeze HH: Chapter 443 - Cysteine Proteinase-7 of Dictyostelium discoideum. 2nd ed. Elsevier; 2013

10. Powers ET, Morimoto RI, Dillin A, Kelly JW, Balch WE: Biological and Chemical Approaches to Diseases of Proteostasis Deficiency. *Annu. Rev. Biochem.* 78: 959–991, 2009

11. Hua Y, Nair S: Proteases in cardiometabolic diseases: Pathophysiology, molecular mechanisms and clinical applications. *Biochim. Biophys. Acta* 1852: 195–208, 2015

12. Pejler G, Ronnberg E, Waern I, Wernersson S: Mast cell proteases: multifaceted regulators of inflammatory disease. *Blood* 115: 4981–4990, 2010

13. De Strooper B: Proteases and Proteolysis in Alzheimer Disease: A Multifactorial View on the Disease Process. *Physiol. Rev.* 90: 465–494, 2010

14. Turk B: Targeting proteases: successes, failures and future prospects. *Nat. Rev. Drug Discov.* 5: 785–799, 2006

15. Edwards DR, Murphy G: Proteases — invasion and more. *Nature* 394: 527–528, 1998

16. Koblinski JE, Ahram M, Sloane BF: Unraveling the role of proteases in cancer. *Clin. Chim. Acta* 291: 113–135, 2000

17. Frejlich E, Rudno-Rudzińska J, Janiszewski K, Salomon Ł, Kotulski K, Pelzer O, Grzebieniak Z, Tarnawa R, Kielan W: Caspases and their role in gastric cancer. *Adv. Clin. Exp. Med.* 22: 593–602, 2013

18. Olsson M, Zhivotovsky B: Caspases and cancer. *Cell Death Differ.* 18: 1441–1449, 2011

References

19. Matarrese P, Ascione B, Ciarlo L, Vona R, Leonetti C, Scarsella M, Mileo AM, Catricalà C, Paggi MG, Malorni W: Cathepsin B inhibition interferes with metastatic potential of human melanoma: an in vitro and in vivo study. *Mol. Cancer* 9: 207–221, 2010

20. Vasiljeva O, Turk B: Dual contrasting roles of cysteine cathepsins in cancer progression: Apoptosis versus tumour invasion. *Biochimie* 90: 380–386, 2008

21. Rakash S: Role of proteases in cancer: A review. *Biotechnol. Mol. Biol. Rev.* 7: 90–101, 2012

22. Levin I: Changes in the tissue surrounding a growing tumor and the significance of the precancerous state. *J. Exp. Med.* 16: 149–54, 1912

23. Jabłońska-Trypuć A, Matejczyk M, Rosochacki S: Matrix metalloproteinases (MMPs), the main extracellular matrix (ECM) enzymes in collagen degradation, as a target for anticancer drugs. *J. Enzyme Inhib. Med. Chem.* 31: 177–183, 2016

24. Sternlicht MD, Werb Z: How matrix metalloproteinases regulate cell behavior. *Annu. Rev. Cell Dev. Biol.* 17: 463–516, 2001

25. Rawlings ND, Waller M, Barrett AJ, Bateman A: MEROPS : the database of proteolytic enzymes, their substrates and inhibitors. *Nucleic Acids Res.* 42: D503–D509, 2014

26. Rawlings ND, Barrett AJ, Finn R: Twenty years of the MEROPS database of proteolytic enzymes, their substrates and inhibitors. *Nucleic Acids Res.* 44: D343–D350, 2016

27. Quesada V, Ordonez GR, Sanchez LM, Puente XS, Lopez-Otin C: The Degradome database: mammalian proteases and diseases of proteolysis. *Nucleic Acids Res.* 37: D239–D243, 2009

28. Abbenante G, Fairlie D: Protease Inhibitors in the Clinic. *Med. Chem. (Los. Angeles).* 1: 71–104, 2005

29. Van Cutsem E, Sagaert X, Topal B, Haustermans K, Prenen H: Gastric cancer. *Lancet* 388: 2654–2664, 2016

30. Laurén P: The two histological main types of gastric carcinoma: diffure ans so-called intestinal-type carcinoma. *Acta Pathol. Microbiol. Scand.* 64: 31–49, 1965

31. Layke JC, Lopez PP: Gastric cancer: diagnosis and treatment options. *Am. Fam. Physician* 69: 1133–40, 2004

32. Shah MA, Khanin R, Tang L, Janjigian YY, Klimstra DS, Gerdes H, Kelsen DP: Molecular classification of gastric cancer: A new paradigm. *Clin. Cancer Res.* 17: 2693–2701, 2011

33. Lei Z, Tan IB, Das K, Deng N, Zouridis H, Pattison S, Chua C, Feng Z, Guan YK, Ooi CH, Ivanova T, Zhang S, Lee M, Wu J, Ngo A, Manesh S, Tan E, Teh BT, So JBY, Goh LK, Boussioutas A, Lim TKH, Flotow H, Tan P, Rozen SG: Identification of Molecular Subtypes of Gastric Cancer With Different Responses to PI3-Kinase Inhibitors and 5-Fluorouracil. *Gastroenterology* 145: 554–565, 2013

34. Network CGAR: Comprehensive molecular characterization of gastric adenocarcinoma. *Nature* 513: 202–209, 2014

35. Burke AP, Yen TS, Shekitka KM, Sobin LH: Lymphoepithelial carcinoma of the stomach with Epstein-Barr virus demonstrated by polymerase chain reaction. *Mod. Pathol.* 3: 377–80, 1990

36. Marshall BJ: Helicobacter pylori: a primer for 1994. *Gastroenterologist* 1: 241–7, 1993

37. Chung S min, Kawai K: Protease activities in gastric cancer tissues. *Clin. Chim. Acta* 189: 205–210, 1990

38. Jee C Do, Lee HS, Bae SI, Yang HK, Lee YM, Rho MS, Kim WH: Loss of caspase-1 gene expression in human gastric carcinomas and cell lines. *Int. J. Oncol.* 26: 1265–71, 2005

39. Yoo NJi, Lee JW, Kim YJ, Soung YH, Kim SY, Nan SW, Park WS, Lee JY, Lee SH: Loss of caspase-2, -6 and -7 expression in gastric cancers. *APMIS* 112: 330–335, 2004

40. Zhang M, Zhao J, Tang W, Wang Y, Peng P, Li L, Song S, Wu H, Li C, Yang C, Wang X, Zhang C, Gu J: High Hepsin expression predicts poor prognosis in Gastric Cancer. *Sci. Rep.* 6: 36902, 2016

41. Allgayer H, Babic R, Grützner KU, Beyer BC, Tarabichi A, Schildberg FW, Heiss MM: Tumor-associated proteases and inhibitors in gastric cancer: analysis of prognostic impact and individual risk protease patterns. *Clin. Exp. Metastasis* 16: 62–73, 1998

42. Labisso WL, Seifu D: Application of Proteases as Molecular Imaging Tools for Early Gastric Cancer Detection: In Vitro and Ex Vivo Investigation. *J. Mol. Biomark. Diagn.* 8: 6, 2017

43. Thornberry NA, Rano TA, Peterson EP, Rasper DM, Timkey T, Garcia-Calvo M, Houtzager VM, Nordstrom PA, Roy S, Vaillancourt JP, Chapman KT, Nicholson DW: A Combinatorial Approach Defines Specificities of Members of the Caspase Family and Granzyme B. *J. Biol. Chem.* 272: 17907–17911, 1997

44. Harris JL, Backes BJ, Leonetti F, Mahrus S, Ellman JA, Craik CS: Rapid and general profiling of protease specificity by using combinatorial fluorogenic substrate libraries. *Proc. Natl. Acad. Sci.* 97: 7754–7759, 2000

45. Kasperkiewicz P, Poreba M, Groborz K, Drag M: Emerging challenges in the design of selective substrates, inhibitors and activity-based probes for indistinguishable proteases. *FEBS J.* 284: 1518–1539, 2017

46. Cravatt B: Chemical strategies for the global analysis of protein function. *Curr. Opin. Chem. Biol.* 4: 663–668, 2000

47. Adam GC, Sorensen EJ, Cravatt BF: Chemical Strategies for Functional Proteomics. *Mol. Cell. Proteomics* 1: 781–790, 2002

48. Liu Y, Patricelli MP, Cravatt BF: Activity-based protein profiling: The serine hydrolases.

*Proc. Natl. Acad. Sci.* 96: 14694–14699, 1999

49. Weissleder R, Tung C-H, Mahmood U, Bogdanov A: In vivo imaging of tumors with protease-activated near-infrared fluorescent probes. *Nat. Biotechnol.* 17: 375–378, 1999

50. Withana NP, Garland M, Verdoes M, Ofori LO, Segal E, Bogyo M: Labeling of active proteases in fresh-frozen tissues by topical application of quenched activity-based probes. *Nat. Protoc.* 11: 184–191, 2016

51. Thomson JJ: Cathode Rays. *Philos. Mag.* 44: 293, 1897

52. Aston FW: LXXIV. A positive ray spectrograph. *London, Edinburgh, Dublin Philos. Mag. J. Sci.* 38: 707–714, 1919

53. Comisarow MB, Marshall AG: Fourier transform ion cyclotron resonance spectroscopy. *Chem. Phys. Lett.* 25: 282–283, 1974

54. A O Nier: A double-Focusing Mass Spectrometer. *Mass Spectrosc. Phys. Res. Natl. Bur. Stand. Circ.* 522: 29, 1953

55. Wolff MM, Stephens WE: A Pulsed Mass Spectrometer with Time Dispersion. *Rev. Sci. Instrum.* 24: 616–617, 1953

56. Cameron AE, Eggers DF: An Ion ``Velocitron''. *Rev. Sci. Instrum.* 19: 605–607, 1948

57. Paul W, Steinwedel H: Notizen: Ein neues Massenspektrometer ohne Magnetfeld. *Phys. Sci. Zeitschrift für Naturforsch. A* 8: 448–450, 1953

58. Fenn J, Mann M, Meng C, Wong S, Whitehouse C: Electrospray ionization for mass spectrometry of large biomolecules. *Science (80-. ).* 246: 64–71, 1989

59. Karas M, Bachmann D, Hillenkamp F: Influence of the wavelength in high-irradiance ultraviolet laser desorption mass spectrometry of organic molecules. *Anal. Chem.* 57: 2935–2939, 1985

60. Shariatgorji M, Svenningsson P, Andrén PE: Mass Spectrometry Imaging, an Emerging Technology in Neuropsychopharmacology. *Neuropsychopharmacology* 39: 34–49, 2014

61. Caprioli RM, Farmer TB, Gile J: Molecular Imaging of Biological Samples: Localization of Peptides and Proteins Using MALDI-TOF MS. *Anal. Chem.* 69: 4751–4760, 1997

62. Norris JL, Caprioli RM: Imaging mass spectrometry: a new tool for pathology in a molecular age. *Proteomics. Clin. Appl.* 7: 733–8, 2013

63. Zavalin A, Todd EM, Rawhouser PD, Yang J, Norris JL, Caprioli RM: Direct imaging of single cells and tissue at sub-cellular spatial resolution using transmission geometry MALDI MS. *J. Mass Spectrom.* 47: i, 2012

64. Aichler M, Walch A: MALDI Imaging mass spectrometry: current frontiers and perspectives in pathology research and practice. *Lab. Investig.* 95: 422–431, 2015

65. Goodwin RJ a, Pennington SR, Pitt AR: Protein and peptides in pictures: Imaging with

MALDI mass spectrometry. *Proteomics* 8: 3785–3800, 2008

66. Fox CH, Johnson FB, Whiting J, Roller PP: Formaldehyde fixation. *J. Histochem. Cytochem.* 33: 845–853, 1985

67. Werner M, Chott A, Fabiano A, Battifora H: Effect of formalin tissue fixation and processing on immunohistochemistry. *Am. J. Surg. Pathol.* 24: 1016–9, 2000

68. Kokkat TJ, Patel MS, McGarvey D, LiVolsi VA, Baloch ZW: Archived Formalin-Fixed Paraffin-Embedded (FFPE) Blocks: A Valuable Underexploited Resource for Extraction of DNA, RNA, and Protein. *Biopreserv. Biobank.* 11: 101–106, 2013

69. Shi SR, Key ME, Kalra KL: Antigen retrieval in formalin-fixed, paraffin-embedded tissues: an enhancement method for immunohistochemical staining based on microwave oven heating of tissue sections. *J. Histochem. Cytochem.* 39: 741–748, 1991

70. Pileri SA, Roncador G, Ceccarelli C, Piccioli M, Briskomatis A, Sabattini E, Ascani S, Santini D, Piccaluga PP, Leone O, Damiani S, Ercolessi C, Sandri F, Pieri F, Leoncini L, Falini B: Antigen retrieval techniques in immunohistochemistry: comparison of different methods. *J. Pathol.* 183: 116–123, 1997

71. Fowler CB, O'Leary TJ, Mason JT: Protein Mass Spectrometry Applications on FFPE Tissue Sections. 2011

72. Hood BL, Conrads TP, Veenstra TD: Mass spectrometric analysis of formalin-fixed paraffin-embedded tissue: Unlocking the proteome within. *Proteomics* 6: 4106–4114, 2006

73. Link AJ, Eng J, Schieltz DM, Carmack E, Mize GJ, Morris DR, Garvik BM, Yates JR: Direct analysis of protein complexes using mass spectrometry. *Nat. Biotechnol.* 17: 676–82, 1999

74. Catherman AD, Skinner OS, Kelleher NL: Top Down proteomics: Facts and perspectives. *Biochem. Biophys. Res. Commun.* 445: 683–693, 2014

75. Aebersold R, Mann M: Mass spectrometry-based proteomics. *Nature* 422: 198–207, 2003

76. Minerva L, Clerens S, Baggerman G, Arckens L: Direct profiling and identification of peptide expression differences in the pancreas of control and ob/ob mice by imaging mass spectrometry. *Proteomics* 8: 3763–3774, 2008

77. Rauser S, Marquardt C, Balluff B, Deininger S-O, Albers C, Belau E, Hartmer R, Suckau D, Specht K, Ebert MP, Schmitt M, Aubele M, Höfler H, Walch A: Classification of HER2 Receptor Status in Breast Cancer Tissues by MALDI Imaging Mass Spectrometry. *J. Proteome Res.* 9: 1854–1863, 2010

78. Maier SK, Hahne H, Gholami AM, Balluff B, Meding S, Schoene C, Walch AK, Kuster B: Comprehensive Identification of Proteins from MALDI Imaging. *Mol. Cell. Proteomics* 12: 2901–2910, 2013

79. Cillero-Pastor B, Eijkel GB, Kiss A, Blanco FJ, Heeren RMA: Matrix-assisted laser desorption ionization-imaging mass spectrometry: A new methodology to study human osteoarthritic cartilage. *Arthritis Rheum.* 65: 710–720, 2013

80. Heijs B, Carreira RJ, Tolner EA, de Ru AH, van den Maagdenberg AMJM, van Veelen PA, McDonnell LA: Comprehensive Analysis of the Mouse Brain Proteome Sampled in Mass Spectrometry Imaging. *Anal. Chem.* 87: 1867–1875, 2015

81. Longuespée R, Kriegsmann K, Cremer M, Zgorzelski C, Casadonte R, Kazdal D, Kriegsmann J, Weichert W, Schwamborn K, Fresnais M, Schirmacher P, Kriegsmann M: In MALDI-Mass Spectrometry Imaging on Formalin-Fixed Paraffin-Embedded Tissue Specimen Section Thickness Significantly Influences m/z Peak Intensity. *PROTEOMICS - Clin. Appl.* 1800074, 2018

82. Battifora H: The multitumor (sausage) tissue block: novel method for immunohistochemical antibody testing. *Lab. Invest.* 55: 244–8, 1986

83. Groseclose MR, Andersson M, Hardesty WM, Caprioli RM: Identification of proteins directly from tissue:in situ tryptic digestions coupled with imaging mass spectrometry. *J. Mass Spectrom.* 42: 254–262, 2007

84. Stauber J, Lemaire R, Franck J, Bonnel D, Croix D, Day R, Wisztorski M, Fournier I, Salzet M: MALDI Imaging of Formalin-Fixed Paraffin-Embedded Tissues: Application to Model Animals of Parkinson Disease for Biomarker Hunting. *J. Proteome Res.* 7: 969–978, 2008

85. Ronci M, Bonanno E, Colantoni A, Pieroni L, Di Ilio C, Spagnoli LG, Federici G, Urbani A: Protein unlocking procedures of formalin-fixed paraffin-embedded tissues: Application to MALDI-TOF Imaging MS investigations. *Proteomics* 8: 3702–3714, 2008

86. Groseclose MR, Massion PP, Chaurand P, Caprioli RM: High-throughput proteomic analysis of formalin-fixed paraffin-embedded tissue microarrays using MALDI imaging mass spectrometry. *Proteomics* 8: 3715–3724, 2008

87. Gravius S, Randau TM, Casadonte R, Kriegsmann M, Friedrich MJ, Kriegsmann J: Investigation of neutrophilic peptides in periprosthetic tissue by matrix-assisted laser desorption ionisation time-of-flight imaging mass spectrometry. *Int. Orthop.* 39: 559–567, 2015

88. Stauber J, MacAleese L, Franck J, Claude E, Snel M, Kaletas BK, Wiel IMVD, Wisztorski M, Fournier I, Heeren RMA: On-tissue protein identification and imaging by MALDI-Ion mobility mass spectrometry. *J. Am. Soc. Mass Spectrom.* 21: 338–347, 2010

89. Gustafsson JOR, Oehler MK, McColl SR, Hoffmann P: Citric acid antigen retrieval (CAAR) for tryptic peptide imaging directly on archived formalin-fixed paraffin-embedded tissue. *J. Proteome Res.* 9: 4315–28, 2010

90. Casadonte R, Caprioli RM: Proteomic analysis of formalin-fixed paraffin-embedded

tissue by MALDI imaging mass spectrometry. *Nat. Protoc.* 6: 1695–1709, 2011

91.    Enthaler B, Trusch M, Fischer M, Rapp C, Pruns JK, Vietzke J-P: MALDI imaging in human skin tissue sections: focus on various matrices and enzymes. *Anal. Bioanal. Chem.* 405: 1159–1170, 2013

92.    Powers TW, Neely BA, Shao Y, Tang H, Troyer DA, Mehta AS, Haab BB, Drake RR: MALDI Imaging Mass Spectrometry Profiling of N-Glycans in Formalin-Fixed Paraffin Embedded Clinical Tissue Blocks and Tissue Microarrays. *PLoS One* 9: e106255, 2014

93.    De Sio G, Smith AJ, Galli M, Garancini M, Chinello C, Bono F, Pagni F, Magni F: A MALDI-Mass Spectrometry Imaging method applicable to different formalin-fixed paraffin-embedded human tissues. *Mol. Biosyst.* 11: 1507–1514, 2015

94.    Casadonte R, Kriegsmann M, Deininger S-O, Amann K, Paape R, Belau E, Suckau D, Fuchser J, Beckmann J, Becker M, Kriegsmann J: Imaging mass spectrometry analysis of renal amyloidosis biopsies reveals protein co-localization with amyloid deposits. *Anal. Bioanal. Chem.* 407: 5323–5331, 2015

95.    Heijs B, Tolner EA, Bovée JVMG, van den Maagdenberg AMJM, McDonnell LA: Brain Region-Specific Dynamics of On-Tissue Protein Digestion Using MALDI Mass Spectrometry Imaging. *J. Proteome Res.* 14: 5348–5354, 2015

96.    Diehl HC, Beine B, Elm J, Trede D, Ahrens M, Eisenacher M, Marcus K, Meyer HE, Henkel C: The challenge of on-tissue digestion for MALDI MSI— a comparison of different protocols to improve imaging experiments. *Anal. Bioanal. Chem.* 407: 2223–2243, 2015

97.    Holst S, Heijs B, de Haan N, van Zeijl RJM, Briaire-de Bruijn IH, van Pelt GW, Mehta AS, Angel PM, Mesker WE, Tollenaar RA, Drake RR, Bovée JVMG, McDonnell LA, Wuhrer M: Linkage-Specific in Situ Sialic Acid Derivatization for N-Glycan Mass Spectrometry Imaging of Formalin-Fixed Paraffin-Embedded Tissues. *Anal. Chem.* 88: 5904–5913, 2016

98.    Oetjen J, Lachmund D, Palmer A, Alexandrov T, Becker M, Boskamp T, Maass P: An approach to optimize sample preparation for MALDI imaging MS of FFPE sections using fractional factorial design of experiments. *Anal. Bioanal. Chem.* 408: 6729–6740, 2016

99.    Mascini NE, Teunissen J, Noorlag R, Willems SM, Heeren RMA: Tumor classification with MALDI-MSI data of tissue microarrays: A case study. *Methods* 151: 21–27, 2018

100.    Angel PM, Comte-Walters S, Ball LE, Talbot K, Mehta A, Brockbank KGM, Drake RR: Mapping Extracellular Matrix Proteins in Formalin-Fixed, Paraffin-Embedded Tissues by MALDI Imaging Mass Spectrometry. *J. Proteome Res.* 17: 635–646, 2018

101.    Brenton AG, Godfrey AR: Accurate mass measurement: terminology and treatment of data. *J. Am. Soc. Mass Spectrom.* 21: 1821–35, 2010

102.    Mann M, Kelleher NL: Precision proteomics: The case for high resolution and high mass

accuracy. *Proc. Natl. Acad. Sci.* 105: 18132–18138, 2008

103. O'Rourke MB, Djordjevic SP, Padula MP: The quest for improved reproducibility in MALDI mass spectrometry. *Mass Spectrom. Rev.* 37: 217–228, 2018

104. Wilk ZA, Viswanadham SK, Sharkey AG, Hercules DM: Factors affecting the quantitation of organic compounds in laser mass spectrometry. *Anal. Chem.* 60: 2338–2346, 1988

105. Preston LM, Murray KK, Russell DH: Reproducibility and quantitation of matrix-assisted laser desorption ionization mass spectrometry: Effects of nitrocellulose on peptide ion yields. *Biol. Mass Spectrom.* 22: 544–550, 1993

106. Djidja M-C, Claude E, Snel MF, Francese S, Scriven P, Carolan V, Clench MR: Novel molecular tumour classification using MALDI–mass spectrometry imaging of tissue micro-array. *Anal. Bioanal. Chem.* 397: 587–601, 2010

107. Steurer S, Borkowski C, Odinga S, Buchholz M, Koop C, Huland H, Becker M, Witt M, Trede D, Omidi M, Kraus O, Bahar AS, Seddiqi AS, Singer JM, Kwiatkowski M, Trusch M, Simon R, Wurlitzer M, Minner S, Schlomm T, Sauter G, Schlüter H: MALDI mass spectrometric imaging based identification of clinically relevant signals in prostate cancer using large-scale tissue microarrays. *Int. J. Cancer* 133: 920–928, 2013

108. Jones EA, Deininger S-O, Hogendoorn PCW, Deelder AM, McDonnell LA: Imaging mass spectrometry statistical analysis. *J. Proteomics* 75: 4962–4989, 2012

109. Rabe J-H, A. Sammour D, Schulz S, Munteanu B, Ott M, Ochs K, Hohenberger P, Marx A, Platten M, Opitz CA, Ory DS, Hopf C: Fourier Transform Infrared Microscopy Enables Guidance of Automated Mass Spectrometry Imaging to Predefined Tissue Morphologies. *Sci. Rep.* 8: 313, 2018

110. Thompson J, Epting T, Schwarzkopf G, Singhofen A, Eades-Perner A-M, van der Putten H, Zimmermann W: A transgenic mouse line that develops early-onset invasive gastric carcinoma provides a model for carcinoembryonic antigen-targeted tumor therapy. *Int. J. Cancer* 86: 863–869, 2000

111. Schneider CA, Rasband WS, Eliceiri KW: NIH Image to ImageJ: 25 years of image analysis. *Nat. Methods* 9: 671–5, 2012

112. Schwamborn K, Caprioli RM: Molecular imaging by mass spectrometry — looking beyond classical histology. *Nat. Rev. Cancer* 10: 639–646, 2010

113. Cupp-Enyard C: Sigma's Non-specific Protease Activity Assay - Casein as a Substrate. *J. Vis. Exp.* 19: 899, 2008

114. Hinsenkamp I, Schulz S, Roscher M, Suhr A-M, Meyer B, Munteanu B, Fuchser J, Schoenberg SO, Ebert MPA, Wängler B, Hopf C, Burgermeister E: Inhibition of Rho-Associated Kinase 1/2 Attenuates Tumor Growth in Murine Gastric Cancer. *Neoplasia* 18: 500–11, 2016

115. Erich K, Reinle K, Müller T, Munteanu B, Sammour DA, Hinsenkamp I, Gutting T, Burgermeister E, Findeisen P, Ebert MP, Krijgsveld J, Hopf C: Spatial Distribution of Endogenous Tissue Protease Activity in Gastric Carcinoma Mapped by MALDI Mass Spectrometry Imaging. *Mol. Cell. Proteomics* 18: 151–161, 2019

116. Schramm T, Hester A, Klinkert I, Both J-P, Heeren RMA, Brunelle A, Laprévote O, Desbenoit N, Robbe M-F, Stoeckli M, Spengler B, Römpp A: imzML — A common data format for the flexible exchange and processing of mass spectrometry imaging data. *J. Proteomics* 75: 5106–5110, 2012

117. Palmer A, Phapale P, Chernyavsky I, Lavigne R, Fay D, Tarasov A, Kovalev V, Fuchser J, Nikolenko S, Pineau C, Becker M, Alexandrov T: FDR-controlled metabolite annotation for high-resolution imaging mass spectrometry. *Nat. Methods* 14: 57–60, 2017

118. Ihaka R, Gentleman R: R: A Language for Data Analysis and Graphics. *J. Comput. Graph. Stat.* 5: 299–314, 1996

119. Fülöp A, Sammour DA, Erich K, von Gerichten J, van Hoogevest P, Sandhoff R, Hopf C: Molecular imaging of brain localization of liposomes in mice using MALDI mass spectrometry. *Sci. Rep.* 6: 33791, 2016

120. Erich K, Sammour DA, Marx A, Hopf C: Scores for standardization of on-tissue digestion of formalin-fixed paraffin-embedded tissue in MALDI-MS imaging. *Biochim. Biophys. Acta - Proteins Proteomics* 1865: 907–915, 2017

121. Syngenta Austria: Water sensitive paper. 2018 Available from: https://www.syngenta.com.au/awri [cited 2018 Aug 30]

122. R. D. Fox, R. C. Derksen, J. A. Cooper, C. R. Krause, H. E. Ozkan: Visual and image system measurement of spray deposits using water-sensitive paper. *Appl. Eng. Agric.* 19: 549, 2003

123. Taylor AJ, Dexter A, Bunch J: Exploring Ion Suppression in Mass Spectrometry Imaging of a Heterogeneous Tissue. *Anal. Chem.* 90: 5637–5645, 2018

124. Scholz B, Sköld K, Kultima K, Fernandez C, Waldemarson S, Savitski MM, Söderquist M, Borén M, Stella R, Andrén P, Zubarev R, James P: Impact of Temperature Dependent Sampling Procedures in Proteomics and Peptidomics – A Characterization of the Liver and Pancreas Post Mortem Degradome. *Mol. Cell. Proteomics* 10: M900229-MCP200, 2011

125. Ihler F, Vetter EV, Pan J, Kammerer R, Debey-Pascher S, Schultze JL, Zimmermann W, Enders G: Expression of a Neuroendocrine Gene Signature in Gastric Tumor Cells from CEA 424-SV40 Large T Antigen-Transgenic Mice Depends on SV40 Large T Antigen. *PLoS One* 7: e29846, 2012

126. Munteanu B, Meyer B, von Reitzenstein C, Burgermeister E, Bog S, Pahl A, Ebert MP,

Hopf C: Label-Free in Situ Monitoring of Histone Deacetylase Drug Target Engagement by Matrix-Assisted Laser Desorption Ionization-Mass Spectrometry Biotyping and Imaging. *Anal. Chem.* 86: 4642–4647, 2014

127. Goodwin RJ a, Nilsson A, Borg D, Langridge-Smith PRR, Harrison DJ, Mackay CL, Iverson SL, Andrén PE: Conductive carbon tape used for support and mounting of both whole animal and fragile heat-treated tissue sections for MALDI MS imaging and quantitation. *J. Proteomics* 75: 4912–4920, 2012

128. Wang H-YJ, Liu C Bin, Wu H-W: A simple desalting method for direct MALDI mass spectrometry profiling of tissue lipids. *J. Lipid Res.* 52: 840–849, 2011

129. Ritchie ME, Phipson B, Wu D, Hu Y, Law CW, Shi W, Smyth GK: limma powers differential expression analyses for RNA-sequencing and microarray studies. *Nucleic Acids Res.* 43: e47–e47, 2015

130. Stoeckli M, Chaurand P, Hallahan DE, Caprioli RM: Imaging mass spectrometry: A new technology for the analysis of protein expression in mammalian tissues. *Nat. Med.* 7: 493–496, 2001

131. Caprioli RM, Farmer TB, Gile J: Molecular Imaging of Biological Samples: Localization of Peptides and Proteins Using MALDI-TOF MS. *Anal. Chem.* 69: 4751–4760, 1997

132. Sun N, Fernandez IE, Wei M, Wu Y, Aichler M, Eickelberg O, Walch A: Pharmacokinetic and pharmacometabolomic study of pirfenidone in normal mouse tissues using high mass resolution MALDI-FTICR-mass spectrometry imaging. *Histochem. Cell Biol.* 145: 201–211, 2016

133. Nilsson A, Goodwin RJ a., Shariatgorji M, Vallianatou T, Webborn PJH, Andrén PE: Mass Spectrometry Imaging in Drug Development. *Anal. Chem.* 87: 1437–1455, 2015

134. Qin L, Zhang Y, Liu Y, He H, Han M, Li Y, Zeng M, Wang X: Recent advances in matrix-assisted laser desorption/ionisation mass spectrometry imaging (MALDI-MSI) for in situ analysis of endogenous molecules in plants. *Phytochem. Anal.* 29: 351–364, 2018

135. Hall-Andersen J, Kaasgaard SG, Janfelt C: MALDI imaging of enzymatic degradation of glycerides by lipase on textile surface. *Chem. Phys. Lipids* 211: 100–106, 2018

136. Jadoul L, Longuespée R, Noël A, De Pauw E: A spiked tissue-based approach for quantification of phosphatidylcholines in brain section by MALDI mass spectrometry imaging. *Anal. Bioanal. Chem.* 407: 2095–2106, 2015

137. Balluff B, Rauser S, Meding S, Elsner M, Schöne C, Feuchtinger A, Schuhmacher C, Novotny A, Jütting U, Maccarrone G, Sarioglu H, Ueffing M, Braselmann H, Zitzelsberger H, Schmid RM, Höfler H, Ebert MP, Walch A: MALDI Imaging Identifies Prognostic Seven-Protein Signature of Novel Tissue Markers in Intestinal-Type Gastric Cancer. *Am. J. Pathol.* 179: 2720–2729, 2011

138. Bauer JA, Chakravarthy AB, Rosenbluth JM, Mi D, Seeley EH, De Matos Granja-Ingram

N, Olivares MG, Kelley MC, Mayer IA, Meszoely IM, Means-Powell JA, Johnson KN, Tsai CJ, Ayers GD, Sanders ME, Schneider RJ, Formenti SC, Caprioli RM, Pietenpol JA: Identification of Markers of Taxane Sensitivity Using Proteomic and Genomic Analyses of Breast Tumors from Patients Receiving Neoadjuvant Paclitaxel and Radiation. *Clin. Cancer Res.* 16: 681–690, 2010

139. Schwamborn K, Krieg RC, Jirak P, Ott G, Knüchel R, Rosenwald A, Wellmann A: Application of MALDI imaging for the diagnosis of classical Hodgkin lymphoma. *J. Cancer Res. Clin. Oncol.* 136: 1651–1655, 2010

140. Meding S, Nitsche U, Balluff B, Elsner M, Rauser S, Schöne C, Nipp M, Maak M, Feith M, Ebert MP, Friess H, Langer R, Höfler H, Zitzelsberger H, Rosenberg R, Walch A: Tumor classification of six common cancer types based on proteomic profiling by MALDI imaging. *J. Proteome Res.* 11: 1996–2003, 2012

141. Casadonte R, Kriegsmann M, Zweynert F, Friedrich K, Bretton G, Otto M, Deininger S-O, Paape R, Belau E, Suckau D, Aust D, Pilarsky C, Kriegsmann J: Imaging mass spectrometry to discriminate breast from pancreatic cancer metastasis in formalin-fixed paraffin-embedded tissues. *Proteomics* 14: 956–964, 2014

142. Balluff B, Elsner M, Kowarsch A, Rauser S, Meding S, Schuhmacher C, Feith M, Herrmann K, Röcken C, Schmid RM, Höfler H, Walch A, Ebert MP: Classification of HER2/neu Status in Gastric Cancer Using a Breast-Cancer Derived Proteome Classifier. *J. Proteome Res.* 9: 6317–6322, 2010

143. Willems SM, van Remoortere A, van Zeijl R, Deelder AM, McDonnell LA, Hogendoorn PC: Imaging mass spectrometry of myxoid sarcomas identifies proteins and lipids specific to tumour type and grade, and reveals biochemical intratumour heterogeneity. *J. Pathol.* 222: 400–409, 2010

144. Balluff B, Frese CK, Maier SK, Schöne C, Kuster B, Schmitt M, Aubele M, Höfler H, Deelder AM, Heck A, Hogendoorn PCW, Morreau J, Maarten Altelaar AF, Walch A, McDonnell LA, Hogendoorn PCW, Morreau J, Maarten Altelaar AF, Walch A, McDonnell LA: De novo discovery of phenotypic intratumour heterogeneity using imaging mass spectrometry. *J. Pathol.* 235: 3–13, 2015

145. Hillenkamp F, Karas M: Mass spectrometry of peptides and proteins by matrix-assisted ultraviolet laser desorption/ionization. Academic Press; 1990

146. Hillenkamp F, Karas M: The MALDI Process and Method. Weinheim, Germany: Wiley-VCH Verlag GmbH & Co. KGaA; 2007

147. Topic E, Nikolac N, Panteghini M, Theodorsson E, Salvagno GL, Miler M, Simundic A-M, Infusino I, Nordin G, Westgard S: How to assess the quality of your analytical method? *Clin. Chem. Lab. Med.* 53: 1707–1718, 2015

148. Taverniers I, De Loose M, Van Bockstaele E: Trends in quality in the analytical

laboratory. II. Analytical method validation and quality assurance. *TrAC Trends Anal. Chem.* 23: 535–552, 2004

149. Green JM: A Practical Guide to Analytical Method Validation. *Anal. Chem.* 68: 305A–309A, 1996

150. Food and Drug Administration: Guidance for Industry: Bioanalytical Method Validation. 2001

151. Chaurand P, Latham JC, Lane KB, Mobley JA, Polosukhin V V., Wirth PS, Nanney LB, Caprioli RM: Imaging Mass Spectrometry of Intact Proteins from Alcohol-Preserved Tissue Specimens: Bypassing Formalin Fixation. *J. Proteome Res.* 7: 3543–3555, 2008

152. Damodaran S, Wood TD, Nagarajan P, Rabin RA: Evaluating peptide mass fingerprinting-based protein identification. *Genomics. Proteomics Bioinformatics* 5: 152–7, 2007

153. Meyer B, Papasotiriou DG, Karas M: 100% protein sequence coverage: a modern form of surrealism in proteomics. *Amino Acids* 41: 291–310, 2011

154. Stoeckli M, Staab D: Reproducible Matrix Deposition for MALDI MSI Based on Open-Source Software and Hardware. *J. Am. Soc. Mass Spectrom.* 26: 911–914, 2015

155. Hankin JA, Barkley RM, Murphy RC: Sublimation as a method of matrix application for mass spectrometric imaging. *J. Am. Soc. Mass Spectrom.* 18: 1646–1652, 2007

156. Albrethsen J: Reproducibility in Protein Profiling by MALDI-TOF Mass Spectrometry. *Clin. Chem.* 53: 852–858, 2007

157. Tsiatsiani L, Heck AJR: Proteomics beyond trypsin. *FEBS J.* 282: 2612–2626, 2015

158. Zaima N, Hayasaka T, Goto-Inoue N, Setou M: Matrix-Assisted Laser Desorption/Ionization Imaging Mass Spectrometry. *Int. J. Mol. Sci.* 11: 5040–5055, 2010

159. Sadeghi M: Crystallite size dependence of volatilization in matrix-assisted laser desorption ionization. *Appl. Surf. Sci.* 127–129: 226–234, 1998

160. SunChrom: Influence of crystal size of matrix layer on resolution in MALDI Imaging Laser beam diameter and hot zone. 2017

161. Li S, Zhang Y, Liu J, Han J, Guan M, Yang H, Lin Y, Xiong S, Zhao Z: Electrospray deposition device used to precisely control the matrix crystal to improve the performance of MALDI MSI. *Sci. Rep.* 6: 37903, 2016

162. Schulz S, Gerhardt D, Meyer B, Seegel M, Schubach B, Hopf C, Matheis K: DMSO-enhanced MALDI MS imaging with normalization against a deuterated standard for relative quantification of dasatinib in serial mouse pharmacology studies. *Anal. Bioanal. Chem.* 405: 9467–9476, 2013

163. Aikawa H, Hayashi M, Ryu S, Yamashita M, Ohtsuka N, Nishidate M, Fujiwara Y, Hamada A: Visualizing spatial distribution of alectinib in murine brain using quantitative mass spectrometry imaging. *Sci. Rep.* 6: 23749, 2016

164. Clemis EJ, Smith DS, Camenzind AG, Danell RM, Parker CE, Borchers CH: Quantitation of spatially-localized proteins in tissue samples using MALDI-MRM imaging. *Anal. Chem.* 84: 3514–22, 2012

165. Prideaux B, Dartois V, Staab D, Weiner DM, Goh A, Via LE, Barry CE, Stoeckli M, Stoeckli M: High-sensitivity MALDI-MRM-MS imaging of moxifloxacin distribution in tuberculosis-infected rabbit lungs and granulomatous lesions. *Anal. Chem.* 83: 2112–8, 2011

166. Stoeckli M, Staab D, Schweitzer A: Compound and metabolite distribution measured by MALDI mass spectrometric imaging in whole-body tissue sections. *Int. J. Mass Spectrom.* 260: 195–202, 2007

167. Marko-Varga G, Fehniger TE, Rezeli M, Döme B, Laurell T, Végvári Á: Drug localization in different lung cancer phenotypes by MALDI mass spectrometry imaging. *J. Proteomics* 74: 982–992, 2011

168. Rubakhin SS, Sweedler J V: Mass Spectrometry Imaging. Totowa, NJ: Humana Press; 2010

169. Rzagalinski I, Volmer DA: Quantification of low molecular weight compounds by MALDI imaging mass spectrometry – A tutorial review. *Biochim. Biophys. Acta - Proteins Proteomics* 1865: 726–739, 2017

170. Yi J, Liu Z, Craft D, O'Mullan P, Ju G, Gelfand CA: Intrinsic Peptidase Activity Causes a Sequential Multi-Step Reaction (SMSR) in Digestion of Human Plasma Peptides. *J. Proteome Res.* 7: 5112–5118, 2008

171. Bouchoux G: Gas phase basicities of polyfunctional molecules. Part 3: Amino acids. *Mass Spectrom. Rev.* 31: 391–435, 2012

172. Zenobi R, Knochenmuss R: Ion formation in MALDI mass spectrometry. *Mass Spectrom. Rev.* 17: 337–366, 1998

173. Nadler WM, Waidelich D, Kerner A, Hanke S, Berg R, Trumpp A, Rösli C: MALDI versus ESI: The Impact of the Ion Source on Peptide Identification. *J. Proteome Res.* 16: 1207–1215, 2017

174. Everette JD, Bryant QM, Green AM, Abbey YA, Wangila GW, Walker RB: Thorough Study of Reactivity of Various Compound Classes toward the Folin−Ciocalteu Reagent. *J. Agric. Food Chem.* 58: 8139–8144, 2010

175. Speers AE, Wu CC: Proteomics of Integral Membrane ProteinsTheory and Application. *Chem. Rev.* 107: 3687–3714, 2007

176. Meyer B: Charakterisierung und Identifizierung von Membranproteinen auf der Ebene von Peptiden. 2007

177. Goldberg GI, Frisch SM, He C, Wilhelm SM, Reich R, Collier IE: Secreted Proteases. *Ann. N. Y. Acad. Sci.* 580: 375–384, 1990

178. Sevenich L, Joyce JA: Pericellular proteolysis in cancer. *Genes Dev.* 28: 2331–2347, 2014

179. Brix K: Lysosomal Proteases: Retrieval of the Sleeping Beauty. Austin (TX): Landes Bioscience; 2005

180. Baruch A, Jeffery DA, Bogyo M: Enzyme activity – it's all about image. *Trends Cell Biol.* 14: 29–35, 2004

181. Funovics M, Weissleder R, Tung C-H: Protease sensors for bioimaging. *Anal. Bioanal. Chem.* 377: 956–963, 2003

182. Poreba M, Drag M: Current Strategies for Probing Substrate Specificity of Proteases. *Curr. Med. Chem.* 17: 3968–3995, 2012

183. Rut W, Kasperkiewicz P, Byzia A, Poreba M, Groborz K, Drag M: Recent advances and concepts in substrate specificity determination of proteases using tailored libraries of fluorogenic substrates with unnatural amino acids. *Biol. Chem.* 396: 329–37, 2015

184. Liu H-W, Chen L, Xu C, Li Z, Zhang H, Zhang X-B, Tan W: Recent progresses in small-molecule enzymatic fluorescent probes for cancer imaging. *Chem. Soc. Rev.* 47: 7140–7180, 2018

185. Garland M, Yim JJ, Bogyo M: A Bright Future for Precision Medicine: Advances in Fluorescent Chemical Probe Design and Their Clinical Application. *Cell Chem. Biol.* 23: 122–136, 2016

186. Cutter JL, Cohen NT, Wang J, Sloan AE, Cohen AR, Panneerselvam A, Schluchter M, Blum G, Bogyo M, Basilion JP: Topical Application of Activity-based Probes for Visualization of Brain Tumor Tissue. *PLoS One* 7: e33060, 2012

187. Fisher S, Yasui Y, Dabbs K, Winget M: Re-excision and survival following breast conserving surgery in early stage breast cancer patients: a population-based study. *BMC Health Serv. Res.* 18: 94, 2018

188. Somerset HL, Kleinschmidt-DeMasters BK: Approach to the Intraoperative Consultation for Neurosurgical Specimens. *Adv. Anat. Pathol.* 18: 446–449, 2011

189. Bivehed E, Strömvall R, Bergquist J, Bakalkin G, Andersson M: Region-specific bioconversion of dynorphin neuropeptide detected by in situ histochemistry and MALDI imaging mass spectrometry. *Peptides* 87: 20–27, 2017

190. Gross J, Lapiere CM: Collagenolytic activity in amphibian tissues: a tissue culture assay. *Proc. Natl. Acad. Sci.* 48: 1014–1022, 1962

191. Stöcker W, Grams F, Reinemer P, Bode W, Baumann U, Gomis-Rüth F-X, Mckay DB: The metzincins - Topological and sequential relations between the astacins, adamalysins, serralysins, and matrixins (collagenases) define a super family of zinc-peptidases. *Protein Sci.* 4: 823–840, 2008

192. Wyganowska-Świątkowska M, Tarnowski M, Murtagh D, Skrzypczak-Jankun E, Jankun

J: Proteolysis is the most fundamental property of malignancy and its inhibition may be used therapeutically (Review). *Int. J. Mol. Med.* 43: 15–25, 2019

193. Vaysse P-M, Heeren RMA, Porta T, Balluff B: Mass spectrometry imaging for clinical research – latest developments, applications, and current limitations. *Analyst* 142: 2690–2712, 2017

194. Sköld K, Svensson M, Norrman M, Sjögren B, Svenningsson P, Andrén PE: The significance of biochemical and molecular sample integrity in brain proteomics and peptidomics: Stathmin 2-20 and peptides as sample quality indicators. *Proteomics* 7: 4445–4456, 2007

195. Ferrer I, Santpere G, Arzberger T, Bell J, Blanco R, Boluda S, Budka H, Carmona M, Giaccone G, Krebs B, Limido L, Parchi P, Puig B, Strammiello R, Ströbel T, Kretzschmar H: Brain Protein Preservation Largely Depends on the Postmortem Storage Temperature. *J. Neuropathol. Exp. Neurol.* 66: 35–46, 2007

196. McCombie G, Staab D, Stoeckli M, Knochenmuss R: Spatial and Spectral Correlations in MALDI Mass Spectrometry Images by Clustering and Multivariate Analysis. *Anal. Chem.* 77: 6118–6124, 2005

197. Almond J, Cohen G: The proteasome: a novel target for cancer chemotherapy. *Leukemia* 16: 433–443, 2002

198. Manasanch EE, Orlowski RZ: Proteasome Inhibitors in Cancer Therapy. *Nat. Rev. Clin. Oncol.* 14: 417–433, 2017

199. Hensley P, Mishra M, Kyprianou N: Targeting caspases in cancer therapeutics. *Biol. Chem.* 394: 831–843, 2013

200. Rinderknecht H: Activation of pancreatic zymogens. *Dig. Dis. Sci.* 31: 314–321, 1986

201. Berg J, Tymczko J, Stryer L: Section 10.5 Many Enzymes are activated by specific proteolytic cleavage. New York, NY: W H Freeman; 2002

202. Banno K, Niwa Y, Miyahara R, Nakamura M, Nagaya T, Nagasaka T, Watanabe O, Ando T, Kawashima H, Ohmiya N, Itoh A, Hirooka Y, Goto H: Confocal endomicroscopy for phenotypic diagnosis of gastric cancer. *J. Gastroenterol. Hepatol.* 25: 712–718, 2010

203. Otsuka Y, Niwa Y, Ohmiya N, Ando N, Ohashi A, Hirooka Y, Goto H: Usefulness of magnifying endoscopy in the diagnosis of early gastric cancer. *Endoscopy* 36: 165–169, 2004

204. Tsurudome I, Miyahara R, Funasaka K, Furukawa K, Matsushita M, Yamamura T, Ishikawa T, Ohno E, Nakamura M, Kawashima H, Watanabe O, Nakaguro M, Satou A, Hirooka Y, Goto H: In vivo histological diagnosis for gastric cancer using endocytoscopy. *World J. Gastroenterol.* 23: 6894–6901, 2017

205. Takahashi T, Saikawa Y, Kitagawa Y: Gastric Cancer: Current Status of Diagnosis and Treatment. *Cancers (Basel).* 5: 48–63, 2013

206. DeClerck YA, Mercurio AM, Stack MS, Chapman HA, Zutter MM, Muschel RJ, Raz A, Matrisian LM, Sloane BF, Noel A, Hendrix MJ, Coussens L, Padarathsingh M: Proteases, extracellular matrix, and cancer: a workshop of the path B study section. *Am. J. Pathol.* 164: 1131–9, 2004

207. Egeblad M, Nakasone ES, Werb Z: Tumors as organs: complex tissues that interface with the entire organism. *Dev. Cell* 18: 884–901, 2010

208. Tan P, Yeoh K-G: Genetics and Molecular Pathogenesis of Gastric Adenocarcinoma. *Gastroenterology* 149: 1153–1162.e3, 2015

209. Busuttil RA, George J, Tothill RW, Ioculano K, Kowalczyk A, Mitchell C, Lade S, Tan P, Haviv I, Boussioutas A: A Signature Predicting Poor Prognosis in Gastric and Ovarian Cancer Represents a Coordinated Macrophage and Stromal Response. *Clin. Cancer Res.* 20: 2761–2772, 2014

210. Kang HC, Menias CO, Gaballah AH, Shroff S, Taggart MW, Garg N, Elsayes KM: Beyond the GIST: Mesenchymal Tumors of the Stomach. *RadioGraphics* 33: 1673–1690, 2013

211. Tarazona N, Gambardella V, Huerta M, Roselló S, Cervantes A: Personalised Treatment in Gastric Cancer: Myth or Reality? *Curr. Oncol. Rep.* 18: 41, 2016

212. Jackson SE, Chester JD: Personalised cancer medicine. *Int. J. Cancer* 137: 262–266, 2015

213. Kriegsmann J, Kriegsmann M, Casadonte R: MALDI TOF imaging mass spectrometry in clinical pathology: A valuable tool for cancer diagnostics (Review). *Int. J. Oncol.* 46: 893–906, 2015

214. Buck A, Ly A, Balluff B, Sun N, Gorzolka K, Feuchtinger A, Janssen K-P, Kuppen PJ, van de Velde CJ, Weirich G, Erlmeier F, Langer R, Aubele M, Zitzelsberger H, Aichler M, Walch A: High-resolution MALDI-FT-ICR MS imaging for the analysis of metabolites from formalin-fixed, paraffin-embedded clinical tissue samples. *J. Pathol.* 237: 123–132, 2015

215. Mandel J: Repeatability and Reproducibility. *Interlab. Test. Tech.* 40–48, 1978

216. Buck A, Heijs B, Beine B, Schepers J, Cassese A, Heeren RMA, McDonnell LA, Henkel C, Walch A, Balluff B: Round robin study of formalin-fixed paraffin-embedded tissues in mass spectrometry imaging. *Anal. Bioanal. Chem.* 410: 5969–5980, 2018

217. Brownridge P, Beynon RJ: The importance of the digest: Proteolysis and absolute quantification in proteomics. *Methods* 54: 351–360, 2011

218. Proc JL, Kuzyk MA, Hardie DB, Yang J, Smith DS, Jackson AM, Parker CE, Borchers CH: A Quantitative Study of the Effects of Chaotropic Agents, Surfactants, and Solvents on the Digestion Efficiency of Human Plasma Proteins by Trypsin. *J. Proteome Res.* 9: 5422–5437, 2010

219. Scherl A, Tsai YS, Shaffer SA, Goodlett DR: Increasing information from shotgun proteomic data by accounting for misassigned precursor ion masses. *Proteomics* 8: 2791–2797, 2008

220. Veličković D, Saulnier L, Lhomme M, Damond A, Guillon F, Rogniaux H: Mass Spectrometric Imaging of Wheat ( Triticum spp.) and Barley ( Hordeum vulgare L.) Cultivars: Distribution of Major Cell Wall Polysaccharides According to Their Main Structural Features. *J. Agric. Food Chem.* 64: 6249–6256, 2016

221. Schulz S, Becker M, Groseclose MR, Schadt S, Hopf C: Advanced MALDI mass spectrometry imaging in pharmaceutical research and drug development. *Curr. Opin. Biotechnol.* 55: 51–59, 2019

# 9 PUBLICATIONS

Fülöp A, Sammour DA, **Erich K,** von Gerichten J, van Hoogevest P, Sandhoff R, Hopf C: Molecular imaging of brain localization of liposomes in mice using MALDI mass spectrometry. *Sci. Rep.* 6: 33791, 2016

**Erich K\***, Sammour DA\*, Marx A, Hopf C: Scores for standardization of on-tissue digestion of formalin-fixed paraffin-embedded tissue in MALDI-MS imaging. *Biochim. Biophys. Acta - Proteins Proteomics*. 1865: 907-915, 2017

\* these authors contributed equally

Seyrantepe V, Demir SA, Timur ZK, Gerichten J Von, Marsching C, Erdemli E, Oztas E, Takahashi K, Yamaguchi K, Ates N, Demir BD, Dalkara T, **Erich K**, Hopf C, Sandhoff R, Miyagi T: Murine Sialidase Neu3 facilitates GM2 degradation and bypass in mouse model of Tay-Sachs disease. *Exp. Neurol.* 299: 26-41, 2017

**Erich K**, Reinle K, Müller T, Munteanu B, Sammour DA, Hinsenkamp I, Gutting T, Burgermeister E, Findeisen P, Ebert MP, Krijgsveld J, Hopf C: Spatial distribution of endogenous tissue protease activity in gastric carcinoma mapped by MALDI mass spectrometry imaging. *Mol. Cell. Proteomics*. 18: 151-161, 2019

# 10 CURRICULUM VITAE

115

## PERSONALIEN

| | |
|---|---|
| Name | Katrin Erich |
| Geburtsdatum | 10.05.1989 |
| Geburtsort | Bad Dürkheim a.d.W., Deutschland |
| Nationalität | Deutsch |
| Familienstand | Verheiratet, ein Kind |

## AKADEMISCHER WERDEGANG

| | |
|---|---|
| 02/2015 - heute | **Institut für Medizintechnologie der Universität Heidelberg und der Hochschule Mannheim**<br>Doktorarbeit (Dr. sc. hum.) betreut von Prof. Dr. Carsten Hopf am Center for Mass Spectrometry and Optical Spectroscopy (CeMOS), Hochschule Mannheim |
| 09/2012 - 03/2014 | **Hochschule Mannheim**<br>Biotechnology (Master of Science)<br>Focus: Biomedical Science and Technology<br>Abschluss: Master of Science, Note: 1,2 |
| 03/2009 - 09/2012 | **Hochschule Mannheim**<br>Biologische Chemie<br>Abschluss: Bachelor of Science, Note: 1,8 |
| 04/2008 - 02/2009 | **Technische Universität Kaiserslautern**<br>Lehramt Chemie und Mathematik<br>Kein Abschluss |
| 08/2005 - 03/2008 | **IGS Ernst Bloch Ludwigshafen**<br>Abschluss: Abitur, Note: 1,6 |

## BERUFSERFAHRUNG

| | |
|---|---|
| 09/2018 - heute | **Referentin für Wasser und Boden,** Landesanstalt für Umwelt Baden-Württemberg LUBW, Labor Wasser und Boden, Sachgebiet Organik |
| 03/2014 - 02/2015 | **Wissenschaftliche Mitarbeiterin,** Hochschule Mannheim. Institut für Instrumentelle Analytik und Bioanalytik<br>*Themen: Liposomal formulations and their diffusion through the blood-brain barrier; MALDI MSI of toxins used in Antibody-drug-conjugates* |
| 09/2013 - 03/2014 | **Master Thesis**, Hochschule Mannheim, Applied Research center Biomedical Mass Spectrometry (ABIMAS)<br>*Thema: Development of brain-penetrant liposomal drug formulations* |
| 04/2012 - 08/2012 | **Bachelor Thesis**, BASF SE, Limburgerhof:<br>*Thema: Determination of HPLC-UV relative response factors using NMR integrals* |
| 09/2011 - 02/2013 | **Lehrerin für Naturwissenschaften**, Studienkreis in Bad Dürkheim |
| 03/2011 - 09/2011 | **Praxissemester,** Kings College London, Department of Forensic Science and Drug Monitoring<br>*Thema: Investigation of red blood cells transcriptome and possibilities of storage related changes as an indication of autologous blood doping* |
| 11/2010 - 02/2011<br>11/2011 - 01/2012<br>05/2013 - 07/2013 | **Tutorin für Biochemie** Hochschule Mannheim (für Studenten des 3. Semesters der Fakultät Biotechnology) |

# 11 ACKNOWLEDGEMENT